IMPROVEMENT OF ANTI-LOCK BRAKING ALGORITHMS THROUGH PARAMETER SENSITIVITY ANALYSIS AND IMPLEMENTATION OF AN INTELLIGENT TIRE

Joshua Aaron Caffee

Thesis submitted to the faculty of the Virginia Polytechnic Institute and State University in partial fulfillment of the requirements for the degree of

Master of Science

In

Mechanical Engineering

Saied Taheri, Chair

John B. Ferris

Mehdi Ahmadian

November 18, 2010

Danville, VA

Keywords: stability control, intelligent tire, sliding mode controller, force, slip

IMPROVEMENT OF ANTI-LOCK BRAKING ALGORITHMS THROUGH PARAMETER SENSITIVITY ANALYSIS AND IMPLEMENTATION OF AN INTELLIGENT TIRE

Joshua Aaron Caffee

Abstract

The contact patch of the tire is responsible for all of the transmission of a vehicle's motion to the road surface. This small area is responsible for the acceleration, stopping and steering control of the vehicle. Throughout the development of vehicle safety and stability control systems, it is desirable to possess the exact forces and moments at the tire contact patch. The tire is a passive element in the system, supplying no explicit information to vehicle control systems. Current safety and stability algorithms use estimated forces at the tire contact patch to develop these control strategies. An "intelligent" tire that is capable of measuring and transmitting the instantaneous forces and moments at the contact patch to the control algorithms in real-time holds promise to improve vehicle safety and performance. Using the force and friction information measured at the contact patch, an anti-lock braking control strategy is developed using sliding mode control. This strategy is compared to the performance of a current commercial anti-lock braking system that has been optimized by performing a threshold sensitivity analysis. The results show a definite improvement in control system strategy having known information at the tire contact patch.

Dedication

To my father Wayne and mother Sharon…

Acknowledgements

I would like to sincerely thank my committee chair Dr. Saied Taheri for his continuous support of this research and for the professional mentorship over the past year and a half. I would also like to thank my committee members Dr. Mehdi Ahmadian and Dr. John Ferris for always taking time out of their busy schedules to answer questions and provide insightful comments.

Thank you to Virginia Tech and the Institute for Advanced Learning and Research in Danville, VA for providing the facilities to perform this research. Special thanks go to the IT department at the IALR for all their assistance with the video conferencing for broadcast courses and to Jeff Forlines for all of his help with the laboratory needs.

I would like to thank the Goodyear Tire and Rubber Company who made this research possible and helped me grow professionally.

I would like to thank the members of the Intelligent Transportation Laboratory, Brad Hopkins and Kanwar Bharat Singh, for their help in this research. Thank you for continually contributing ideas and assistance throughout the research process.

Lastly but surely not least, I would like to thank my parents, Wayne and Sharon Caffee, along with my girlfriend Heather Chemistruck, for their constant support and encouragement throughout my graduate studies.

Contents

List of Figures

List of Tables

1 Introduction

According to the National Highway Traffic Safety Administration (NHTSA) Fatality Analysis Reporting System (FARS), there are approximately 36,000 fatal crashes in the United States and over two million people injured each year [1]. It is estimated that there are more than six million car accidents annually totaling more than $164 billion [1]. A study performed by the European Transport Safety Council (ETSC) presents that road condition is the most significant single parameter causing the loss of vehicle control and leading to an accident. Slippery road conditions due to rain, ice and snow are responsible for more than 55% of accidents that lead to personal injury [2].

1.1 Introduction

In order to reduce the number of accidents in the U.S., vehicle development is focused on developing new technology to increase vehicle safety by implementing electronically controlled strategies to assist drivers in maintaining vehicle stability. Over the past several years, the direction of safety devices has shifted from passive components to active technologies. Active safety elements are employed in an effort to reduce safety related accidents due to road conditions and undesired vehicle handling by using information gathered from the vehicle's environment, including the tire's interaction with the road surface.

1.2 Approach

Introducing innovative sensors to the tire that can gather accurate information and provide quick measurement of important dynamic variables of the tire are necessary for effective active safety control systems. An intelligent tire (IT) has the capability to provide accurate measurements to feed to the active control systems in order to improve control algorithms. For the scope of this work, an intelligent tire is defined as an active sensor which is capable of directly measuring the longitudinal, lateral and vertical forces of the tire at each wheel as well as the friction coefficient between the tire and the road. Directly measuring these values from the tire eliminates the need to estimate these

parameters in the control algorithm. Employing an intelligent tire that can detect tire forces holds a high potential of accident prevention.

1.3 Contributions

The specific contributions of this work are as follows:

1) A threshold parameter sensitivity analysis is conducted for the full-vehicle anti-lock braking system simulation to identify the upper bound improvement to the current anti-lock braking system controller, and
2) Using information gained from an intelligent tire, an improvement to current anti-lock braking control systems is proposed by employing the use of a sliding-mode control method.

1.4 Thesis Outline

This work documents recent studies on an intelligent tire with an emphasis on the use of force and friction information at the contact patch to improve the performance of active vehicle safety systems, specifically anti-lock braking systems (ABS). The scope of this work as defined by the research sponsor includes performing a study on current ABS to determine the upper bound improvement to these current algorithms. The research then explores how employing an intelligent tire into ABS can improve braking performance. The overall goal of this study is to determine if employing an IT into new ABS algorithms improves braking performance enough to warrant further development of an IT. The remainder of this work is developed as follows. Chapter 2 presents the role pneumatic tires have on vehicle dynamics, as well as important tire parameters and their effects on vehicle handling. The evolution from passive to active vehicle control systems is also discussed. Chapter 3 provides an overview of the testing completed on an IT and its feasibility of implementation. Chapter 4 details the baseline vehicle simulation and control methods that are currently in-place on passenger vehicles. The simulation is a full representation of the driver, vehicle dynamics and control method which has been validated against real-world testing. Chapter 5 presents a sensitivity study on the current ABS simulation to identify areas of potential gain. Chapter 6 presents and develops a sliding mode control method to implement with the anti-lock braking system. This

control strategy introduces a robust control method capable of quickly actuating and increasing the performance of current anti-lock braking systems. The performance of this system is compared to the currently employed commercial control methods. Chapter 7 summarizes the work presented in this thesis and ends with concluding remarks.

2 Background

This Chapter presents a literature review of the state-of-the-art in vehicle safety control systems. The Chapter begins by identifying the tire coordinate system used in this work and also introduces necessary tire terminology. Passive and active safety control systems are briefly introduced to identify the capabilities and contributions to increase safety to the driver and passengers. More in-depth detail is presented in the sense of which systems are affected by specific tire forces and the ultimate focus of this work is presented- the anti-lock braking system.

2.1 Role of Pneumatic Tire

The pneumatic tire plays a major role in the operational properties of a road vehicle. The forces and moments acting on the tire originate from the location where the tire is in contact with the terrain surface. This interaction site is known as the tire contact patch and the response of the vehicle is the result of the dynamic interaction between the tire contact patch and the road surface. The forces and moments generated at the contact patch are altered by driver input based on various handling maneuvers. Vehicle dynamic behavior is primarily controlled through three driver inputs: 1) accelerator and 2) brake pedal, which control the vehicle longitudinal motion, and 3) steering wheel which provides directional control over lateral motion of the vehicle. These driver inputs indirectly control the vehicle motion by affecting the tire forces. The forces experienced through the tire are the primary forces affecting vehicle handling dynamics. The forces that can be transferred from the tire to the driving surface are limited by the contact patch area, the vertical load on the tire and the coefficient of friction between the tire and road surface.

2.1.1 Tire Coordinate System

The tire forces and moments using the SAE tire axis coordinate system, as shown in Figure 1, are defined in this section according to the J670 standard [3]. The origin of this coordinate system is located at the center of the tire contact patch, defined with the

tire being stationary on a level road. The *x-axis* is defined as the intersection of the wheel plane with the road plane in the longitudinal direction of travel, with the positive defined to the front of the vehicle. The *y-axis* is perpendicular to the *x-axis* and lies in the road plane, with positive defined to the right of the vehicle. The *z-axis* is vertical and passes through the origin, with positive defined downward. The longitudinal force, F_x, acts in the direction of the wheel plane and is a function of the longitudinal slip ratio. The lateral force, F_y, is in the horizontal road plane and is perpendicular to the direction of travel, as long as no inclination angle exists. The normal force, defined as F_z, is responsible for determining the amount of force available to accelerate the vehicle, both laterally and longitudinally, and is defined positive in the negative z direction. The overturning moment, defined as M_x, is the component of the tire moment vector trying to rotate the tire about the *x-axis* and is positive clockwise when looking in the positive direction of the *x-axis*. Rolling resistance, M_y, is the moment vector of the tire which rotates about the *y-axis*, and is taken positive clockwise when looking in the positive *y* direction. M_z represents the self-aligning moment and is defined as positive clockwise when looking in the direction of the *z-axis*. The slip angle of the tire, defined as α, is the angle between the direction of wheel travel and the actual direction of the wheel heading (the wheel plane). The inclination angle, or camber angle, represented by γ, is the angle between the wheel center plane and the axis normal to the ground plane when viewed from behind the wheel. The wheel angular velocity is represented by Ω and wheel angular acceleration by $\dot{\Omega}$.

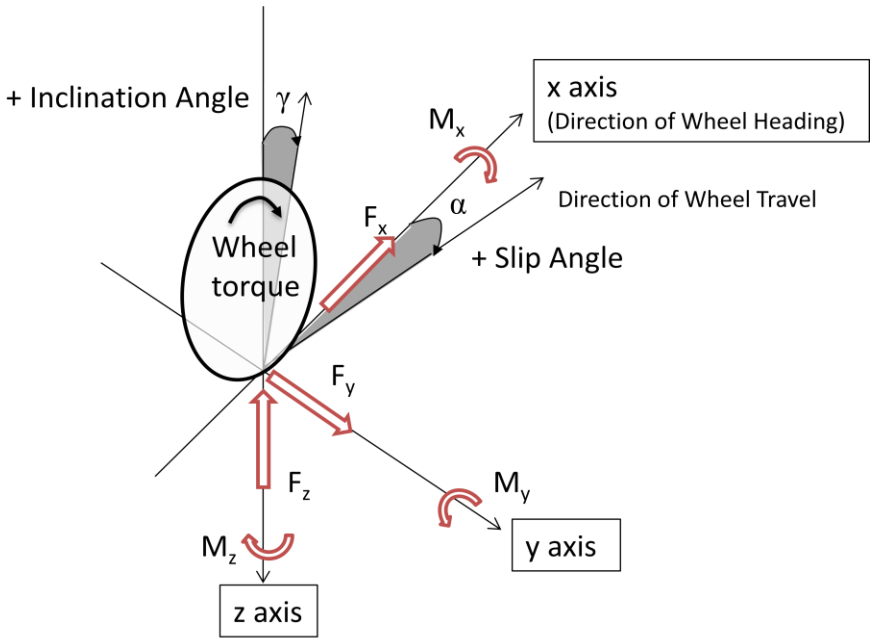

Figure 1. Diagram of SAE standard tire forces and moments acting at the center of the contact patch.

2.1.2 Tire Terminology

Slip

A fundamental property common to all pneumatic tires is the concept of slip of a rolling tire. Slip ratio, defined by κ, is what causes longitudinal force generation and slip angle α, causes lateral force generation of the tire. Slip ratio is the difference in speed between the vehicle body and the angular speed at the wheels. Slip ratio is expressed as a percentage and is represented by Equation 1, where V_x is the free rolling vehicle longitudinal speed, Ω is the angular velocity of the wheel, and r is the effective rolling radius of the tire. Slip ratio is defined as positive during braking, when the wheel speed is slightly less than the vehicle's free rolling velocity.

$$\kappa = \frac{V_x - r\Omega}{V_x} \qquad \text{Equation 1}$$

Slip angle is defined as the ratio of the inverse tangent between a rolling wheel's lateral velocity and forward velocity. As a wheel turns, the slip angle induces a deformation of tread elements, resulting in a force perpendicular to the wheel's direction of travel. This force is responsible for the lateral force generation and directional control

of the vehicle. Slip angle is defined in Equation 2, where α is the slip angle, V_y is the lateral velocity of the wheel and V_x is the forward velocity of the wheel. The sign of α was chosen such that the side force is positive for positive slip angle, according to the SAE coordinate system.

$$\alpha = -\arctan\left(\frac{V_y}{V_x}\right) \qquad \text{Equation 2}$$

At small angles and ratios of slip, the forces depend mainly on elastic deformation of the tire and are associated with a linear trend. At higher levels of slip, the horizontal forces are limited by the friction between the tire and the road and vertical load on the tire. The concept of slip is critical for understanding the vehicle response during extreme maneuvers.

Lateral Tire Characteristics

Figure 2 shows a lateral force versus slip angle plot for a passenger tire. Initially, the lateral force increases linearly with slip angle (the linear range of the tire), then curves, reaches a peak value and saturates in the non-linear region of the tire. Assuming a constant vehicle velocity, the linear region of the tire corresponds to small slip angles, in which the tire experiences more predictable forces. As the slip angle increases, the tire moves into the transitional region, in which the cornering stiffness of the tire, or slope of the lateral force versus slip angle curve, becomes less predictable. As the slip ratio continues to increase at the constant vehicle velocity, it will reach a point where the tire lateral force reaches its maximum friction with the road surface. After this point, the tire is within the 'frictional' region of the plot and the tire is unable to perform as expected, which can lead to loss of control of the vehicle. As the tire operates in the frictional region, the elements in the contact patch interacting with the road surface begin to slide, with the proportion of elements sliding increasing as slip ratio increases. As a result of the lateral properties of the tire, the vehicle response to driver input can change abruptly when the maximum limit of adhesion is reached [4]. For example, during cornering maneuvers, the vehicle yaw remains proportional to the steering input while the tires operate in the linear range. Once the tires move into the transitional and frictional range,

this relationship no longer holds and the vehicle can no longer follow the driver's desired path.

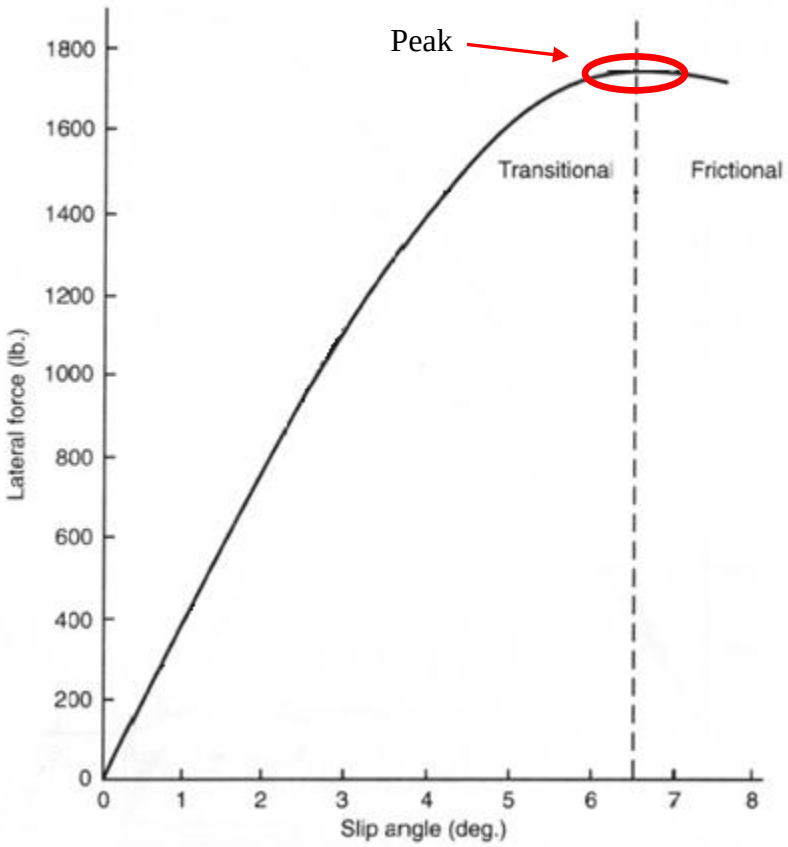

Figure 2. Lateral tire force as a function of slip angle.

Longitudinal Tire Characteristics

Longitudinal characteristics of the tire play an important role in both vibration characteristics of a car and its tractive performance in acceleration and braking. Specifically, longitudinal tire forces, which are primarily a function of the longitudinal slip ratio, experience a similar characteristic curve to that of lateral tire force vs. slip angle. Initially, longitudinal force increases linearly with slip ratio, curves, reaches a maximum value then saturates, as shown in Figure 3. The origin point of this graph corresponds to a non-accelerating vehicle. During acceleration, (the left hand side of this graph) as the slip ratio increases, the longitudinal force increases linearly. As the slip ratio continues to increase, the tire horizontal force will eventually reach its maximum adhesion point for the road surface, represented by the blue dotted line, and the wheel

will begin to slip, causing a reduction in longitudinal force. Excessive throttle application can lead to high slip ratios which can cause excessive wheel spin and loss of vehicle control. Similarly, during a braking maneuver (the right hand side of this graph) where brake pedal force is increasing, the vehicle speed initially decreases proportionally to the brake pedal force. As the brake pedal force reaches its maximum saturation value, the tire braking force saturates, which leads to a decrease in stopping force due to wheel lock-up as well as a loss of steer control. The point where the maximum longitudinal force is attained during braking, along with the corresponding slip ratio, is highlighted by the red dotted line.

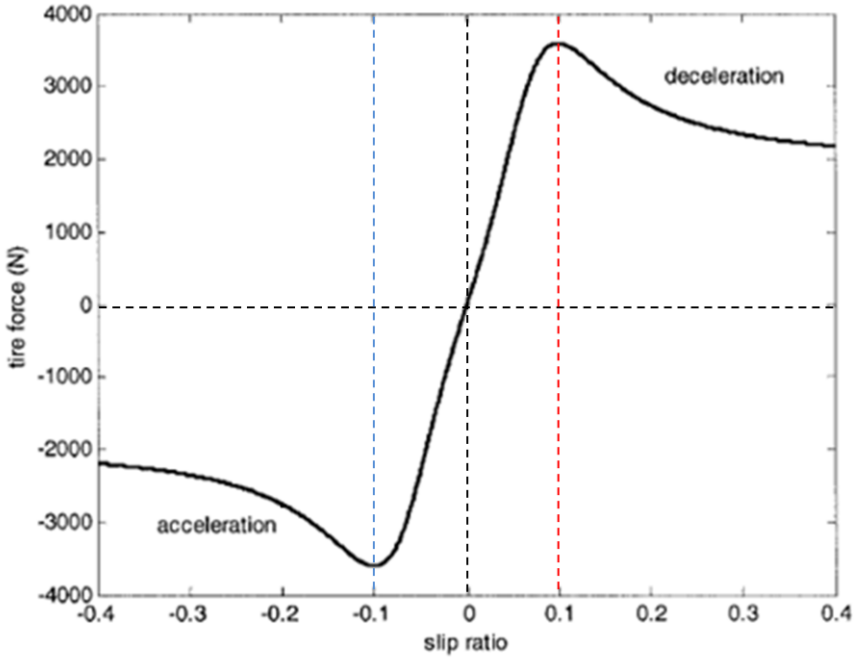

Figure 3. Longitudinal tire force as a function of slip ratio.

2.2 Vehicle Safety Systems

Vehicle safety systems can be separated into two main categories: passive and active safety systems. Passive safety systems have been used in vehicles for many years to aid in the reduction of injury to passengers. Passive safety systems only help reduce injury to the passengers after a collision has occurred. Active safety systems are responsible for aiding in the prevention of accidents by improving vehicle stability and performance during extreme maneuvers.

2.2.1 Passive Safety Systems

Passive safety control systems are a major part of nearly all passenger and commercial vehicles on the road today. Passive safety systems are defined as any safety mechanism on the vehicle that will help reduce injury to the driver and passengers upon impact. Well-known examples of these types of systems are safety restraints such as seat belts and air bags. The installation of seat belts by automotive manufacturers was made mandatory in 1966 by the Highway Safety Act and the National Traffic Motor Vehicle Safety Act [5]. Many newer vehicles are equipped with multiple air bags, which are commonly located in the dashboard, interior door panels and the A- and C-pillars. Other passive safety systems are built into the chassis of the vehicle and include crumple zones on the front and rear of the vehicle. These crumple zones are designed so that when the vehicle is involved in a collision, the chassis structure will attenuate and absorb as much of the impact as possible, limiting the damage transmitted to the passenger compartment. While passive safety systems have dramatically improved survivability and aided in the reduction of injury to the passengers, the damage sustained by the vehicle because of these systems has increased significantly. To put this into perspective, the cost to repair damage to vehicles designed with a crumple zone and many air bags that have been involved in relatively minor collisions can cost thousands of dollars, if the vehicle is not considered 'totaled'.

2.2.2 Active Safety Systems

Active control systems are quickly becoming a standard on many vehicles and have already been introduced on some high-end luxury cars (i.e. Lexus, Cadillac, Mercedes, BMW, etc.). Vehicle stability control systems gather information from vehicle sensors and sensors describing the surrounding environment. These sensors range from a single accelerometer mounted on the chassis, to wheel speed sensors at each wheel, to highly advanced 360 degree sensor arrays that enable autonomous driving [6]. Some common standard vehicle stability control systems are Anti-Lock Braking Systems (ABS) [7-9], Traction Control Systems (TCS) [8, 10-12] and Electronic Stability Programs (ESP) [4, 13-15]. Chassis and suspension controllers are able to assist the

driver in maintaining control of the vehicle during extreme maneuvers or under adverse driving conditions; specifically, these safety control systems engage to prevent the vehicle from skidding or slipping out of control. Currently, the majority of these systems are actuated by data gathered indirectly or estimated information from on-board sensors, however, these control systems can benefit from higher fidelity tire-road interface information by implementing information acquired from an intelligent tire.

Impact of Tire Parameters

The APOLLO consortium, consisting of several tire and vehicle companies, performed a study of an intelligent tire (IT) and its effects on accident free traffic [2, 16]. Table 1 presents their findings from which control and driver assistance systems stand to benefit from information gathered from the tire. The categories are judged on what tire information is available and how much the system would benefit from the availability of tire information. Their findings reveal that ABS, TCS and ESP are greatly affected from the availability of friction and force information from the tire. Other driver assistance programs greatly influenced on this information from the tire include Adaptive Cruise Control (ACC), automatic emergency braking and collision avoidance. These active control systems and others will be discussed in the following sections of this Chapter to discuss the added effects of pairing these systems with an intelligent tire.

Table 1. APOLLO findings on how information gained from an intelligent tire will affect vehicle control systems.

		Friction Information	Slip Angle	Wheel Forces	Tire Condition	Road Parameters
Vehicle Control	ABS					
	TCS					
	ESP					
	Rollover Avoidance					
Advanced Driver Assistance System	ACC					
	Emergency Braking					
	Collision Avoidance					
Driver Information	Information Level					
	Warning Level					
Potential the application will benefit from available tire information		Greatly		Somewhat		Little

Anti-Lock Braking Systems

ABS is a safety system which prevents the wheels from locking up, or ceasing to rotate, during a braking event. ABS allows the driver to maintain steering control while also reducing stopping distance in many cases. Currently, ABS consists of a sensor to detect wheel lock-up along with a brake pressure controller which is used to momentarily relieve brake pressure to prevent the wheel from skidding [12]. This process of releasing and applying brake pressure to the wheel to prevent skidding must happen quickly for the system to perform satisfactorily. Modern vehicles are equipped with these sensor and brake pressure valves at each wheel to allow for independent actuation from one another to maximize braking forces at each wheel by maintaining the longitudinal sip ratio around an optimum value. A common sensor used to detect wheel lock is a wheel speed sensor - a toothed disc attached to the hub of the wheel and a magnetic sensor. This magnetic sensor detects each projection of the disc and sends a signal to the brake pressure valve if lock-up is detected. Currently these systems are designed to use wheel speed and acceleration as the only parameters to predict if the wheel will lock up. Some newer ABS use estimated forces at the contact patch to try and improve the performance of these algorithms. ABS controllers are designed with the intent of preventing the wheels from locking using an assumed longitudinal slip ratio. This longitudinal slip ratio is tuned to be close to an ideal optimal value. The actual value is unknown and is determined from look-up tables based on wheel speed and acceleration. The look up table takes into account the current deceleration of the wheel, the measured wheel acceleration and slip ratio at that time. If the wheel acceleration is greater than a specified rate and the slip ratio is greater than the ideal value, the brake controller is triggered to release the brake. If the wheel acceleration is lower than the specified value and the slip ratio is quickly decreasing, the brake controller will reapply the brake. The slip ratio value and maximum available longitudinal force vary depending on road surface condition, so these parameters require extensive on-vehicle tuning to perform properly. Additional detail on ABS systems can be found in the Longitudinal Control Section of this Chapter.

Traction Control System

TCS is a safety system which prevents excessive slip, or wheel spinning, during acceleration. Wheel spin is defined as loss of traction because the force supplied to the wheel exceeds the maximum available tractive force between the tire and road surface. It allows the driver to maintain control of the vehicle when excessive throttle is applied or adverse road conditions exist that would result in wheel spin. TCS reacts much the same way as ABS, with the objective of the controller being to prevent wheel spin (instead of wheel lock-up). The goal of TCS is to reduce drive torque to the wheels by applying the brakes when the wheel speed sensors detect the wheel is about to spin. However, wheel spin is more difficult to measure than wheel lock-up. TCS must be more sensitive to longitudinal slip to differentiate the wheel speed at each wheel when the vehicle is being driven around a corner. That is the inside and outside wheels of the vehicle will experience different speeds since they are not traveling along the same radius path. Again, TCS is controlled without knowing the available longitudinal force of the tire-road interaction, so iterative estimations must be performed to determine when, and at what drive torque, maximum adhesion to the road surface is achieved. Additional detail on TCS systems can be found in the Longitudinal Control Section of this Chapter.

Electronic Stability Program

ESP is an integrated safety system that improves vehicle stability by detecting and minimizing skid. ESP generally uses a combination of differential braking [7, 14, 17-20], steer-by-wire (SBW) systems [20-22] and active torque distribution [20, 23, 24]. ESP employs a yaw control sensor mounted on the vehicle to ensure the vehicle maintains stability during cornering and on split friction coefficient surfaces. ESP uses differential braking to control brake forces at each wheel in order to counter excessive yaw moment of the vehicle. Active torque distribution is used for the same purpose except during acceleration and SBW is employed to assist the driver. These systems will be discussed in more detail in the Lateral Controls section of this Chapter.

2.3 Longitudinal Vehicle Control

2.3.1 Longitudinal Forces

Several factors contribute to the generation of longitudinal forces acting on a vehicle. Figure 4 shows a diagram of a vehicle on an inclined surface. The forces acting on the vehicle in the longitudinal direction include gravitational forces, longitudinal tire forces, rolling resistance forces and aerodynamic drag forces. The longitudinal tractive and braking forces for the front and rear tires are represented by F_{xf} and F_{xr}, respectively. RR_{xf} and RR_{xr} are the rolling resistances of the front and rear tires. To simplify this diagram, the longitudinal force and the rolling resistance are assumed to be the combination of the left and right tires at both the front and rear axles. In reality, the forces and rolling resistances will be accounted for at each tire. The mass of the vehicle is denoted by m, the acceleration due to gravity, g and the aerodynamic forces are represented as F_{aero}. The angle of the incline is given as θ.

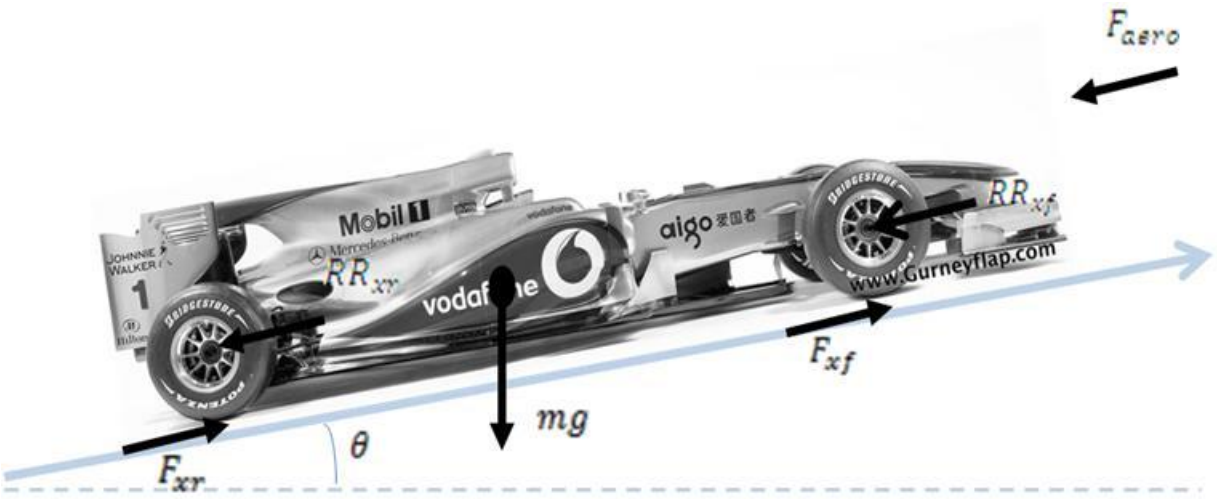

Figure 4. Longitudinal forces acting on a vehicle on an inclined road. Used under fair use, http://gurneyflap.com/Resources/MC02.jpg, 2010.

Performing a force balance along the vehicle longitudinal axis yields the equation:

$$m\ddot{x} = F_{xf} + F_{xr} - F_{aero} - RR_{xf} - RR_{xr} - mgsin(\theta) \qquad \text{Equation 3}$$

Equation 3 shows that the net longitudinal forces are positive, relating to the friction force of the wheel with the road surface, under vehicle acceleration. Experimental results

have established that the pure longitudinal tire force generated at each tire depends on the slip ratio, κ, the normal load on the tire, F_z, and the friction coefficient between the tire and the road, μ [8]. The aerodynamic drag force is heavily influenced by the frontal area and the speed of the vehicle and plays a significant role at higher speeds. The rolling resistance acts to oppose the motion of the vehicle due to internal damping and deformation of the tire and frictional losses in the rotating powertrain components. Assuming negligible lateral forces, the normal force on the tires can be calculated knowing the height and fore-aft location of the center of gravity, longitudinal acceleration of the vehicle, aerodynamic drag forces and the inclination of the road. With the assistance of an intelligent tire, the longitudinal and normal loads acting on the tire can be measured directly.

2.3.2 Longitudinal Control Systems

All of the tire forces are either directly or indirectly related to the tire interaction with the road. It is assumed that an intelligent tire is capable of measuring these forces to enable the design of effective active longitudinal controllers. Longitudinal controllers are any control system that controls the longitudinal motion, such as the velocity or acceleration of the host vehicle (in case of a platoon) or distance from the host vehicle to preceding vehicles. Longitudinal controllers consist of cruise control, adaptive cruise control (ACC), automated highway systems (AHS), anti-lock braking systems (ABS), and traction control systems (TCS).

Cruise Control and Adaptive Cruise Control

Cruise control is offered as a dealer option on every present day vehicle and allows the driver to set the car at a desired velocity. The car will maintain the desired velocity until the driver intervenes and either applies the brake, accelerator or turns the system off. An adaptive cruise control (ACC) system is an extension of the standard cruise control system. ACC consists of a laser, radar or other sensor that measures the distance to preceding vehicles [25]. If there is no other vehicle upstream, the cruise control will travel at a user-set speed. However, if a vehicle is detected ahead of the user's vehicle, the ACC determines if the desired speed can be maintained or if the ACC

must take control and switch to spacing control. Spacing control enables the ACC to control the brakes or throttle in order to maintain a safe spacing from the preceding vehicle. An addition to ACC is a collision avoidance system [26, 27] that makes use of the corrective throttle reduction or braking action in order to slow the vehicle to avoid an accident. The visual forward looking sensors must be able to positively identify obstacles in the direct path of the vehicle while not returning false signals due to vehicles in adjacent lanes. ACC must respond quickly if another vehicle cuts into its path at a slower speed and immediate collision avoidance is necessary. While ACC is a convenience to drivers, these systems still require ultimate driver attention. This system is not investigated further in this thesis because it does not lend itself to improvement with the implementation of an intelligent tire. It is discussed here to present all of the current safety systems available to passenger vehicles.

Automated Highway Systems

Automated highway systems (AHS) are a level apart from cruise control, and do not currently exist for public use, but would allow vehicles to travel together in a tightly spaced pack on the highway. Several AHS have been constructed and tested at several locations and have proven successful. The system requires fully instrumented vehicles to travel autonomously on the interstate. AHS can greatly increase traffic capacity and help reduce gas consumption of cars within the pack due to decreased aerodynamic drag. Most importantly, AHS would allow for a huge reduction if not elimination of highway related traffic accidents because the driver is removed from the equation. However, AHS requires either extensive infrastructure expansion, or the addition of communication and position sensors to each vehicle. AHS requires a high capital cost to develop and maintain infrastructure. It would be possible to implement current vehicles with the necessary sensors and software to be compatible for AHS, but is not a cost effective solution at this time. Some aspects of the AHS system, such as emergency braking, would benefit from the implementation of an intelligent tire, but this system is outside the scope of this work.

Anti-Lock Braking System (ABS)

ABS was developed to prevent wheel lock-up during hard braking. Newer ABS does this more efficiently by attempting to maximize the braking forces generated by the tires on the road surface. This is accomplished by maintaining the longitudinal slip ratio around an optimum value. ABS systems prevent the wheels from locking during braking, thus allowing the driver to maintain relative control over the direction of the vehicle. If the wheels lock and begin to slide during braking, the vehicle stopping distance increases and the driver does not have control over the direction of the vehicle. In order for ABS to maximize the braking forces, the system requires the knowledge of the maximum longitudinal force available at each wheel. This value is dependent on the surface friction available at the road and the normal load at each tire. During heavy braking, the normal load is prone to variation since a large percentage of the vehicle weight is transferred forward as the nose of the vehicle dives during braking. The maximum longitudinal force that can be obtained for the front and rear tires is presented in Equation 4 and Equation 5 respectively.

$$F_{xf} = \mu F_{zf} \qquad \text{Equation 4}$$

$$F_{xr} = \mu F_{zr} \qquad \text{Equation 5}$$

The friction coefficient is μ and F_{zf} and F_{zr} are the normal loads of the front and rear tires, respectively. The longitudinal force is dependent on the available friction between the tire and the road and normal load at each tire. If the force information is accurately known at each wheel, a more effective controller can be developed. Implementation of an intelligent tire would eliminate the need to calculate the normal force acting on each tire since longitudinal force can be calculated directly, and provide the means for a more efficient controller.

Traction Control Systems

TCS provides a similar benefit as ABS except during acceleration. TCS attempts to maximize tractive forces generated by the tires on the road surface by preventing wheel spin and keeping longitudinal slip from exceeding an optimal value. This results in controlled vehicle acceleration and the ability to maintain speed in adverse conditions.

As an added benefit, TCS also allow for sports cars to maximize the rate of acceleration by reducing longitudinal slip. It again relies on the maximum longitudinal force equations presented in Equation 4 and Equation 5. TCS has great potential for improvement with the addition of an intelligent tire.

2.4 Lateral Vehicle Control

2.4.1 Lateral Forces

The lateral forces on a vehicle are generated at each tire by the driver inputting a steering angle to the front wheels. The rotation of the wheels results in the deformation of the tire tread, resulting in slip angle generation. The steering angle input is defined by δ and is the directional input to the tire from the driver. The slip angle is given by α and is the amount of tire deflection that results in the heading of the vehicle. The slip angle is responsible for the lateral force generation at the tires. The steering angle input differs from the slip angle slightly due to the tread element deflection in the tire, generally resulting in a steering angle greater than the slip angle. Figure 5 presents a diagram of the lateral forces for a bicycle model. The lateral forces of the front and rear tires are given by $F_{y,F}$, $F_{y,R}$, respectively. The introduction of lateral force to a vehicle results in a rotation of the vehicle around the vehicle's vertical axis at the center of gravity. This rotation is defined as yaw and is represented by ψ. Yaw is typically used in lateral control systems to define the stability of the vehicle during cornering. If yaw exceeds a predetermined value, the vehicle is considered unstable. Measuring the lateral force using an intelligent tire could be used to estimate the slip angle for use in lateral safety control systems. The velocity of the vehicle is denoted by V. The distances from the vehicle center of gravity to the centerline of the front and rear wheels are l_f and l_r, respectively.

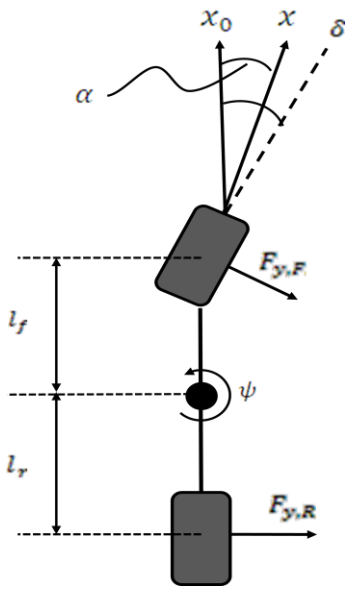

Figure 5. Lateral forces acting on a vehicle.

2.4.2 Lateral Control Systems

Lateral control systems include lane departure warning systems (LDWS) [28], lane keeping systems (LKS) [29, 30], yaw stability control systems and active front steering (AFS) [8]. LDWS and LKS have gained quick popularity and acceptance since their introduction. NHTSA reported that as many as 1,600,000 accidents occur each year due to distracted drivers, many of which occur due to unintended lane departures [1]. LDWS and LKS are both equipped with sensors located on the vehicle which monitor the vehicles position with respect to the lane markings. If the LDWS detects the driver drifting into an adjacent lane or off the roadway it will provide a warning to the driver. The LKS takes this a step further and can make minor corrections to the steering angle of the car in order to keep the vehicle within the lane. LKS systems are cable of following a curved roadway independently using a visual monitoring system or differential GPS. LDWS and LKS are primarily safety systems and would not benefit from implementation of an intelligent tire. .

Yaw Control System

The purpose of a yaw control system is to assist the driver to maintain a safe path throughout a turning maneuver by preventing the vehicle from “spinning out” or drifting.

Figure 6 shows a diagram on the operation of a yaw control system. For example, on a high friction surface at low vehicle speed, the driver is able to maneuver the car around a sharp turn with relative ease. In this case, the high friction surface allows adequate lateral force generation required by the vehicle to negotiate the turn. However, if the coefficient of friction were small due to adverse road conditions, or the vehicle speed were too high, then the vehicle would be unable to follow the nominal motion required by the driver, shown in the large radius curve on the right hand side of Figure 6. The yaw control system works to restore the yaw velocity to a safe rate and set the vehicle to the desired motion expected by the driver. If the friction coefficient is too small or the vehicle speed is too high, it may not be possible to achieve the nominal path desired by the driver, but the yaw control system can be expected to partially succeed by making the vehicle yaw velocity approach the desired yaw rate, as seen in the middle curve of Figure 6. Yaw control systems can work in several ways including differential braking, steer-by-wire, or active torque distribution.

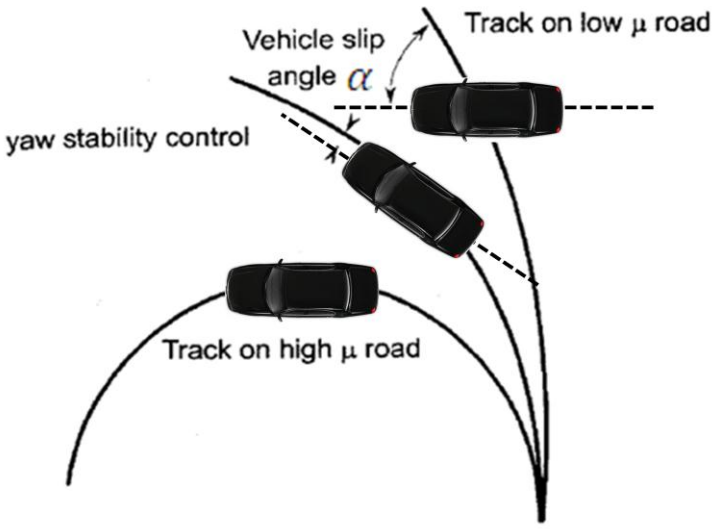

Figure 6. The function of a yaw control system.

Just as pure longitudinal force is a function of friction coefficient and normal load corresponding to the front or rear wheels, pure lateral force can also be defined for the front and rear wheels, as shown in Equation 6 and Equation 7 respectively.

$$F_{yf} = \mu F_{zf} \quad \text{Equation 6}$$

$$F_{yr} = \mu F_{zr} \quad \text{Equation 7}$$

Again, it can be shown that the friction available and normal force at the contact patch for each tire plays a major role in determining the lateral dynamics of the vehicle. Equation 6 and Equation 7 show the benefit of being able to measure the maximum available lateral force at each wheel. If these values are known, lateral control methods can be improved to help keep the vehicle on the driver's intended path. The knowledge of these forces can be provided with the implementation of an intelligent tire.

Differential Braking

The differential braking technique has shown the most promise for correcting vehicle yaw instability. Differential braking employs the ABS on the vehicle to brake the right and left, front and rear wheels independently to control the yaw moment. The yaw moment of the vehicle is generally measured using a yaw sensor attached to the vehicle chassis. If the yaw velocity measured exceeds a predetermined yaw moment that the vehicle is unable to maintain, differential braking will be employed to maintain stability of the vehicle. The most significant effects from differential braking come from braking the outside front tire for vehicles that are experiencing oversteer and braking the inside rear tire for vehicles that are experiencing understeer through a turn [22]. An oversteering vehicle, when traveling through a turn, means that the rear tires reach the limit of adhesion before the front tires, resulting in the back end of the car swinging outward. An understeering vehicle, when going through a turn, will have the front tires reach their limit of adhesion before the rear tires, resulting in the front end pushing outward. The drawback to employing only differential braking is that it can cause a significant reduction in vehicle speed during cornering [4]. Differential braking also stands to greatly benefit from the implementation of an intelligent tire. Direct knowledge of both longitudinal and lateral forces would be able to maintain yaw stability of the vehicle while keeping the reduction in vehicle velocity minimal.

Steer-by-Wire

A steer-by-wire (SBW) system is designed with the intent of modifying the driver's steering input angle by transmitting the control electronically to the steering wheels. A SBW system replaces the mechanical linkages and steering shaft with a fully electrical system. SBW holds several benefits over a traditional mechanical system including the ability to actively correct steering input for LKS and yaw stability systems. By actively changing the steering angle of the front or rear wheels, active steer systems directly affect slip angles of the corresponding axle, and therefore the tire forces. Steering system response can also be adjusted and optimized for driver response and feel. For example, if a driver is entering a sharp turn too quickly and the driver over rotates the steering wheel, this would normally cause the vehicle to become unstable. A SBW control system would only allow the front wheels to steer to the maximum angle at which the car would remain stable and in control, however, this would remove some of the control from the driver's hands. If the system were to underestimate the adhesion levels of the tire and road interface, it could cause the vehicle to leave the desired path altogether. SBW systems could have a small benefit from the introduction of an intelligent tire, but will not be explored further due to the scope of this work.

Active Torque Distribution

Active torque distribution utilizes active differentials of vehicles equipped with all-wheel drive to independently control the drive torque distributed to each wheel. This provides active control for both TCS and yaw moment. The use of active torque distribution can help achieve the desired yaw rate without the use of differential braking. The advantage of active torque distribution over differential braking is that it does not decelerate the vehicle during yaw stability control. This control system is useful when driving in adverse conditions such as rain, snow or ice or on split-μ surfaces where the coefficient of friction is different between the left and right side of the vehicle. This system relies heavily on TCS to prevent the wheel from spinning and also on yaw control to make sure the vehicle maintains stability. Active torque distribution, just like ABS, would benefit from the implementation of an intelligent tire. Knowing the direct forces

at the contact patch would allow for increased performance in distributing torque to the wheels.

2.4.3 Vehicle Stability Control Systems

Current stability control systems employ a combination of both longitudinal and lateral control systems. Additional implementation of active suspension systems can be incorporated to help control the pitch and roll of the vehicle. Stability control systems take on many names from different manufacturers but all take the form of an Electronic Stability Programs (ESP). Since ESP incorporates both longitudinal and lateral control systems, the maximum force generations for pure lateral and pure longitudinal forces introduced in Equation 4 through Equation 7 are no longer completely valid. The maximum force the contact patch can transfer from the vehicle to the tire is a combination of both lateral and longitudinal forces. This can most easily be represented using a friction circle, such as the one shown in Figure 7. Varying levels of lateral and longitudinal slip are shown in the graph, with the outermost circle showing the total vector sum of both lateral and longitudinal forces that remain within the frictional capabilities of the tire, μF_z. Any values of slip ratio and slip angle within this circle are within the frictional capabilities of the tire. Any values outside of the outermost circle are conditions where the tire is experiencing excessive slip and are defined to be in the sliding region of the tire. As can be seen, when the magnitude of the longitudinal force grows larger, the lateral force saturates, and vice versa. The total slip σ is composed of the normalized longitudinal slip ratio and lateral slip angle as shown in Equation 8,

$$\sigma = \sqrt{\sigma_x^2 + \sigma_y^2} \qquad \text{Equation 8}$$

where σ_x is the longitudinal slip component and σ_y is the lateral slip component. The longitudinal and lateral forces are given by Equation 9 and Equation 10

$$F_x = \frac{\sigma_x}{\sigma} F \qquad \text{Equation 9}$$

$$F_y = \frac{\sigma_y}{\sigma} F \qquad \text{Equation 10}$$

where F is the magnitude of the total force. The intelligent tire would be able to further improve the performance of vehicle stability control systems by improving ABS and providing accurate knowledge of the forces at the contact patch to all other related systems. This would eliminate the need for estimating force parameters for load distribution so each system could be optimized.

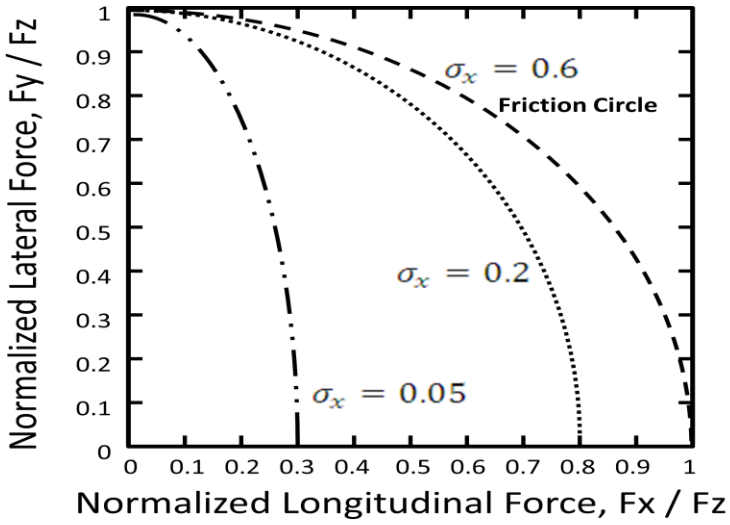

Figure 7. Friction circle showing lateral force versus longitudinal force for a typical passenger tire.

2.4.4 Active Suspensions

An active suspension employs some type of force actuator into the suspension that is able to control the suspension dynamics of the vehicle. Examples of these actuators are Continuous Damping Control (CDC), Magnetorheological (MR) dampers and active roll bars. CDC generally employs an electrical system to soften or harden the damping characteristics. MR dampers control the magnetorheological fluid through a magnetic field to achieve the same effect. Roll bars can stiffen to change the load transfer from side to side. Both of the damper systems allow for soft damping characteristics during normal driving to increase driver comfort, but can stiffen the dampers to improve vehicle handling during extreme maneuvers. Stiffening the dampers acts to balance the force

distribution of the vehicle and can be used to maximize the friction available at the tire contact patch. If applied during emergency maneuvers, active dampers can help prevent excessive pitch and roll dynamics or distribute the vehicle load to maximize traction to each wheel. These systems use a variety of inputs including lateral movement, vehicle speed, driver reaction and road conditions, most of which are determined using look-up tables. Through testing it has been shown that using active suspension to control the load transfer for maximizing the force available at each tire for yaw control is beneficial. However, the maximum corrective yaw control moment generated by using MR dampers and active roll bars are about four times smaller than the maximum values achievable by active steering or braking [4]. An intelligent tire could potentially help improve these systems by eliminating the need to use look-up tables to determine the forces on the vehicle due to load transfer during extreme maneuvers.

2.4.5 Electronic Stability Program

ESP is a computerized integration of controllers that allow the longitudinal and lateral control systems to work together to actively control the vehicle in order to improve safety. Active suspension systems can be included as a subset of ESP. Figure 8 shows a breakdown of the functions of vehicle dynamics control [17]. This figure shows that firstly, the driver has ultimate control over the system. The vehicle dynamics are then broken down into longitudinal, lateral and vertical control and which functions have an influence on each category.

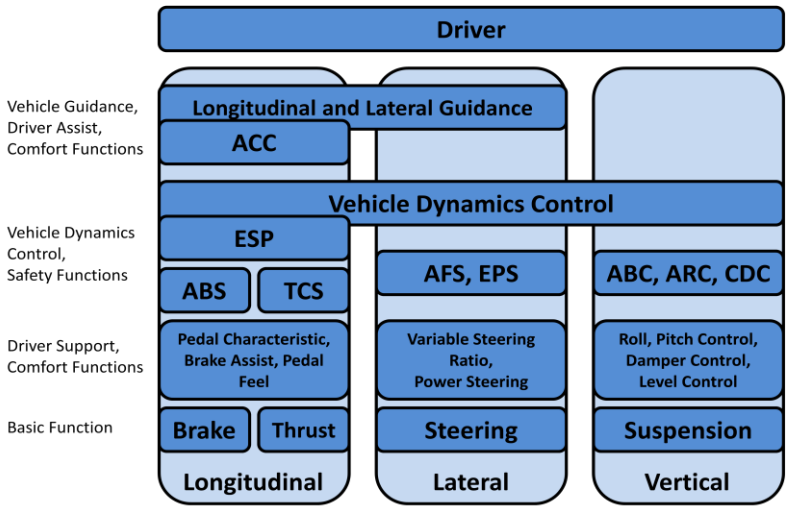

Figure 8. Functions and systems for vehicle dynamics control.

More specifically, control algorithms can be developed for specific systems. An example of this is the integrated yaw controller shown in Figure 9 [17]. This yaw rate controller for an ESP was expanded to include physical interfaces of the steering and suspension system. The closed loop control structure begins by taking the driver steering input, the suspension input and the vehicle dynamics input from vehicle sensors and combining these signals into a signal processing observer. This observer uses the inputs and calculates the desired yaw rate and path for the vehicle to follow. These values are then compared to the current vehicle dynamics and the yaw rate is adjusted and sent through a controller. This controller then adjusts the yaw torque distribution and sends the control signals to the actuators which control the steering, ABS / TCS, and active suspension to make corrections to maintain vehicle stability, if necessary. The yaw and braking controller systems would benefit from an intelligent tire, which would lead to improved overall system performance.

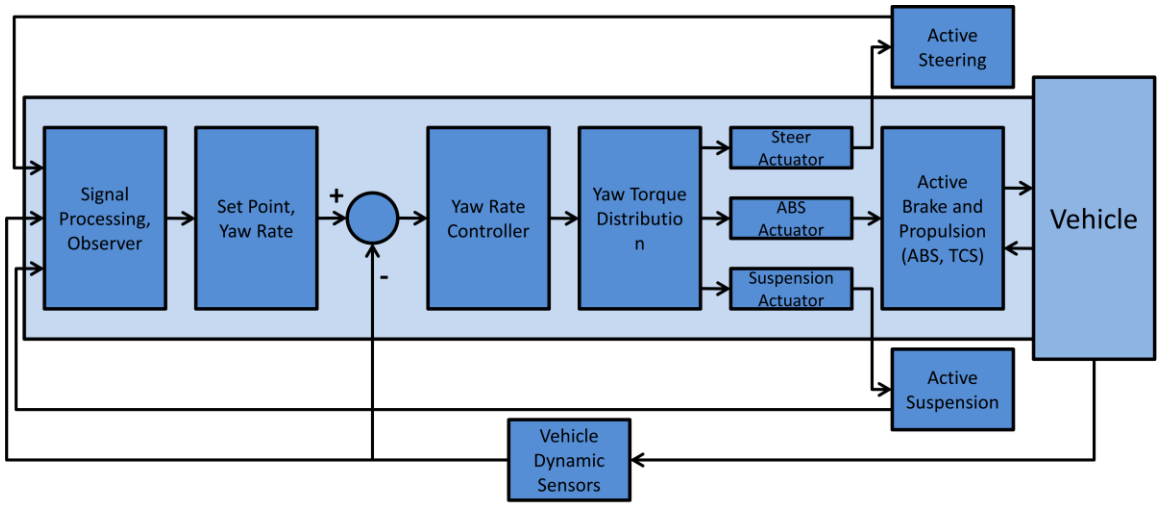

Figure 9. Closed loop control structure of ESP for yaw rate control including steering and suspension system.

2.4.6 Advanced Driver Assistance Systems

Advanced driver assistance systems (ADAS) are systems that help the driver with the driving process. These systems assist the driver in order to improve safety. ADAS are not generally considered emergency stability programs, but are controllers such as ACC, LDWS, and LKS. Other forms of ADAS include hill descent control (HDC) and amenities such as parking assist. HDC uses engine braking to help control the cars motion downhill, but can also be an extension of ABS, using braking at all four wheels to control vehicle motion. HDC allows for smooth and controlled hill descent without requiring the driver to touch the brake pedal. Other ADAS systems include automatic emergency braking and collision avoidance. Collision avoidance systems generally only alert the driver to dangerous conditions on the road including vehicles or obstacles ahead or alert the driver to slow down before taking a turn. Automatic emergency braking acts to assist the driver to quickly apply the brakes and ensure that the maximum braking power is being utilized in an emergency stop situation. Important information could be supplied to the driver, warning of unsafe or unstable conditions using the information from an intelligent tire.

2.5 Focus on Longitudinal Vehicle Control Safety

After performing a literature review of active safety control systems, both for longitudinal and lateral control, it was decided to further study the effect of knowing the exact forces at the tire contact patch in conjunction with ABS. Tire force information was chosen based on information from the APOLLO report, showing potential to affect nearly all active vehicle safety control systems. Force generation at the contact patch was also chosen based on feasibility information gained by the Intelligent Transportation Laboratory, which is presented in Chapter 3. The anti-lock braking control system is the focus of this study since it is a standard system on all modern vehicles. Improving the performance of ABS has the potential to reduce the severity of and prevention of accidents. Additionally, once proper braking control can be achieved, it can be incorporated into vehicle stability control methods, since these systems are actuated based on differential braking. Thus, using tire force in conjunction with ABS is a good starting point to prove and quantify the performance improvement to vehicle safety systems.

3 Intelligent Tire Development

3.1 Introduction

In order to properly model vehicle simulations for active safety systems using an intelligent tire (IT), it is important to accurately measure tire forces and moments at the tire contact patch over different road surface types. The forces and moments at the contact patch are vital to developing accurate tractive and stability control algorithms. There have been many recent advancements and literature dedicated to measuring tire parameters at the contact patch. Some approaches used for tire force and moment measurement at the contact patch are introduced in this Chapter. There are two major methodologies for the basis of tire models used in vehicle simulations - physical and empirical. Physical models seek to numerically represent the interaction of the tire with the road surface for specific performance metrics (i.e. ride, handling, reliability, durability, etc.). Empirical tire models are based on experimentally acquired data and seek to represent the actual interaction of the tire with specific road surfaces. The goal of the ITL is to empirically acquire information about the interaction of the tire with the terrain surface in order to develop more accurate empirically based tire models for use in simulation of vehicle systems.

The objective of this Chapter is to identify the capabilities of an IT through experimental testing. A brief background is presented on a current tire force and moment testing trailer (TTT) and IT. The results from the IT are correlated to the TTT and the feasibility of implementing an IT are discussed, followed by the concluding remarks.

3.2 Intelligent Tire and Tire Testing Trailer

With the number of electronic systems in vehicles quickly growing, there has been a shift from passive to active safety devices. Several vehicle systems and components, including steering, suspension and braking, have been used to improve active vehicle safety, ultimately focused on attaining accident free traffic. As a first step, it is important to define the overall performance goals of an IT and also have a way to objectively measure the desired outputs of the system. Quantifying these outputs

accurately will help judge the role and benefit an IT will play within vehicle active safety systems.

3.2.1 Intelligent Tire

Currently, tires are a passive element in the vehicle system, supplying no information to vehicle safety and control systems. An intelligent tire is a tire that has been outfitted with sensors to gather accurate information and provide real-time measurement of important dynamic variables. For the scope of this work, an IT is defined as an active sensor which is capable of directly measuring the longitudinal, lateral and vertical forces at the tire contact patch. Recent government regulations require the use of a tire pressure monitoring system (TPMS) on all vehicles produced after September 1, 2007 [31]. These systems are designed to warn the driver if a tire is severely under-inflated. These systems are an early attempt to use the tire as an active sensor within the vehicle safety system.

New capabilities are required to improve active safety systems including: gaining or sensing information, actuation, control, decision making based on information evaluation and providing this information to control systems [2]. An intelligent tire that can provide detailed information about the tire's interaction with the road has the capability to provide the chassis and traction management systems with valuable information. This force and moment information can be used to improve the control algorithms, which will better develop the decision making process of the control strategies and result in more precise controller actuation. It is also likely that many current control algorithms can be simplified. Now, instead of programs like ABS and stability control having to estimate tire parameters through look-up tables, these values are measured directly. An IT holds great potential to improve active vehicle safety systems.

There are many different types of sensors that can be implemented into the tire in order to measure these variables. These sensors vary in complexity, cost and measurement capabilities. Several common types of sensors used are strain gauges, accelerometers, acoustic sensors and optical sensors. Strain gauges are inexpensive, easy to implement and provide information about the deformation of the tire as it passes

through the contact patch. Accelerometers measure the acceleration of the tire as it rotates through the contact patch and depending on the type of accelerometer used, the acceleration can be measured for up to three-axes. Acoustic sensors measure sound pressure or vibrational wavelength inside the tire and can be used to identify road conditions or tire wear. Optical sensors measure the deformation of the tread section and sidewall of the tire through rotation of the contact patch.

The capabilities and implementation of different types of sensors are not only limited to measurement. The tire also holds great potential for implementation of energy harvesting materials and methods that can be used to power remote sensors within the tire or provide energy back to vehicle chassis systems. Intelligent tires may also prove useful for electric vehicles. Many new electric vehicles are designed to be driven by independent motors at each wheel, where each motor will be able to directly and accurately provide the necessary torque to brake, accelerate and stabilize the vehicle.

3.2.2 Tire Test Trailer and Intelligent Tire Testing Parameters

The ITL designed and fabricated a Mobile Force and Moment Tire Test Trailer (TTT). The objective of the trailer is to collect tire force and moment data for a variety of on- and off-road surfaces. The TTT is a robust, standalone system capable of traversing smooth and rough surfaces under wet and dry conditions. Parallel testing can be completed using a flat track testing machine, which tests tires in an indoor environment. A flat track machine is capable of reproducing exact testing parameters for different tires in a controlled environment. The TTT also allows for test repeatability of dynamic parameters. The key difference between the TTT and a flat track testing machine is that the tire testing trailer can test on the desired terrain surface of interest directly, rather than using a belt.

The testing trailer was designed to test tires ranging from small passenger and motorcycle tires up to large semi-truck tires. The TTT is able to measure and control tire parameters including vertical load, slip angle and camber angle. These parameters can be adjusted to measure the tire's response to varying inputs and test conditions in order to quantify the performance of the tire. Refer to Fox's thesis for a complete description of the TTT and its capabilities [32]. The validation of the TTT to a third party flat track

machine in presented in [33, 34]. In these works, Hopkins's shows that the forces and moments measured about the tire using the TTT match data gathered from the flat track machine within a 10% error. A strict testing procedure is also presented in order to ensure representative, consistent and repeatable results. Representative results are a measurement of the results that accurately reflect each factor that affects performance, including desired outputs. Repeatability of testing is extremely important in order to validate the consistency and reliability of test results.

Testing of an intelligent tire is an extension of testing non-sensored tires using the TTT. The same testing procedure is utilized for testing the IT. When testing an IT, additional sensor information must be collected from the sensors embedded within the tire. Depending on the type of sensor chosen and used within the tire, the output could yield deformation, acceleration, or acoustic information. The sensors that the ITL have tested have all been attached to the inner lining of the tire. In order to transmit data from sensors located within the tire to the data acquisition hardware, special equipment must be used. Figure 10 shows the testing set-up of an IT. The sensors inside the tire are connected to a specialized air-tight feed-through connector, which passes the wires through the wheel bulkhead. This allows the wires to exit the wheel but keep the tire inflated to the desired pressure. The feed-through connector spins with the wheel. Externally, the feed-through connector is attached to a high-speed slip ring. The slip ring is an electromechanical device that allows for the transmission of electrical signals from a rotating structure to a stationary structure. This eliminates tangling and damage to the wires attached to the data acquisition unit during testing.

Figure 10. Photograph during testing of an intelligent tire showing the use of the slip ring.

The signal from the internally mounted sensors is recorded to the data acquisition software. The signal is post-processed to extract any relevant information gained during testing. These signals are then compared with the forces and moments measured from the Kistler dynamometer hub to determine an appropriate signal processing algorithm. The ITL determines if the results can be correlated to the external measured properties of the tire for feasible implementation of an IT.

3.3 Experimental Results

This section presents the validation of the IT. This information illustrates the feasibility of implementing an IT and the ability to complete the testing in-house. This effectively puts the ITL on the forefront of IT testing and algorithm development. Using the empirical information gathered from the test trailer and IT will allow the ITL to develop new safety system algorithms for validation within a simulation environment. This data can also be implemented into hardware-in-the-loop systems and eventually become the standard for commercial vehicle safety system applications.

3.3.1 Intelligent Tire Force Measurement

The ITL has performed testing on several sensor configurations for an IT. For one test case, an accelerometer is mounted to the centerline of the inner lining of the tire, opposite the tread. A triaxial accelerometer is used, so it is able to return accelerations in the longitudinal, lateral and radial (outward) directions. To simplify the explanation, an easier test case and algorithm will be discussed. Utilizing the radial signal from the accelerometer, shown in Figure 11, valuable information can be obtained from the acceleration signal. The plot in the background shows an entire sample set, with the plot in the foreground showing an enlarged portion of the graph. The important information from this graph is the two sets of two peaks. Each pair of peaks has an increasing acceleration signal going up to the first peak, followed by an area of zero acceleration, a second peak with a decreasing acceleration, back down to low acceleration. Physically for the tire, the increasing acceleration signal leading to the first peak is the location where the tire begins to enter the contact patch, or the leading edge. The peak is where this point on the tire transfers from the entry section of the leading edge to the contact of the road surface. The area of zero acceleration between the two peaks is where the sensor is passing through the contact patch. This is to be expected since there will be zero, or small negative acceleration during this time period because the ground will be exerting an upward force on the tire, counteracting the outward radial acceleration experienced as the tire rotates. The second peak and area of declining acceleration is where the sensor exits the contact patch, or trailing edge. Each set of these peaks represents one rotation of the tire as the location where the sensor is mounted passes through the contact patch. From this data set, the portion of the time spent in the area of zero acceleration can be measured in relation to time. From the time spent in the contact patch, the length of the contact patch can be determined [35]. Using Equation 11, the contact patch length can be related to a multiplication factor for the tire under test, a, the diameter of the tire, d, and the ratio of the normal load to the vertical stiffness at a particular inflation pressure, ρ and yield the vertical load on the tire.

$$L = a \cdot 2d \cdot \sqrt{\left(\frac{\tau}{d}\right) - \left(\frac{\tau}{d}\right)^2} \qquad \text{Equation 11}$$

For Equation 11, the multiplication factor is known as a measured value to be $a = 0.65$. Knowing the patch length, the Equation is solved for σ, where

$$\tau = \frac{F_z}{K} \qquad \text{Equation 12}$$

K is the vertical stiffness, measured to be 1600 pounds per inch for this particular tire. The resulting vertical load is then presented in Equation 13.

$$F_z = \tau \cdot K \qquad \text{Equation 13}$$

Calculating the force using the above Equation and averaging the vertical load over several rotations of the tire shows nearly an exact match to the vertical load measured from the Kistler dynamometer force hub.

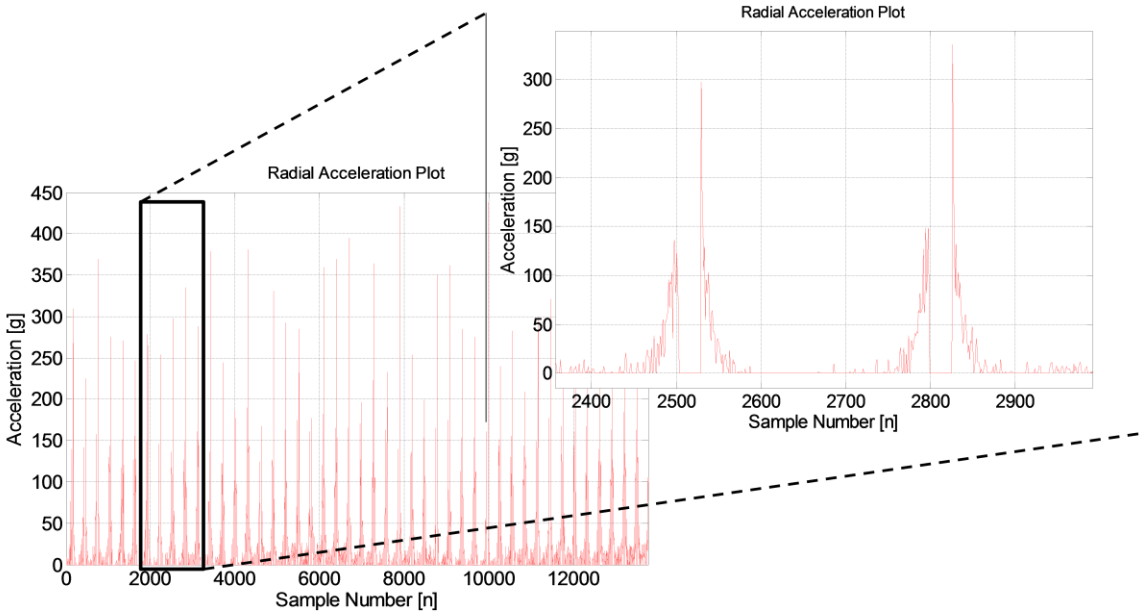

Figure 11. Radial acceleration signal collected during testing of the IT.

The ITL has developed more precise and representative algorithms which utilize additional information in order to increase the accuracy of the described method. Another example of information that can be extracted from the radial acceleration signal

utilizes the power spectral density (PSD). The PSD describes how the signal energy of the time series is distributed with frequency. The plot shown in Figure 12 converts the acceleration signal into the density spectrum and compares the power signal for testing completed on wet and dry surfaces, on the same testing surface. The plot shows a clear difference in signal power between the two surface conditions. This information can be used to help classify surface condition to estimate values or ranges for available surface friction.

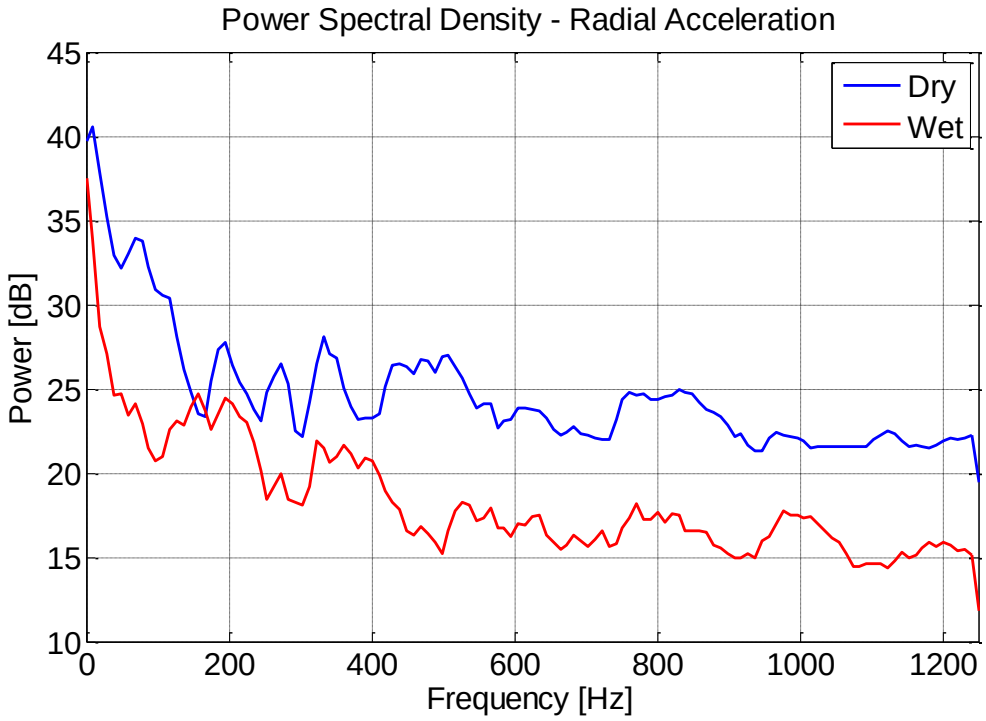

Figure 12. Plot of the PSD of the radial acceleration for dry and wet surfaces.

The ITL has developed more precise algorithms which utilize additional information in order to increase the accuracy of the described methods. This example has been simplified for explanation purposes and will not be detailed any further since it is beyond the scope of work for this project. This information is provided solely to present the feasibility of implementation of an IT.

Future work to improve IT design is to continue exploring different types of sensors and the potential benefit each type of sensor can contribute. The current data processing algorithms return forces that closely correlate to the forces measured using the

TTT. However, current processing requires the averaging of this information over a short period of time, ranging up to several seconds. The data processing techniques are under continual improvement in order to help provide tire force and moment information at the contact patch in real-time. Issues including sensor cost and data transmission from the tire to vehicle systems will prevent an IT from quickly being introduced into the commercial industry. For the near future, the IT will be restricted to laboratory use.

3.4 Conclusions

This Chapter presented the capabilities of the IT. Two simple examples were presented to exhibit the potential of implementing an IT. The information presented shows with good confidence that the implementation of an IT is feasible, if the prohibitive sensor costs can be reduced. The TTT is able to provide tire force and moment information within 10% error from current industry standard testing procedures using a flat track [33]. The force data collected using sensors in an IT correlates closely with the force data collected from the TTT. This presents the capability to measure the forces and moments at the contact patch using an intelligent tire. The next phase of this process is to develop vehicle control algorithms using the information at the contact patch to determine what improvements can be made to vehicle safety systems. In order to develop safety control algorithms, a detailed vehicle simulation model is required to gauge the improvement over currently available systems. This simulation is presented in Chapter 4.

4 Vehicle Simulation and ABS Control

4.1 Introduction

Simulation is a powerful tool used to analyze and design complex systems. It enables the testing of many hypotheses in a virtual environment before performing physical testing. Simulations result in significant cost savings throughout the design process, as well as reducing the time it takes to obtain performance results. Simulation models can describe real-world systems and can be used to test design parameters in a quick, repeatable fashion to produce objective results. Modeling for simulation is generally started with a simple approximation of the system and is refined as necessary to improve the accuracy of the system. Simulation provides a method of testing design processes in order to evaluate ideas, explore the effects of modifications, identify inefficiencies and communicate the integrity and feasibility of design plans. This Chapter explains the operation of anti-lock braking system control and introduces the vehicle simulation used as a baseline comparison for an alternative ABS control algorithm.

4.2 Longitudinal Slip Based ABS Control

The current industry standard for ABS is based on longitudinal slip ratio control. This method of control is utilized since slip ratio can be easily measured and approximated from available on-board vehicle sensors. It is also fairly simple to control the brake application and release depending on the values of slip ratio, vehicle speed and wheel angular acceleration. A basic block diagram of a longitudinal slip based controller is shown in Figure 13. Beginning with the driver block in the lower left hand corner, the driver inputs a demanded brake torque. Based on the driver demand brake torque, a desired slip calculation is determined. This desired longitudinal slip is the value that corresponds to the maximum braking force available, if full braking is applied. This value is determined by the control designer. The slip value chosen is generally less than the optimal slip value where maximum braking force is achieved. This conservative practice is followed to ensure that the tire operates within the stable region and does not

cross into the frictional region of the tire, as presented in Figure 2. The driver demand brake torque and the desired slip ratio are input into a control logic box, which here represents the ABS controller. The additional input to this system is the actual measured longitudinal slip, based on the vehicle and wheel dynamics. The actual slip ratio is compared to the desired slip ratio. The control logic is designed to minimize the difference between the desired slip and actual slip, with the goal to achieve a difference of zero. If the desired slip ratio is greater than the actual slip ratio, the brakes will be applied to the wheel. If the desired slip ratio is less than the actual slip ratio, the brakes will be released. The application and release of the brakes in quick succession is responsible for ABS control. Typical application frequency of ABS control is 10-15 Hz. The ABS controller then calculates and outputs the desired braking torque, depending on the action required to achieve the desired slip ratio.

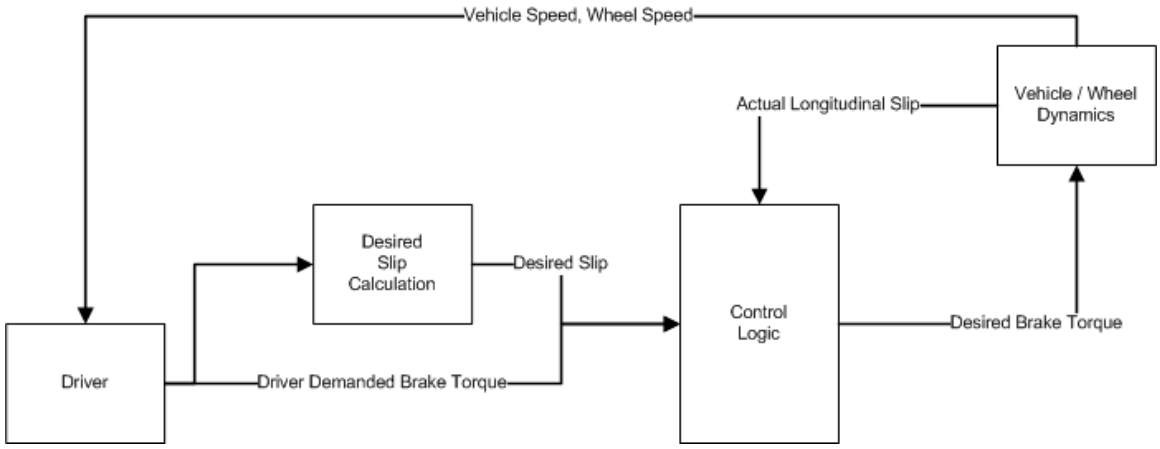

Figure 13. Block diagram representing ABS longitudinal slip based control method.

While the longitudinal slip ratio based ABS control is robust for widespread application, there remain areas for improvement. Current ABS control specifies a single slip ratio value that is used for all ABS application, regardless of surface type and condition. Figure 14 shows the surface friction coefficient versus longitudinal wheel slip for different surface types. Different surface conditions experience their maximum available adhesion coefficient at varying slip ratios. The maximum values of adhesion coefficient also represents the point of maximum force, refer to Equation 4 and Equation 5. The points where the maximum value occurs are highlighted by red points. The points are connected by a dashed line to show how the slip ratio value changes for different

surface conditions. As seen in the Figure, the point where maximum braking force is generated varies as the surface condition changes. Being able to adjust the longitudinal slip ratio using values measured directly from the tire allows for optimization of ABS control regardless of surface type or condition.

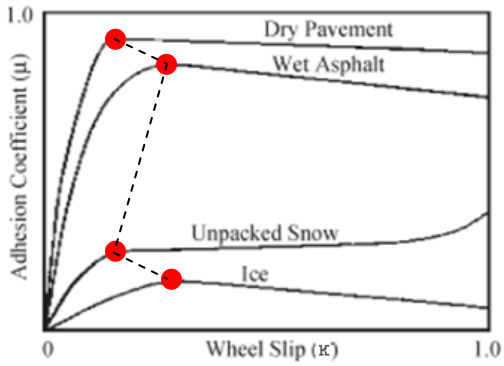

Figure 14. Surface friction coefficient versus longitudinal slip ratio for varying surface types.

It is desirable for ABS controllers to maintain the braking torque to the wheels as close to the determined slip ratio value for two reasons. These reasons are highlighted in Figure 15, which show both the longitudinal force, represented by the solid line and lateral force, represented by the dotted line versus longitudinal slip ratio. If the slip ratio can be held within a specified range encompassing the location where maximum braking force is achieved, the stopping distance is minimized. From the graph, it can also be seen that within the highlighted ABS slip tolerance, the lateral or cornering force is relatively high at slip ratios of less than 0.2. A good ABS controller minimizes braking distance while maintaining lateral control of the vehicle. In vehicles not equipped with ABS, if the wheels lock up, all steering control is lost, creating an even more hazardous situation. For example, for the unpacked snow condition in Figure 14, the maximum adhesion coefficient is reached when the wheels are locked; however, at this value no lateral control of the vehicle is possible, thus eliminating driver directional control of the vehicle. In this case, it would be preferable to have a greater stopping distance so that the driver can maintain control of the vehicle. For a typical passenger car and tire pairing, the slip ratio that results in the maximum available braking force is between 0.1 and 0.2. Again, the exact slip ratio value corresponding to maximum braking force varies for different surface conditions. While these systems are quite effective at controlling the

brake torque to prevent wheel lock up and reducing stopping distance, this method of control requires extensive on-vehicle testing in order to tune the threshold parameters.

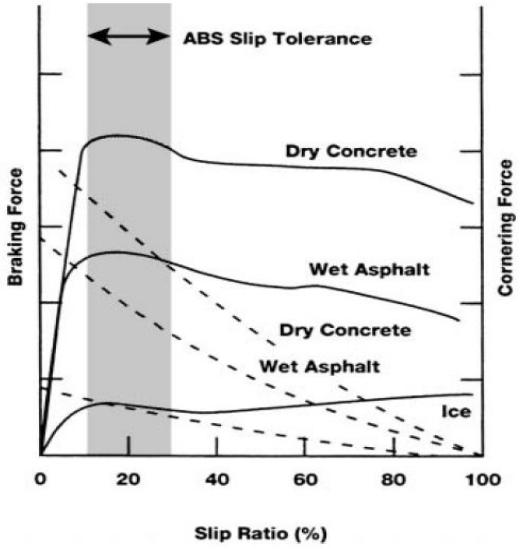

Figure 15. Longitudinal force (solid line) and lateral force (dotted line) versus longitudinal slip ratio.

Implementation of an intelligent tire would allow for the direct, real-time acquisition of the maximum longitudinal force, or braking force. The exact longitudinal slip ratio can be calculated from the measured maximum braking force. Using force information from an IT, a more accurate longitudinal slip based controller can be designed for use in vehicle safety systems.

4.3 Full Vehicle Simulation

To model vehicle safety systems, it is important to have a full vehicle representation that also incorporates the system controller. For this purpose, the ITL developed a full, four wheeled vehicle model along with an ABS controller using Matlab and Simulink. Simulink was chosen as the modeling program due to its relative simplicity for modeling large systems, ability to quickly change parameters to output results and its availability within the laboratory. The simulation consists of a driver model, tire model, vehicle model and ABS controller. Figure 16 shows a block diagram of the overall system. These models and their relating variables will be discussed in detail in the following sections. The more accurate the simulation, the more precise the

control algorithms will be for development and implementation into vehicles. The vehicle used for the basis of this simulation is a small size sport utility vehicle. After the development of the simulation, the results were compared to that of the host vehicle. The simulation and vehicle parameters were tuned so that the simulation very closely matches the real-world vehicle performance. The simulation provides an accurate representation of the actual vehicle and safety control system.

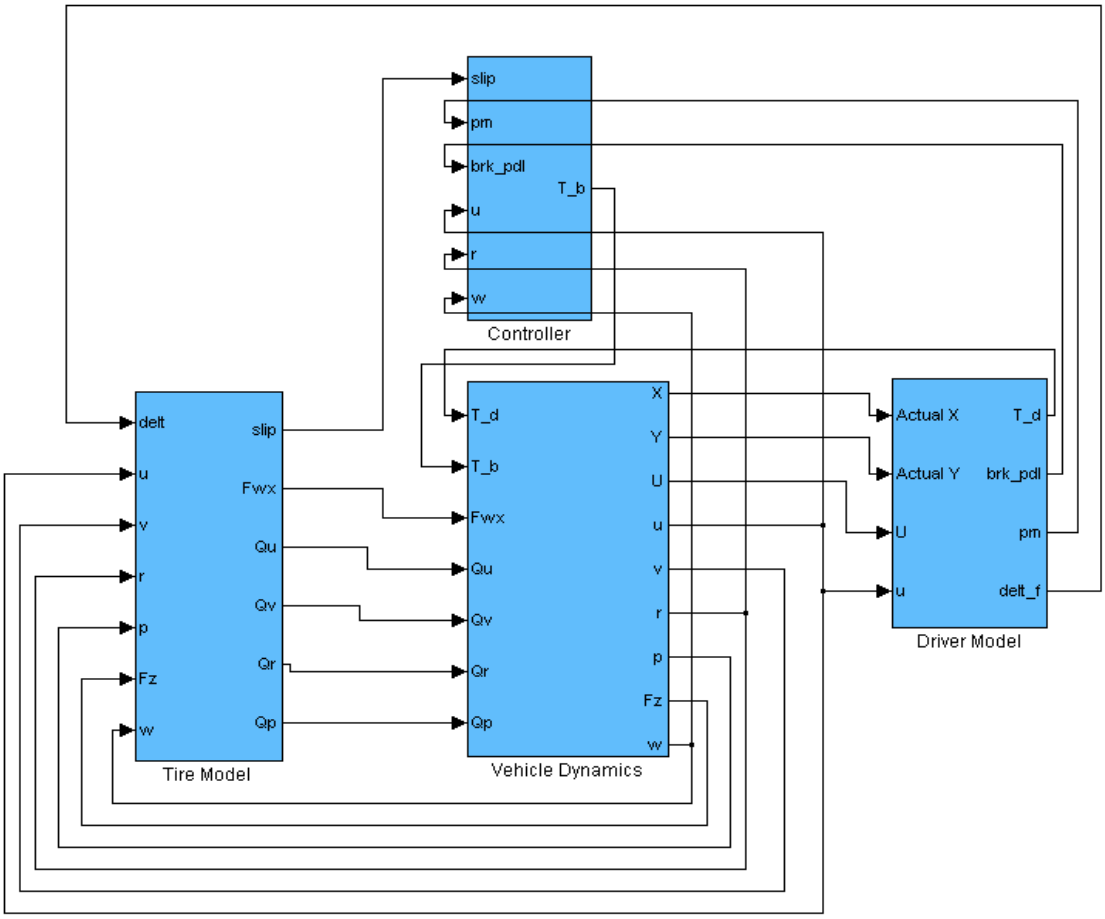

Figure 16. Comprehensive vehicle and controller simulation model.

4.3.1 Driver Model

The driver model used is based on a McRuer style driving model. The driver model computes and simulates driver behavior. The McRuer style model was chosen for its capabilities and relatively simple design. This model can be programmed to carry out any desired maneuver, ranging from straight line emergency braking to double-lane

change, J-turn and Fishhook stability maneuvers. For the ABS simulation, the driver model is set to perform straight line braking, using only small steer control to keep the vehicle traveling straight due to any yaw moment caused from weight transfer during braking. The McRuer model provides driver and mechanical delays to the system, accounting for driver reaction time and brake pedal application. These delays are based on experimental data on average reaction time and are represented using a transfer function [36]. Figure 17 shows a diagram of the driver model, highlighting the inputs and outputs of the system. The inputs of the system include the longitudinal and lateral position of the vehicle within the testing plane, represented by $Actual\ X$ and $Actual\ Y$, respectively. U is the longitudinal velocity, corrected for yaw velocity of the vehicle and u is the pure longitudinal velocity of the vehicle. The difference between U and u, is used to determine the yaw angle. For straight line braking, the yaw angle should ideally be zero, so the difference should be kept to a minimum. If the vehicle begins to yaw, the driver model will correct the steering angle to ensure the vehicle is traveling straight. The outputs of the driver system are the desired braking torque, T_d, the brake command from the driver, brk_pdl, brake pressure actuation, pm and steering correction command, $delt_f$. The brake command gives an on or off condition to determine if the brake pedal is being actuated by the driver. The demand braking torque is the torque required by the driver to slow the vehicle to the desired speed, in this case brake torque equal to emergency braking is necessary to come to a complete stop. The brake pressure actuation is a brake system delay that accounts for the pressure build-up in the brake master cylinder after the brake pedal is applied. The steering correction command ensures the vehicle is kept steering straight.

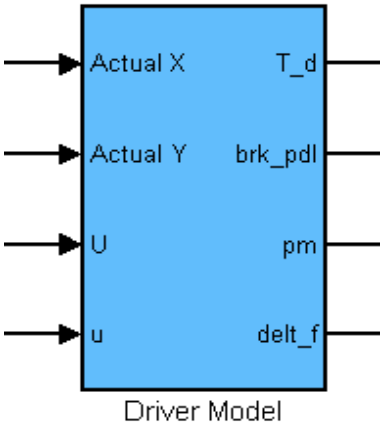

Figure 17. Driver model showing the inputs and outputs of the system.

More current driver models exist that take many more prediction and correction factors into account, but for the scope of designing an ABS controller, the McRuer style driving model is more than adequate to define the braking actuation, steer control and driver delays.

4.3.2 Vehicle Dynamics

The vehicle dynamics model in the simulation, shown in Figure 18, is responsible for calculating the vehicle motion based on the estimated tire parameters and their reaction to the driver model steering and braking input. The vehicle dynamics model is a four wheeled model that accounts for the load transfer, pitch and roll of the vehicle as well as the suspension and roll stiffnesses. The system inputs include T_d, which is the demand torque from the driver. T_b is the calculated necessary braking torque required from the ABS controller. The ABS braking torque is designed to apply and release the brakes rapidly to prevent the wheel from locking up under emergency braking. Fw_x is the calculated maximum longitudinal force available at each tire. This force is estimated in the tire parameters model. Q_u, Q_v, Q_r and Q_p are the combined values for longitudinal, lateral, yaw and damper velocities at all four tires. These values use a single input to represent the velocities at each individual tire to calculate the pitching and rolling moments for the vehicle. The outputs of the vehicle dynamics model are the longitudinal position, X, and lateral position, Y, of the vehicle within the plane. U is the longitudinal

motion corrected with yaw angle and u is the pure longitudinal velocity. These position and velocity terms are fed into the driver model to determine the subsequent driver command. v, r and p are the lateral velocity, yaw velocity and damper velocity of the entire vehicle. F_z is the calculated vertical load at each tire based on the longitudinal load transfer and w is the individual wheel rotational velocities. The vehicle velocities, vertical load and wheel angular velocities are fed into the tire parameters model to calculate and update the individual wheel velocities and maximum longitudinal force which are input back into the vehicle dynamics block.

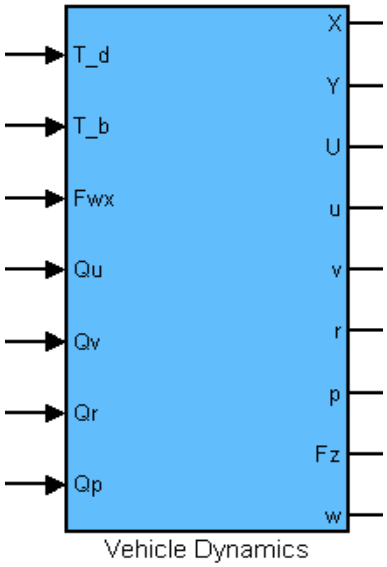

Figure 18. Vehicle dynamics model showing the inputs and outputs of the system.

The vehicle dynamics block uses basic dynamic equations to determine the load transfer about the center of gravity based on the velocities at each wheel along with known, measured values about the car. These parameters include mass, wheelbase, track width, center of gravity location and all corresponding pitch and roll stiffnesses. The values for all of these parameters can be found in Appendix B.

4.3.3 Tire Parameter Estimation

The tire parameter model is a combination of the Pacejka's Magic Formula and the LuGre tire model. The Magic Formula is a semi-empirical series of equations characterized by up to 20 coefficients that can produce a mathematical formula best fit

line for the forces and moments between experimental data and a tire model. These characteristics are obtained through physical testing of the tire and characterize the properties of the tire. For the simulation, the ITL uses a tire with known Magic Formula coefficients and inputs these values into the model. Using these coefficients along with the wheel angular speed, vertical load and velocities calculated from the vehicle dynamics model, the forces and moments of the tire are calculated. The Magic Formula represents the steady-state properties of the tire. The LuGre model is a dynamic tire friction model that can accurately describe the transient characteristics of the tire. Due to nonlinearities, the LuGre model is not capable of calculating the tire parameters [37]. Combining the use of these two tire models together allow for the proper representation of the tire in both transient and steady-state conditions.

The inputs and outputs of the system are shown in Figure 19. All of the velocity and force inputs and outputs for the system have been previously defined. The input $delt$ is the steering control designated from the driver model. For the ABS simulation, the steering input is minimal, only inputting slight steer angles to keep the vehicle heading straight. The output $slip$ is the combined calculated slip for the longitudinal and lateral directions on the tire. The tire parameters model acts as an updating feedback controller with the vehicle dynamics model. During heavy braking, the velocity and load transfer of the vehicle affects the vehicle dynamics. The new velocity and load information from the vehicle dynamics model is then fed into the tire parameters model. The tire parameters are updated from the results of the latest vehicle dynamics model. The wheel velocities and forces are then input back into the vehicle dynamics model, continuing the cycle. These cycles are carried out at small incremental values in order to ensure the consistency of the model.

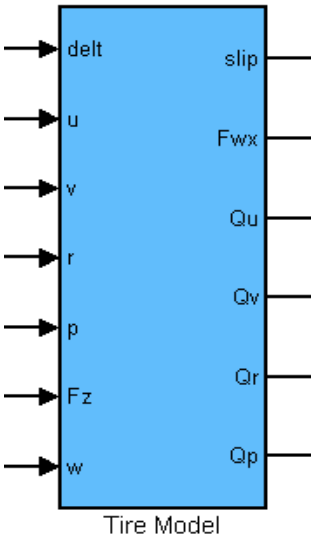

Figure 19. Tire parameters model showing the inputs and outputs of the system.

4.3.4 ABS Control

The ABS control model is an integral part of this simulation. This model is responsible for calculating the required brake torque necessary to decelerate the vehicle as quickly as possible, while not allowing the wheels to lock up. Figure 20 shows the ABS control model with the inputs and outputs. The inputs to the system are $slip$, the combined longitudinal and lateral slip value calculated from the tire parameters block. The brake pedal actuation and brake pressure delay term are inputted from the driver model, which controls the braking action. Variables u, r and w are the longitudinal and yaw velocity of the vehicle and wheel angular velocity at each wheel from the vehicle dynamics model. The sole output of the system is the braking torque required to decelerate the vehicle without locking the wheels.

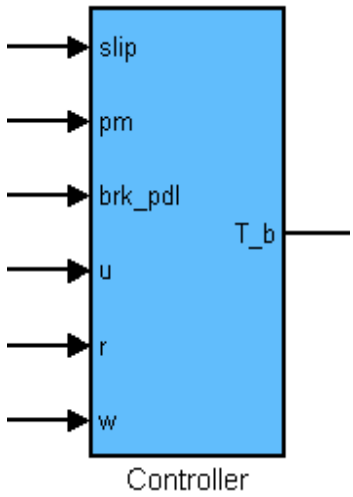

Figure 20. ABS control model showing the inputs and outputs of the system.

Within the ABS model is the mechanical control of the brake, which determines the state of the brake, as well as a fully developed pressure model which calculates the required brake line pressure to achieve the desired braking torque. The brake state is determined using a state-flow decision process. Depending on the internally calculated values of longitudinal slip ratio, vehicle velocity and wheel angular acceleration, threshold values are established to determine if the brakes need to be applied, held or released. For example, if the calculated wheel acceleration is greater than a predetermined value and the measured slip ratio also exceeds a determined value, the brake is applying too much force, which will result in wheel lock up, so the brake is released. Similarly, if the wheel angular acceleration and slip ratio go below predetermined values, the brake is not providing the maximum amount of braking torque, so the brake is applied to slow the vehicle. These upper and lower threshold values are tuned for each vehicle and values are chosen that predict wheel lock up before it occurs. Currently, tuning these values requires extensive on-vehicle testing. With the implementation into an accurate simulation, these threshold values can be tuned near their optimal value, greatly reducing the amount of on-vehicle testing that needs to be completed.

4.4 Results

There are several parameters that need to be studied on the ABS controller in order to quantify system performance. One of the first parameters to study is the overall stopping distance of the vehicle. Other values that quantify ABS performance are the control of the longitudinal slip ratio over time as well as the individual wheel angular acceleration over time. Each of these parameters will be presented to show the system performance for both a high-mu surface, representative of dry asphalt and a low-mu surface, representative of an icy surface.

For the high-mu surface, a friction coefficient of 0.8 is used. The initial velocity of the vehicle is 52 *mph* (83 *kph*). Full brakes are applied at 0.15 seconds. Figure 21 shows the slip ratio response over time for the right front tire. Only one tire will be used for explanation and clarification of the plots. All wheels experience similar traits. From the plot, it can be seen that the slip ratio falls within a tolerance of between 0.05 and 0.2. It is of use to note that longitudinal slip based controllers have a cut-off speed generally around 2 *mph* (3.2 *kph*). This is because the vehicle speed is used to calculate the slip ratio. Recall from Equation 1, the vehicle speed component is located in the denominator. As the vehicle speed approaches zero, the calculated longitudinal slip will approach infinity, corresponding to a slip ratio of one, where the wheel is fully locked. Therefore, a cut-off speed is set and once this speed is reached, ABS is no longer used, leaving the remainder of the braking maneuver to the skill of the driver.

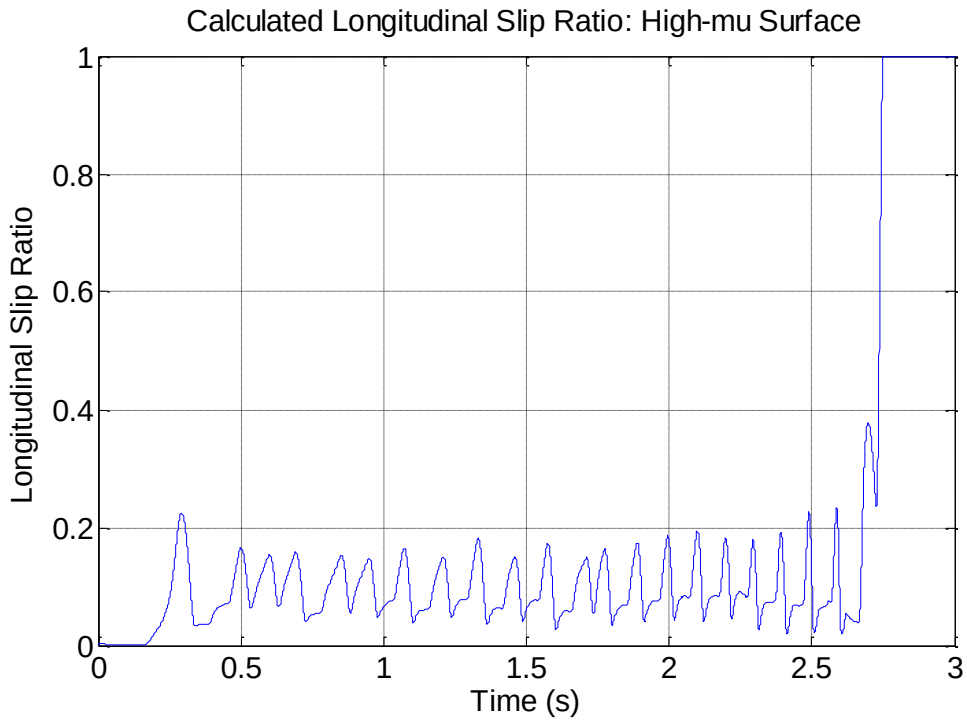

Figure 21. Longitudinal slip versus time response for ABS braking on a high-mu surface.

Another way to show the performance of an ABS controller is to plot the longitudinal braking force versus slip ratio for the entire duration of the braking maneuver. The plot shown in Figure 22 pictures the longitudinal force at the front right tire throughout the braking maneuver. The ABS control logic described in the previous section controls the slip ratio to stay within predetermined bounds. The longitudinal force increases as the brakes are applied at the beginning of the maneuver. Once the slip ratio and wheel acceleration exceed the determined threshold values, the brake is released to reduce brake torque. When the slip ratio and wheel acceleration fall below the chosen design values, the brake is applied to increase the slip ratio and brake torque. This plot shows the longitudinal force variation as the controller maintains the longitudinal slip value by engaging and disengaging the brake throughout the braking maneuver. The longitudinal force calculated at the wheel varies between 1500 *lb* and 2500 *lb* (6.7 *kN* and 11.1 *kN*) throughout the maneuver.

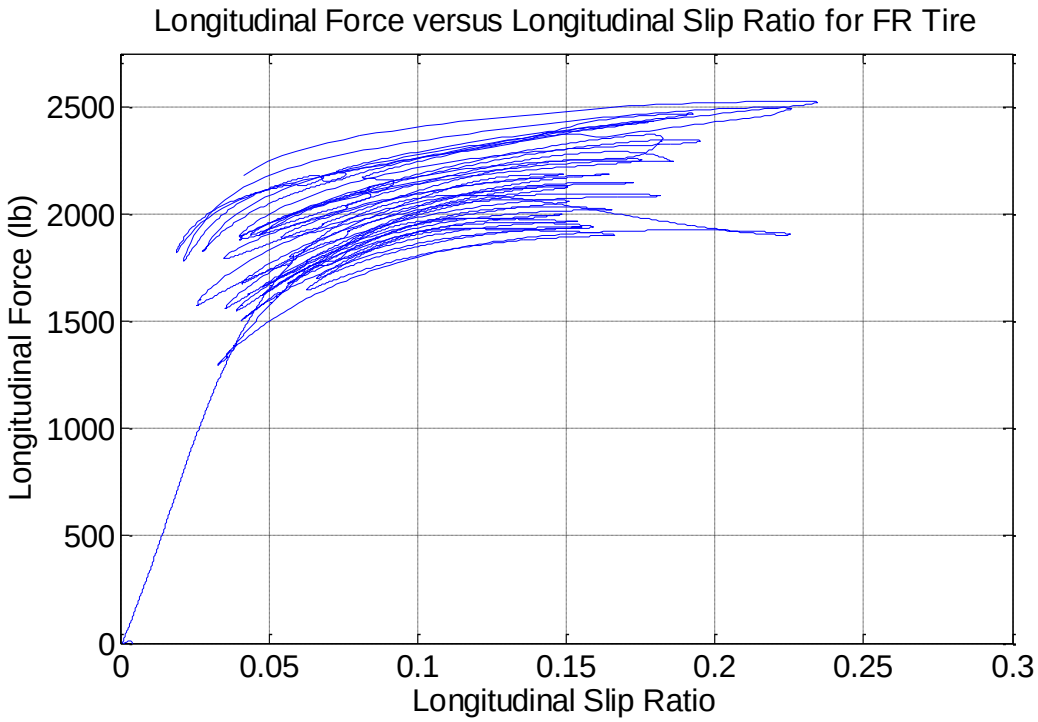

Figure 22. Longitudinal force versus longitudinal slip ratio for the front right tire during ABS braking maneuver for high-mu surface.

Plotting translational wheel speed against the maximum deceleration speed before the wheel begins to lock for the braking maneuver is shown in Figure 23. Again, only the value for the front right tire is shown for clarification. The blue line represents the calculated maximum deceleration of the wheel just before wheel lock occurs. The red line represents the wheel translational speed, which is the product of wheel rotational velocity and the radius of the tire. The wheel speed increases and decreases slightly due to the application and release of the brake from the ABS controller. The closer the wheel speed is to the maximum available deceleration velocity, the quicker the vehicle will come to a stop.

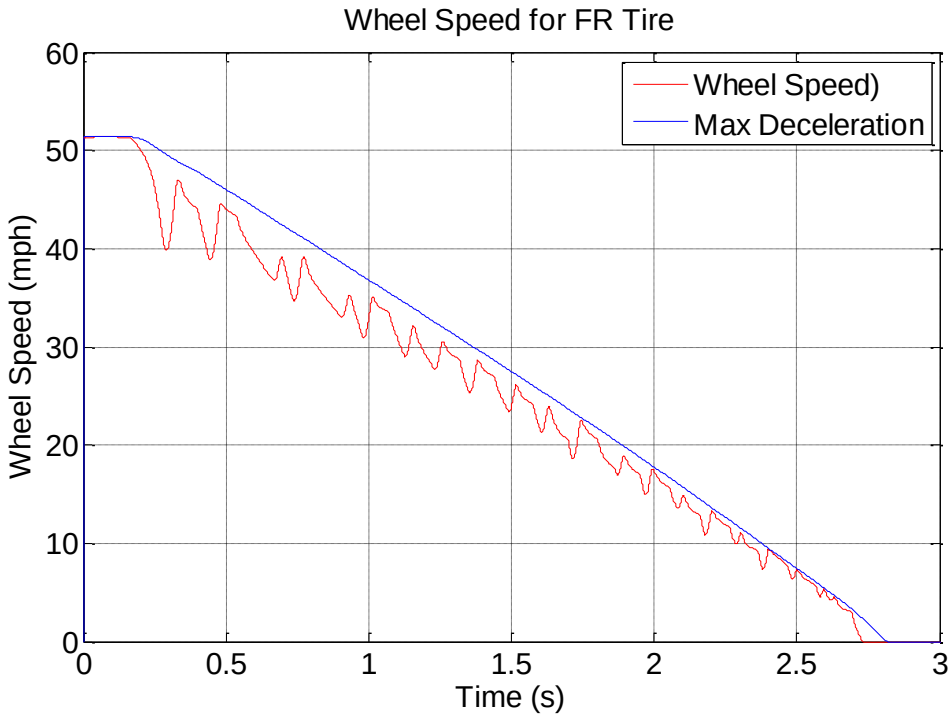

Figure 23. Wheel speed plotted alongside maximum wheel deceleration against time throughout ABS braking maneuver for high-mu surface.

Summarizing the performance of the ABS simulation for a high-mu surface shows that it takes 2.8 seconds for the vehicle to come to rest from an initial velocity of 52 *mph*. The distance required to stop is 118 *ft* (36 *m*). For the low-mu surface, a friction coefficient of 0.2 is used. Again, the initial velocity of the vehicle is 52 *mph* (83 *kph*). Full braking is applied at 0.15 seconds. Figure 24 shows the slip ratio response over time. From this plot it can be seen that the slip ratio tolerance has increased significantly over the high-mu surface, falling within a range from 0.02 to 0.35. The variation of longitudinal slip ratio control has increased significantly over the range from the high-mu surface. The cut-off speed of 2 *mph* (3.2 *kph*) is maintained, resulting in the slip ratio increasing to one as this cut-off speed is achieved.

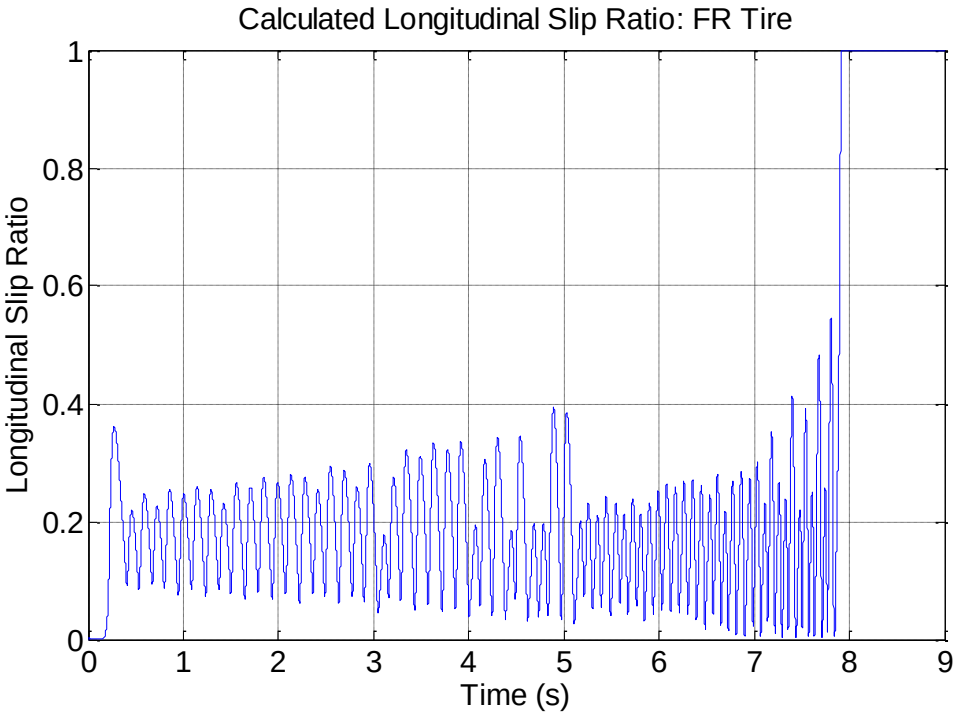

Figure 24. Longitudinal slip versus time response for ABS braking on a low-mu surface.

Figure 24 presents a plot of the longitudinal force as a function of longitudinal slip ratio for a low-mu surface for the ABS braking maneuver. The control of slip ratio on a low-mu surface is not as linear as it was for a high-mu surface. The ABS controller utilizes the same control methods and threshold values, but due to the large reduction in friction coefficient between the tire and road surface, the same control method is not as effective. The variation in slip ratio values is greater, leading to a larger variation in braking force and even allowing the wheel to enter the frictional or unstable zone of the tire. Also, the longitudinal force values are much less than that of a high-mu surface, ranging from 400 *lb* to 650 *lb* (1.8 *kN* to 2.9 *kN*), due to the lower friction coefficient. Recall from Equation 4 that the maximum longitudinal force is a function of the friction coefficient and normal load on the wheel. Due to the longer braking time on the low-mu surface, the ABS controller is engaged over a longer time period, which explains why the plot appears more crowded.

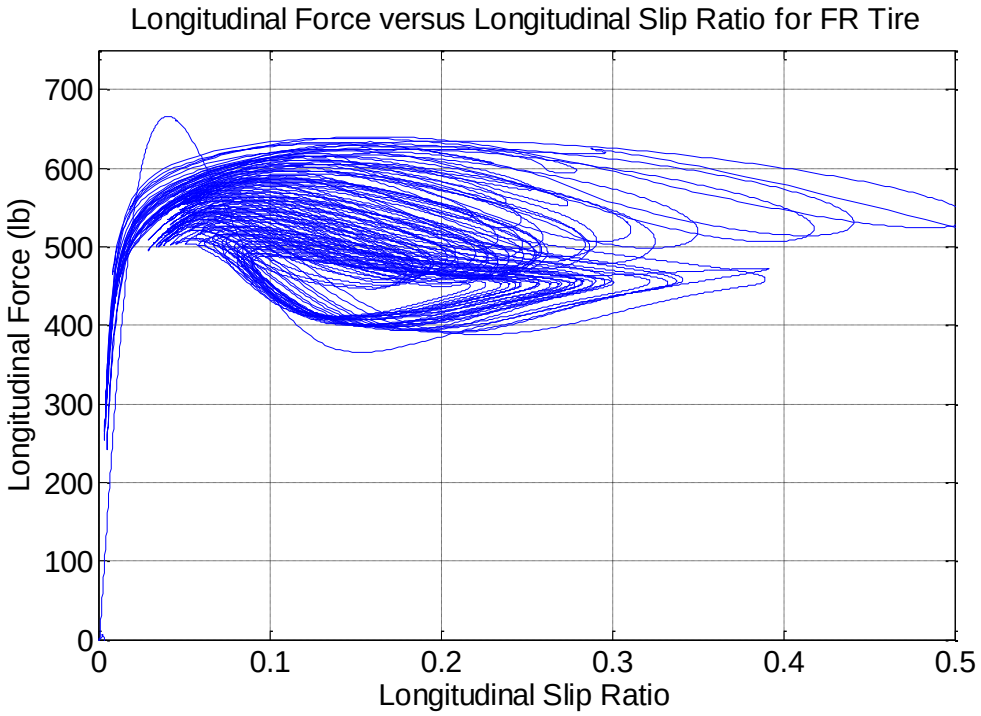

Figure 25. Longitudinal force versus longitudinal slip ratio for the front right tire during ABS braking maneuver for low-mu surface.

The translational wheel speed plotted against time with the maximum deceleration speed is shown in Figure 26. This responds in the same way as described earlier, only acting over a longer braking period. Due to the larger variations in slip ratio on the low-mu surface, the braking periods of brake application and release are longer than for the high-mu simulation. These fluctuations result in larger changes in velocity for the individual wheel speeds, which bring the average wheel deceleration further away from the calculated maximum wheel deceleration velocity, resulting in a longer braking distance.

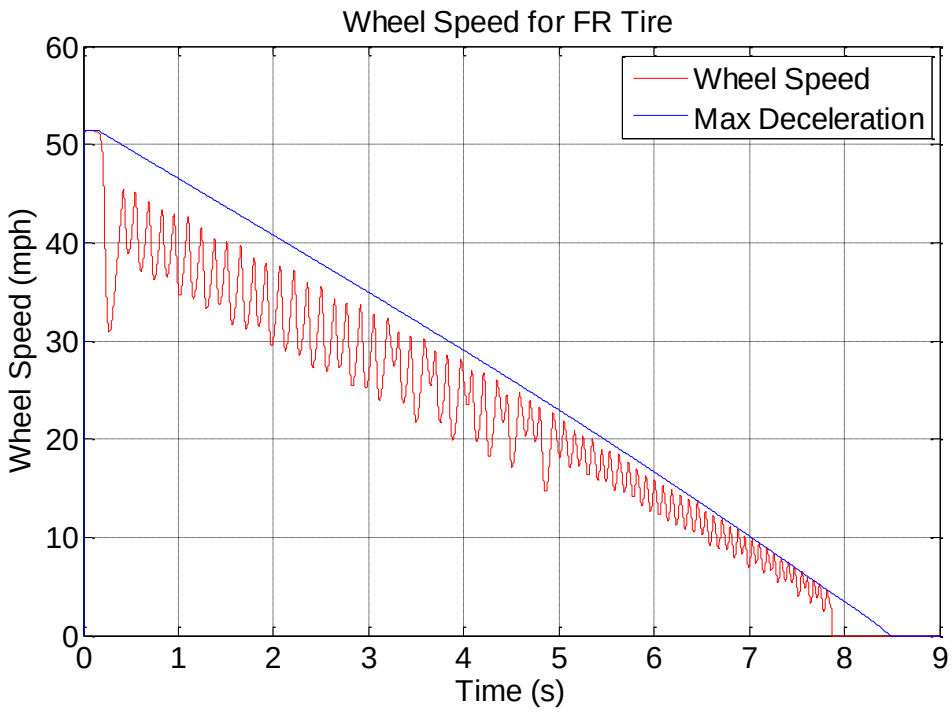

Figure 26. Wheel speed plotted alongside maximum wheel deceleration against time throughout ABS braking maneuver for low-mu surface.

Summarizing the performance of the ABS simulation for the low-mu surface shows that it takes the vehicle 8.5 seconds to come to a rest from an initial velocity of 52 mph. The distance required to stop is 339 ft (103 m).

4.5 Discussion

The vehicle simulation presented in this Chapter is representative of a small sport utility vehicle. The ABS control model used for this simulation is an actual ABS control algorithm and decision process used in commercial vehicles. This simulation provides an accurate representation of vehicle and ABS performance and both of the prescribed scenarios (emergency braking on high- and low-mu surfaces) have been validated with real-world vehicle testing. This ABS control method provides the ITL with the current baseline ABS processes in order to develop a more accurate control method.

In order to improve on the current ABS control method there are two main processes to improve. The most basic and important concept that will improve a longitudinal slip based ABS control is to minimize the longitudinal slip threshold about

which the controller operates. Ideally, this slip range will be as small as possible and be located at the longitudinal slip that corresponds to the maximum braking force. Figure 27 shows the longitudinal force versus slip on a high-mu surface for the front right tire. Using the high-mu simulation as an example, the maximum longitudinal force occurs at a longitudinal slip ratio value of 0.1415. This value is represented by the solid red line. Longitudinal slip values exceeding 0.1415 begin to experience a reduction in longitudinal force due to the tire entering the unstable frictional area. Values below this line do not exploit the maximum braking potential available from the tire. The two dotted red lines on either side of the maximum value represent close to ideal values for the upper and lower limits of slip. If the values of longitudinal slip can be kept within these boundaries, this would result in a shorter stopping distance due to the increased accuracy of the ABS controller. The ideal controller will maintain the slip ratio at the maximum longitudinal force point with no variation.

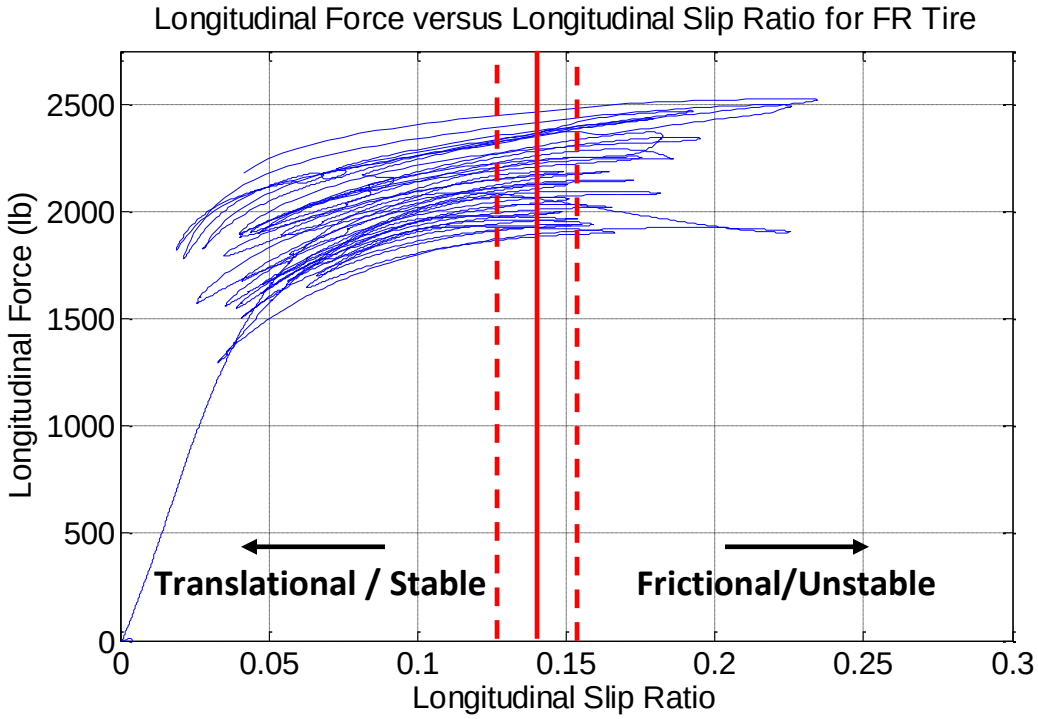

Figure 27. Longitudinal force versus longitudinal slip ratio highlighting ideal ABS components.

Suggested methods to improve the ABS controller so that the correct longitudinal slip value is chosen is to directly measure the longitudinal force from the tire contact patch using an IT. The ideal longitudinal slip ratio can be correlated to the point where

the maximum longitudinal force is measured. This value of slip can be accurately determined for any surface condition from measuring the longitudinal force.

4.6 Conclusions

This Chapter introduced the full vehicle simulation and the longitudinal slip control method employed in commercial ABS. The simulation used by the ITL is representative of a small sport utility vehicle and has been compared and validated by physical testing of the vehicle. The current performance of the commercial ABS system is presented for high-mu and low-mu test cases. Potential methods of improvement to ABS are provided. The next phase of this project is to complete a threshold sensitivity analysis on the current ABS simulation to determine which gain values and prediction parameters most affect the performance of the ABS system. The sensitivity analysis will allow the study of each parameter value that is currently available to the ABS system. The tuning of these variables is explored in order to determine the upper limit of performance of the longitudinal slip ABS algorithm based on the systems currently available to commercial vehicles.

5 ABS Threshold Sensitivity Analysis

5.1 Introduction

Sensitivity analysis is a technique for systematically changing parameters in a model to determine the effects of such changes. This type of analysis is used to determine how sensitive the model is to changes in the value of parameters in the structure of the model. For the ABS model, a parameter sensitivity model is followed, which is performed as a series of tests in which the user specifies different parameter values to see how a change in these values causes a change in the dynamic behavior of the vehicle. Comparing how the model behavior changes with a variation of the parameter values is a useful tool in model evaluation. A sensitivity analysis is performed on the current longitudinal slip based ABS controller to determine the upper bound of system performance. The following sections explain the parameter sensitivity model used, the parameters tested, and the results of this sensitivity analysis on the ABS simulation of Chapter 4.

5.2 Sensitivity Analysis Parameters

In order to perform a parameter sensitivity analysis, the first task is to determine what parameters directly and indirectly affect the operation of the model under study. For the ABS model, the parameters that directly affect the operation are the prediction threshold values introduced in Chapter 4.3.4. These threshold values include longitudinal slip ratio, wheel angular acceleration, and vehicle speed. Values that indirectly affect the performance of ABS are several gain values that specify additional control over determining the correct brake state. Once these parameters are identified, each parameter value is independently tested to evaluate how the parameter affects the dynamic performance of the braking system. The parameters are then ranked into two groups, parameters that improve the overall system performance and parameters that decrease or do not affect ABS performance. The values that increase system performance are further tuned as a group to optimize system performance and determine the upper bound of ABS.

Expanding from Chapter 4.3.4, the goal of the ABS control algorithm is to maintain the vehicle longitudinal slip ratio value at a predetermined desired longitudinal slip ratio by controlling the braking torque provided to each wheel. For commercial ABS, there is a decision process that is responsible for determining the brake state – that is, if the brake needs to be applied to increase braking force, held constant to maintain braking force, or released to decrease the braking force. These brake states are determined by comparing the instantaneous values of longitudinal slip ratio, wheel angular acceleration and vehicle speed. Another parameter that directly affects the application and release speed of the brakes is the line brake pressure and the amount of time required to apply and release this pressure. The longitudinal slip ratio, wheel angular acceleration and vehicle longitudinal speed are each composed of an upper bound and lower bound value which control the longitudinal slip threshold range of the ABS. The prediction parameter threshold bounds for the original ABS simulation are given in Table 2. These ABS results using these parameter values were presented in Figure 21 through Figure 23.

Table 2. Prediction parameter threshold bounds for original ABS simulation.

Prediction Parameter	**Upper Bound**	**Lower Bound**
Vehicle Speed, u $[mph]$	52.5	2
Wheel Acceleration, $\dot{\Omega}$ $[\frac{m}{s^2}]$	2	0.5
Slip Ratio, κ	0.15	0.08
Pressure Ramp, pm	50	0

The vehicle speed parameter is upper-bounded by the initial velocity of the vehicle, for the example covered, the initial velocity was 52.5 *mph*. This value varies with the speed of the vehicle throughout the braking maneuver and is used to calculate the longitudinal slip ratio of the vehicle. The lower bound of vehicle speed is the cut-off speed of ABS. The pressure ramp value is a ramping function that defines how quickly pressure to the system can be applied through the brake lines. The two main parameters that are responsible for the decision making process of the brake state are the wheel angular acceleration and longitudinal slip ratio. These parameters are bounded such that the values predict and change the braking state just before the wheel will lock, and

similarly will reapply the brakes before the slip ratio reaches too low a value. The basic operation of the decision process is summarized in Table 3.

Table 3. Decision process responsible for brake state control.

	Apply Brakes	**Hold**	**Release Brakes**
Wheel Acceleration	≥ 2	$0.5 < \dot{\Omega} < 2$	≤ 0.5
Slip Ratio	≤ 0.08	$0.08 < \kappa < 0.15$	≥ 0.15

In order to determine the braking state, both the wheel angular acceleration and slip ratio decision parameters must be met simultaneously. That is, in order for ABS to apply the brakes, both the wheel acceleration and slip ratio must be outside the specified values in the "Apply Brakes" column. To release the brakes, both parameters must exceed the specified bound values. The braking force is adjustable within the holding state boundaries, until either a new brake state is determined or the vehicle falls below the cut-off speed. The braking pressure range is adjustable throughout the states based on the current parameter values. To explain how the braking pressure is determined within the threshold bounds, an example of a braking maneuver will be given. At the beginning of the braking maneuver, assume both the wheel acceleration and slip ratio are below their lower bounds. During emergency braking, the brakes are applied at full pressure in order to reach the desired slip ratio as quickly as possible. This action causes the slip ratio to increase and the wheel acceleration to decrease. Since these two parameters vary independently of one another, both values do not reach their release brake boundary limit at the same time. So, if one parameter exceeds the upper bound while the other condition is still within the holding state, the braking pressure applied to the wheel will be reduced slightly. This reduction in braking pressure is part of the "prediction" method. Once one parameter exceeds the release brake bounding value, the ABS control algorithm predicts that the second parameter will soon reach the release boundary value. This slight reduction in brake force is completed to reduce the overshoot of the system. For example, if the wheel acceleration reaches the release bound value of $0.5\ m/s^2$ while the slip ratio value is still within the bounds of the holding state, the braking pressure will decrease slightly in order to reduce the overshoot of the system when the slip ratio exceeds 0.15. Once the slip ratio reaches 0.15, the brake pressure will be completely

released, relieving the brake force to the wheel. The same prediction method is used to reapply the brakes once the wheel acceleration and slip ratio exceed the apply brake bound values. Once one parameter reaches the lower bound, a slight amount of brake pressure will be reapplied to the system, again to reduce overshoot from the system. These lower and upper bounds are tuned in order to maintain the longitudinal slip ratio within a desired range by predicting the tire performance.

There are several braking gains which indirectly affect ABS performance. These gains are inputs into the ABS decision process and are responsible for specifying the initial gains of the front and rear wheels, as well as the gains associated with releasing and holding the brakes.

5.3 Parameter Sensitivity Analysis Results

Now that the parameters affecting ABS performance have been identified, the next step is to perform the parameter sensitivity analysis. The sensitivity analysis consists of varying these parameters individually to determine how each parameter affects the braking performance during an emergency stopping maneuver. The parameters are broken down into direct and indirect groups for the study. A series of tests for each parameter was carried out, varying the gain values and threshold bounds independently. These values were chosen incrementally close to the original value and also with large variation from the original value to determine if the initially specified value was optimized for the current system, and to study how large changes to the parameter affected system performance. The following parameter sensitivity analysis is conducted on a high-mu surface.

5.3.1 Threshold Gains

The parameter sensitivity analysis summary for the ABS threshold gains are given in Table 4. The original initial value for the system is listed along with the maximum lower and upper range of values that were tested. Again, these values were tested incrementally between the given bounds, with each parameter tested independently. The overall result in braking distance is given where a positive value results in an increase in braking distance, a negative value corresponds to a decrease in braking distance and a

zero value shows parameter insensitivity to value change. The braking difference is highlighted to correspond to its effect on system performance.

Table 4. Threshold gain sensitivity analysis results summary.

Case	ABS Threshold Gain	Value	Lower Range	Upper Range	Chosen Value	Braking Difference
1	**a1_ini_f**	-15.68	-100	100	-100	0
2	**a1_ini_r**	-21.6	-100	100	-100	0
3	**Ak_f**	10.5	-100	100	100	0
4	**Ak_r**	9	-100	100	100	0
5	**a_hold**	-11	-100	100	-100	0.362
6	**a_hold**	-11	-100	100	20	6.262
	Positive Effect		Insensitive		Negative Effect	

Many of the threshold gain values were shown to be insensitive to value change, with the exception being the gain value for the holding parameter. Cases 1 and 2 in Table 4 represent the initial gains for braking for the front and rear wheels, respectively. Cases 3 and 4 are the secondary gains of the ABS system for controlling applied braking pressure as the parameters reach the release brake state. These values are primarily responsible for insuring stability of the braking pressure. Since the overall braking pressure of the system is so high relative to these values, their change, even to large inputs, is insensitive to the overall ABS performance. Cases 5 and 6 represent two separate tests for the holding parameter gain, each of which has a negative effect on braking distance. As the gain values remain close to the original value, the increase in braking distance is small, but as the values increase away from this parameter, the braking distance increases significantly. To show how varying these parameter values affects the braking dynamics, the longitudinal force versus longitudinal slip ratio plot and wheel speed plot for Case 6 are shown in Figure 28. As can be seen from the plots, the braking system performance is heavily degraded from the original performance shown in Figure 22 and Figure 23. The control of longitudinal slip ratio is not constantly maintained, which results in poor control over the braking torque provided to the wheel, resulting in poor wheel speed control. The results for Case 5 are close to the original system performance, with only slightly slower wheel speed response times, which result

in the longer stopping distance. The initially specified braking gains of the system are optimized for the current ABS algorithm.

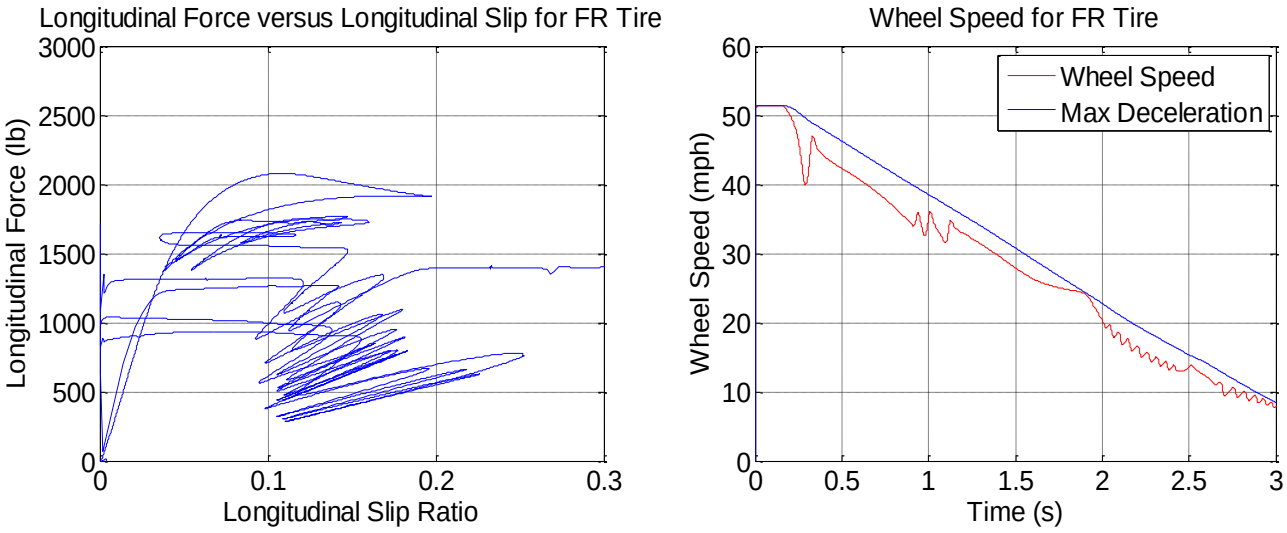

(a) (b)

Figure 28. Braking dynamics for Case 6 showing (a) the longitudinal force versus slip ratio for the FR tire and (b) the wheel speed of the FR tire.

5.3.2 Threshold Prediction Parameters

The threshold prediction parameters are evaluated using the same method as the threshold gains, with the only difference being that a range set must be specified instead of just a maximum and minimum value. A summary of the threshold parameters tested is given in Table 5. Two cases are presented for each prediction parameter to show that depending on the range set specified, the system dynamics change. The main effect of parameter changes to the system was a change in the longitudinal slip ratio over time, since this directly affects the resulting braking torque to the system and control of wheel speed. To compare the ABS performance of the threshold parameter analysis, the longitudinal slip ratio over time is compared to the slip ratio of the original simulation, with the major changes highlighted for each case.

Table 5. Threshold parameter sensitivity analysis results summary.

Case	Prediction Parameters	Original Upper Bound	Original Lower Bound	New Upper Bound	New Lower Bound	Braking Difference
7	**Vehicle Speed**	52.5	2	52.5	0.5	0.012
8	$u \quad [mph]$	52.5	2	52.5	5	-0.014
9	**Wheel Acceleration**	2	0.5	1	0.25	-0.057
10	$\dot{\Omega} \quad [\frac{m}{s^2}]$	2	0.5	3	1	-0.43
11	**Slip Ratio**	0.15	0.08	0.15	0.13	0.469
12	κ	0.15	0.08	0.2	0.15	-0.05
13	**Pressure Ramp**	50	0	10	0	3.72
14	pm	50	0	1000	0	-0.853
	Positive Effect		Insensitive		Negative Effect	

Each of these cases will be presented along with the braking system response and a short explanation of how ABS performance was affected. For the vehicle speed parameters presented in Cases 7 and 8, the changing of the lower bound of vehicle speed affects the cut-off velocity for ABS. For Case 7, shown in Figure 29. , the cut-off speed was lowered to 0.5 mph. Recall from Equation 1, that the vehicle velocity term used to calculate longitudinal slip ratio is located in the denominator of the equation. As this value approaches zero, the resulting slip ratio is driven to infinity. A slip ratio of infinity corresponds to wheel lock. The system will exhibit instability for small velocity values, which results in slightly greater stopping distances. The following plot for Case 7 shows the longitudinal slip ratio with respect to time in (a), with the original system performance shown in (b) for comparison. The area of the longitudinal slip curve affected by this change is the slip corresponding to low vehicle speeds, highlighted by the dashed red box. While reducing the cut-off velocity results in the wheel not locking during the braking maneuver, the tire is still pushed to operate in the frictional range, which would result in a large loss of driver steering control and maximum braking force. Operating at high slip ratio values does not offer much benefit over a fully locked wheel at these low vehicle speeds. It additionally creates an unstable input in the ABS controller, resulting in overall decreased performance at very low vehicle speeds.

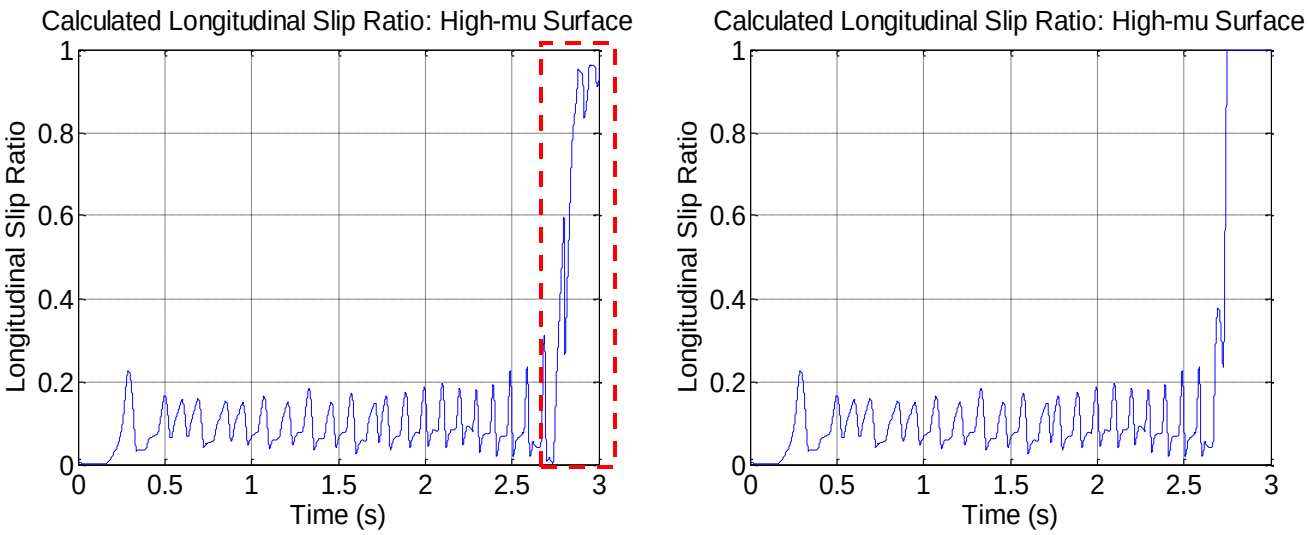

(a) (b)

Figure 29. Braking dynamics for Case 7 (a) showing the change in longitudinal slip ratio versus time for the FR tire and (b) the original longitudinal slip ratio versus time.

Figure 30 presents how raising the ABS cut-off speed from 2 mph to 5 mph affects the braking dynamics in Case 8. This lower bound velocity increase results in a slight decrease in braking distance by approximately 0.5 in (1.4 cm) from the original simulation. This higher cut-off speed results in wheel lock up at a 5 *mph* and provides almost negligible improvements to vehicle stopping distance. Since the wheel locks and beings to skid, this means that the driver loses steering control at a higher velocity than the original test case. So, while this parameter change results in a slightly shorter stopping distance, the loss of steering control to the driver is potentially not worth the trade-off in stopping distance. The earlier effect of wheel lock by increasing the cut-off velocity can be seen in Figure 30 (a), highlighted by the dashed box.

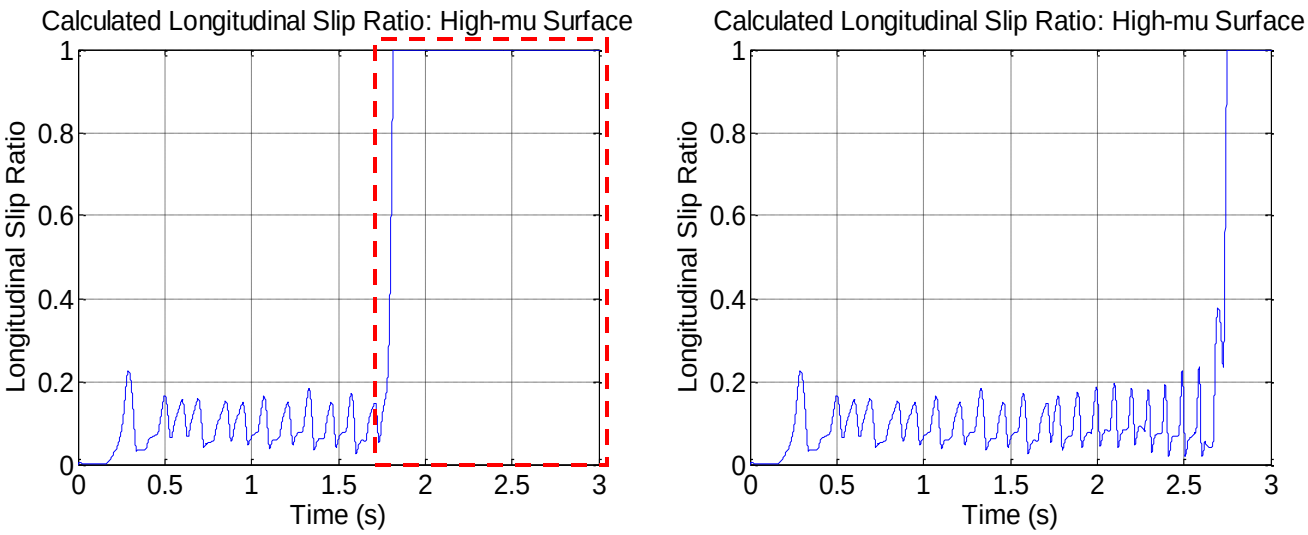

(a) (b)

Figure 30. Braking dynamics for Case 8 (a) showing the change in longitudinal slip ratio versus time for the FR tire and (b) the original longitudinal slip ratio versus time.

For the cut-off velocity parameter, the originally specified speed of 2 mph provides a good balance to the ABS system. It results in a low enough value of cut-off speed to allow the driver to maintain steering control for a majority of the braking maneuver without specifying a value so low as to cause instability in the controller.

The next parameter explored is wheel angular acceleration. Case 9 adjusts the threshold values for wheel angular acceleration, specifying lower bounding values as compared to the original bounds. This should result in a quicker reaction in the decision algorithm for determining the brake state from changes to the wheel angular acceleration. This result affects the entire operation range of the longitudinal slip value, shown in the highlighted portion of plot (a) in Figure 31. Plot (b) of this figure shows the slip ratio response of the original system for comparison. The lower bounding range of wheel acceleration results in a slight initial spike followed by a raised operating range of longitudinal slip, putting the mean value of longitudinal slip closer to the ideal calculated slip ratio of 0.1415. Since the mean slip ratio value is closer to the slip ratio corresponding to the maximum braking force, the braking distance is reduced by approximately 2.25 in (0.057 m).

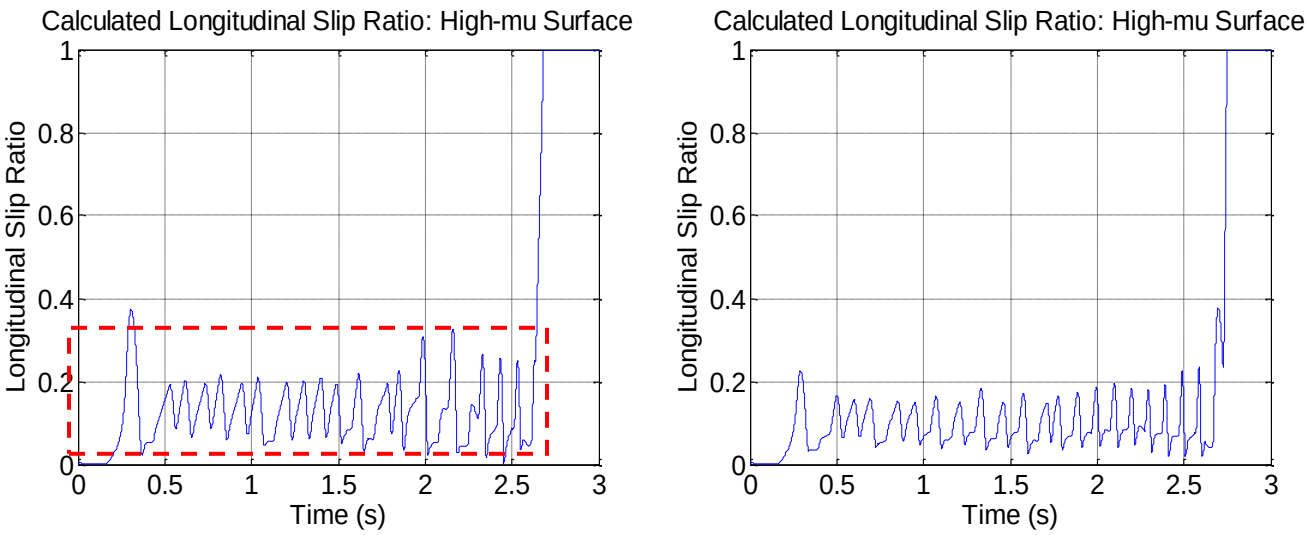

(a) (b)

Figure 31. Braking dynamics for Case 9 (a) showing the change in longitudinal slip ratio versus time for the FR tire and (b) the original longitudinal slip ratio versus time.

Case 10 presents the second case for adjusting the bounds of the wheel angular acceleration. The bound range for this case is higher than the original bounds. For the ABS decision process, this means less overall control of the slip ratio range, since it will take longer for the system to reach these newly defined bounds. Figure 32 (a) shows the longitudinal slip ratio with respect to time for the higher range bounds and (b) the baseline simulation test case with the original values for comparison. As expected, the longitudinal slip ratio range has increased due to the higher boundary values chosen. This results in less control over the longitudinal slip ratio. Again, however, this does raise the mean longitudinal slip ratio value close to the desired slip ratio value for this vehicle on a high-mu surface. Thus, the stopping distance is reduced by 1.4 *ft* (0.43 *m*). Even though the braking distance is reduced, the system exhibits a drawback in the fact that the slip range now begins to enter into the frictional region of the tire, reducing the amount of steering control to the driver, especially during the beginning and end of the braking maneuver.

Cases 9 and 10 show that by adjusting the wheel acceleration threshold ranges, the slip ratio range can be controlled. Raising the slip ratio range holds potential for improvement to braking system performance by reducing stopping distance, however, if not chosen carefully, the tire will begin to enter the frictional region of tire operation.

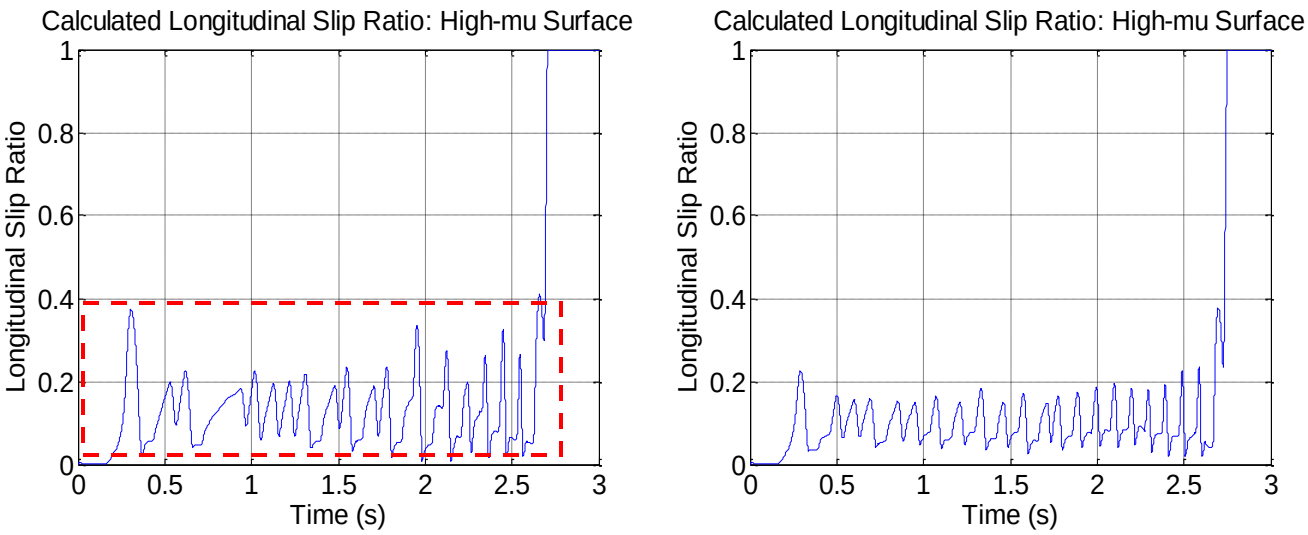

(a) (b)

Figure 32. Braking dynamics for Case 10 (a) showing the change in longitudinal slip ratio versus time for the FR tire and (b) the original longitudinal slip ratio versus time.

Case 11 presents the sensitivity analysis for the slip ratio parameter, choosing a new threshold range directly surrounding the calculated maximum desired slip ratio of 0.1415. The lower and upper bounds were chosen as 0.13 and 0.15 to try and maintain the longitudinal slip within close range of the desired slip value. Figure 33 (a) shows how the new threshold values affect the slip ratio over time with (b) showing the original slip ratio response. The response of the new parameter values, highlighted by the dashed red box, did not respond as expected. Instead of maintaining a slip ratio directly around the desired slip, the slip ratio responded with nonlinearities, beginning to experience step responses midway through the braking maneuver. This nonlinear slip ratio response led to an increase in stopping distance of 1.5 *ft* (0.47 *m*). This is likely due to the ABS controller not responding quickly enough to determine the braking state because all other threshold parameters remained set at the original values used for the baseline simulation.

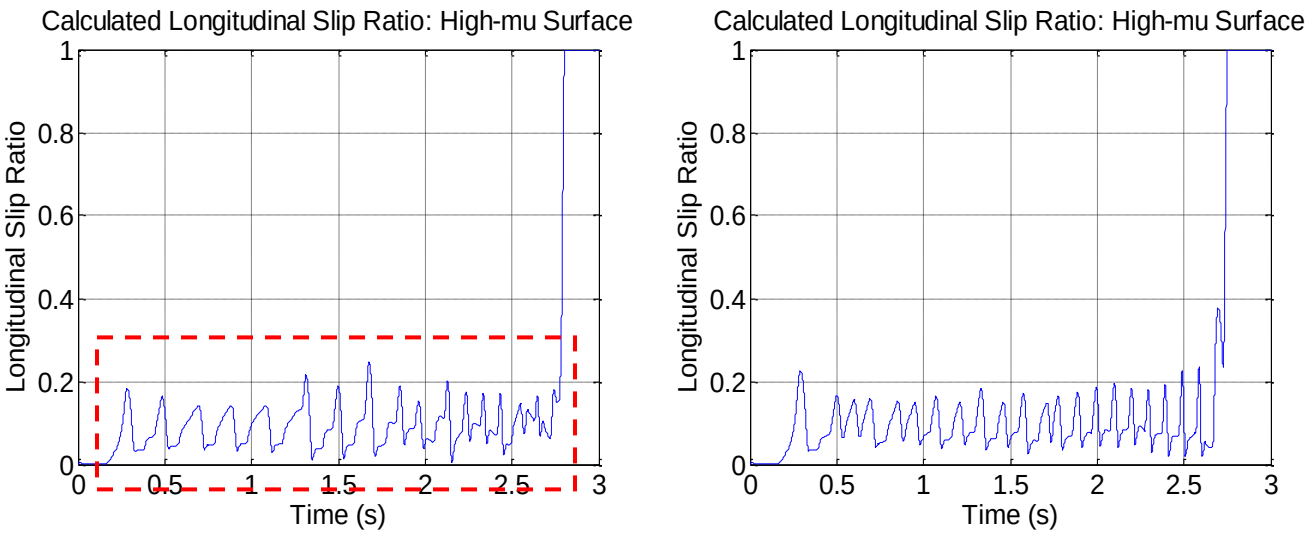

(a) (b)

Figure 33. Braking dynamics for Case 11 (a) showing the change in longitudinal slip ratio versus time for the FR tire and (b) the original longitudinal slip ratio versus time.

Case 12 increases the bounds of the slip ratio threshold values in an attempt to raise the mean slip ratio closer to the desired slip ratio value. These bounds are more evenly spaced, with a difference of 0.05 between the upper and lower values, which results in a smoother, more linear response of the system, as opposed to the closely spaced range in Case 11. The increase of these bounds does little to affect the brake response of the system. The trend of increasing the boundary values shows a slight decrease in braking distance and overall improvement in braking response of approximately 2 *in* (0.05 *m*).

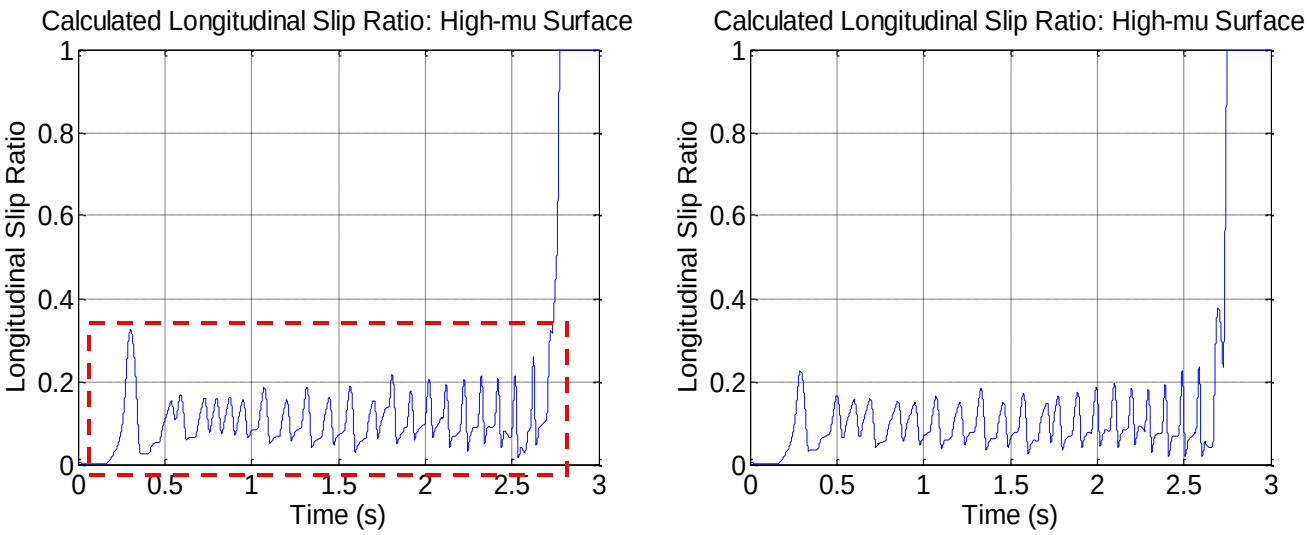

(a) (b)

Figure 34. Braking dynamics for Case 12 (a) showing the change in longitudinal slip ratio versus time for the FR tire and (b) the original longitudinal slip ratio versus time.

Further study of adjusting the slip ratio threshold ranges show that evenly spaced upper and lower boundary values results in a more linear response of the longitudinal slip ratio during braking, but increasing the magnitude of these values alone does not provide significant improvement to braking performance.

Figure 35 (a) shows the response of longitudinal slip ratio with a change of the pressure ramp input for Case 13. The plot in (b) again shows the baseline simulation response. For this case, the ramp input was decreased, resulting in a slower build up in brake pressure. This reduction in braking force specifically affected the beginning of the braking maneuver, resulting in a much slower initial response of the ABS. This resulted in a braking distance increase of 12 *ft* (3.7 *m*). The impact of decreasing the pressure build up in the system is highlighted in plot (a).

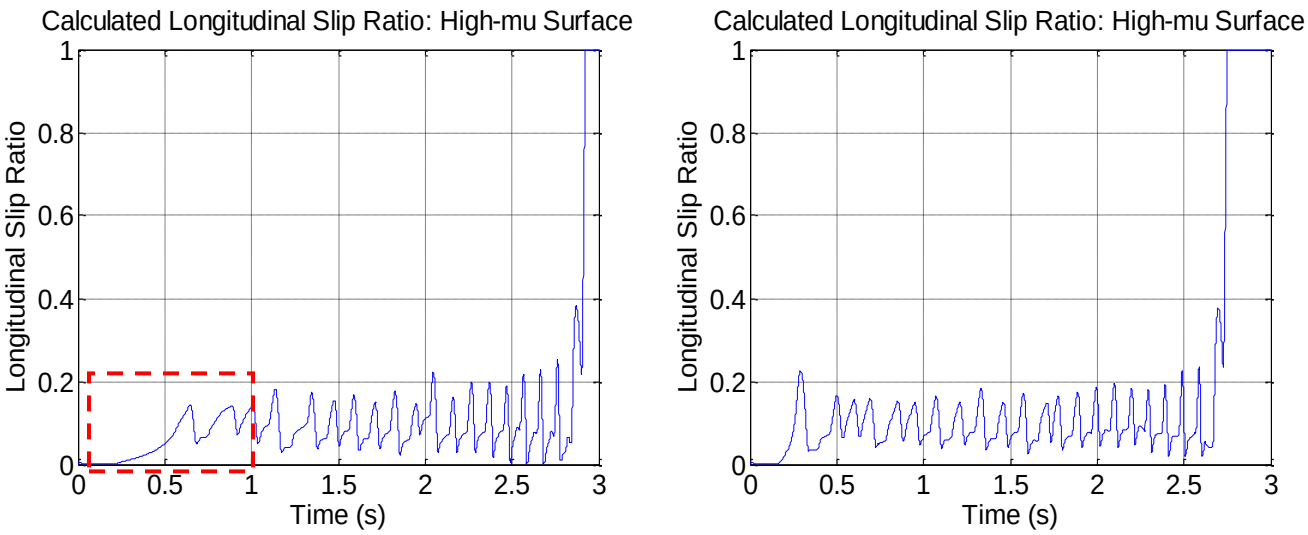

(a) (b)

Figure 35. Braking dynamics for Case 13 (a) showing the change in longitudinal slip ratio versus time for the FR tire and (b) the original longitudinal slip ratio versus time.

Case 14 increases the pressure ramping upper bound significantly from the original value. This pressure increase results in a spike in the initial braking pressure and force and immediately locks the wheel. The ABS then takes a moment to respond and correct for this initial pressure increase. Once the correct braking state is determined and the controller reacts, control of the system is corrected and the slip ratio is maintained within the expected slip range. This increase in the pressure parameter does lead to a decrease in braking distance of 2.8 *ft* (0.85 *m*). This reduction in braking distance does not translate into an increase in overall braking performance however, since the wheel immediately locks upon brake application. This means that the driver briefly loses steering control of the vehicle. The pressure ramp value must be adjusted in order to find an appropriate pressure ramp increase to reduce stopping distance while still allowing the driver to maintain steering control of the vehicle.

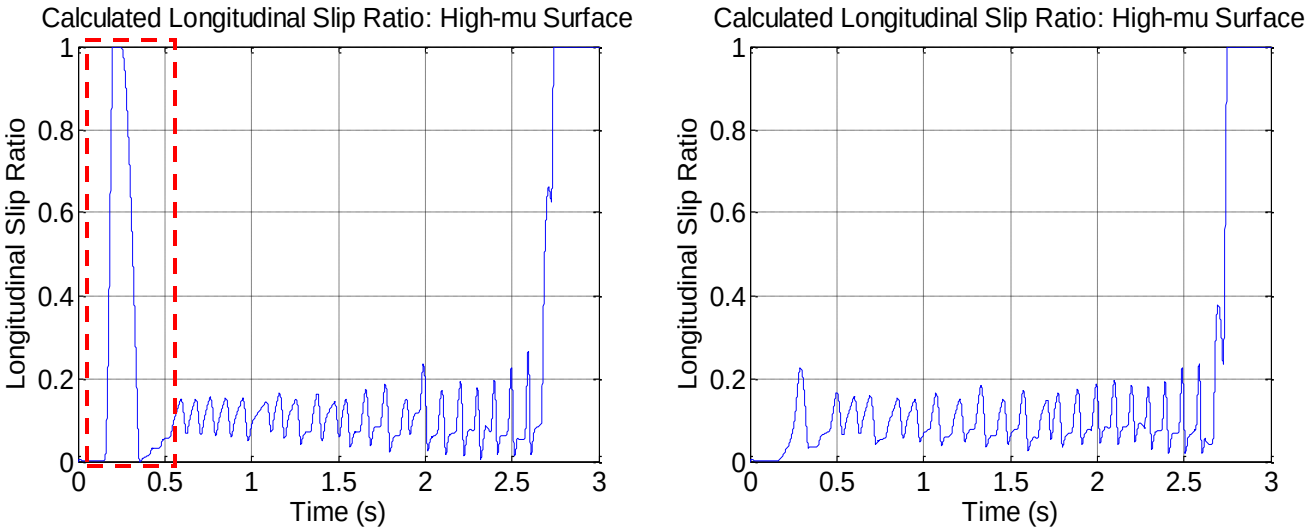

(a) (b)

Figure 36. Braking dynamics for Case 14 (a) showing the change in longitudinal slip ratio versus time for the FR tire and (b) the original longitudinal slip ratio versus time.

5.3.3 Total System Braking Performance Improvement

Once all threshold gains and prediction parameter thresholds were tested individually, the parameters were assigned into two groups. Group one contains parameters that either negatively affected system performance or were insensitive to parameter value changes. Group two contains the parameters that improved braking system performance, either by improving longitudinal slip control or reducing braking distance. These groups are presented in Table 6. The parameters from group two were then studied in more detail. Additional testing was completed which combined the parameter changes and resulting responses of multiple parameter threshold boundaries in order to achieve the best ABS response. The best ABS response is defined as a combination of the greatest reduction in stopping distance while maintaining steering control of the vehicle for the driver. This means that the wheels should not lock before the desired cut-off velocity and the slip ratio range should remain primarily in the linear range of the tire, equating to an average slip ratio of less than 0.3.

Table 6. Grouping the parameter values into positive and negative groups.

Group 1	Group 2
Negative / Insensitive Parameters	**Positive Parameters**
a1_ini_f	Vehicle Speed
a1_ini_r	Wheel Acceleration
Ak_f	Slip Ratio
Ak_r	Pressure Ramp
a_hold	

From the initial parameter sensitivity analysis, it was determined that the threshold prediction parameters were the variables that were most able to positively affect the overall braking performance of ABS. The vehicle speed, wheel angular acceleration, slip ratio and pressure ramp values were studied together, trying to compliment the benefits of changing one parameter variable with all of the others simultaneously. Many tests were conducted measuring the ABS response and the best overall braking performance increase was achieved by using the threshold boundaries given in Table 7. It was discovered that the cut-off velocity of the vehicle was relatively insensitive to changes between 2 to 4 mph and that 2 mph was the lowest value that would not result in braking system instability, while allowing the driver to maintain steering control for the maximum amount of time during the braking maneuver. From the remaining prediction parameters, the sensitivity analysis revealed that the wheel angular acceleration and pressure ramp thresholds were able to produce the most change of all the ABS parameter gains and thresholds. Through extensive testing of these parameters, the threshold values that resulted in the best braking performance were obtained. Once these values were chosen, all threshold gains and parameter values were retested against the newly tuned system parameters to track for any changes due to the new braking dynamics. The variation of these gain values was still insensitive to the new values and the holding gain remained optimized for the new system.

Table 7. Prediction parameter values resulting in the best overall braking performance.

Prediction Parameters	Original Upper Bound	Original Lower Bound	New Upper Bound	New Lower Bound
Vehicle Speed	52.5	2	Same	Same
Wheel Acceleration	2	0.5	3	1
Slip Ratio	0.15	0.08	0.2	0.14
Pressure Ramp	50	0	80	0
Braking Distance Reduction [m]		-0.675		

Figure 37 shows the longitudinal slip ratio response for (a) the best overall braking performance achieved by adjusting the all of the prediction parameters simultaneously and comparing the response to (b) the baseline longitudinal slip ratio with respect to time. From the plot in (a), there is an initial spike due to the increase in the pressure ramp. This spike in braking force results in a reduction in steering force to the driver during the initial portion of the braking maneuver, but never locks the tire. The adjustments of both the wheel angular acceleration and slip ratio threshold values result in an increase in the mean longitudinal slip ratio. This results in a decrease in braking distance, as presented in Cases 9 through 12. These values had to be continually adjusted in order to achieve a linear slip ratio response while ensuring the overall slip ratio remained within the linear response portion of the tire.

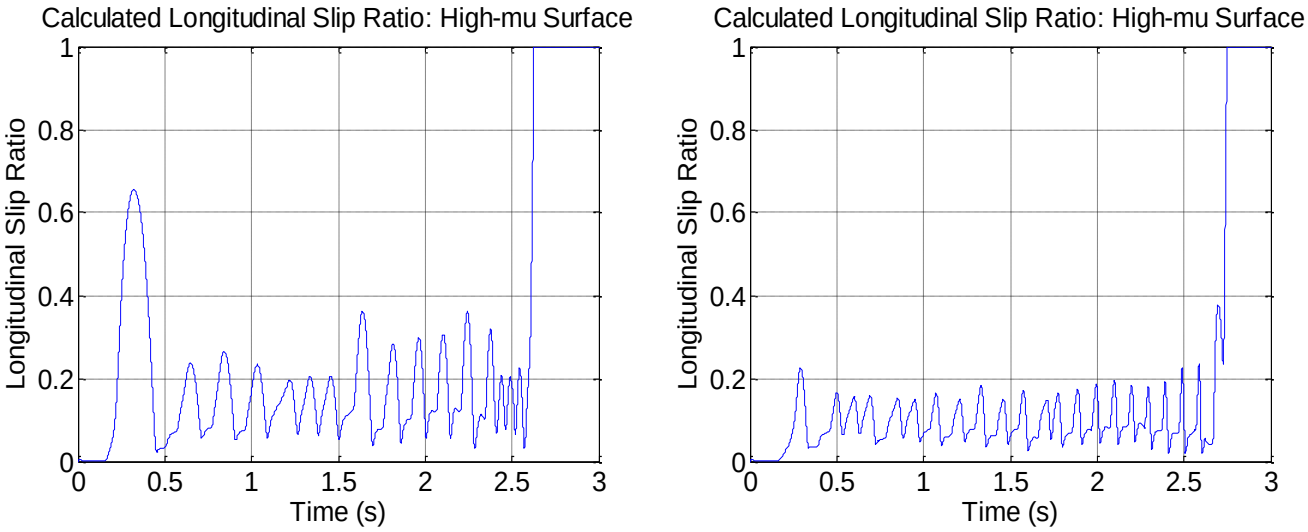

(a) (b)

Figure 37. Braking dynamics for (a) best overall braking performance, showing the change in longitudinal slip ratio versus time for the FR tire and (b) the baseline longitudinal slip ratio versus time.

The wheel velocity response for the front right wheel is shown in Figure 38. Plot (a) shows the response of the newly tuned parameter values and (b) shows the original system performance. There are two noticeable differences in these plots, the first being a slight decrease in wheel speed when braking is initiated. This is due to the pressure ramp increase. The second is the response of the tuned system as the braking maneuver is about to end. The tuned braking response is able to more closely track the maximum deceleration value, allowing for the driver to maintain steering control until the end of the maneuver.

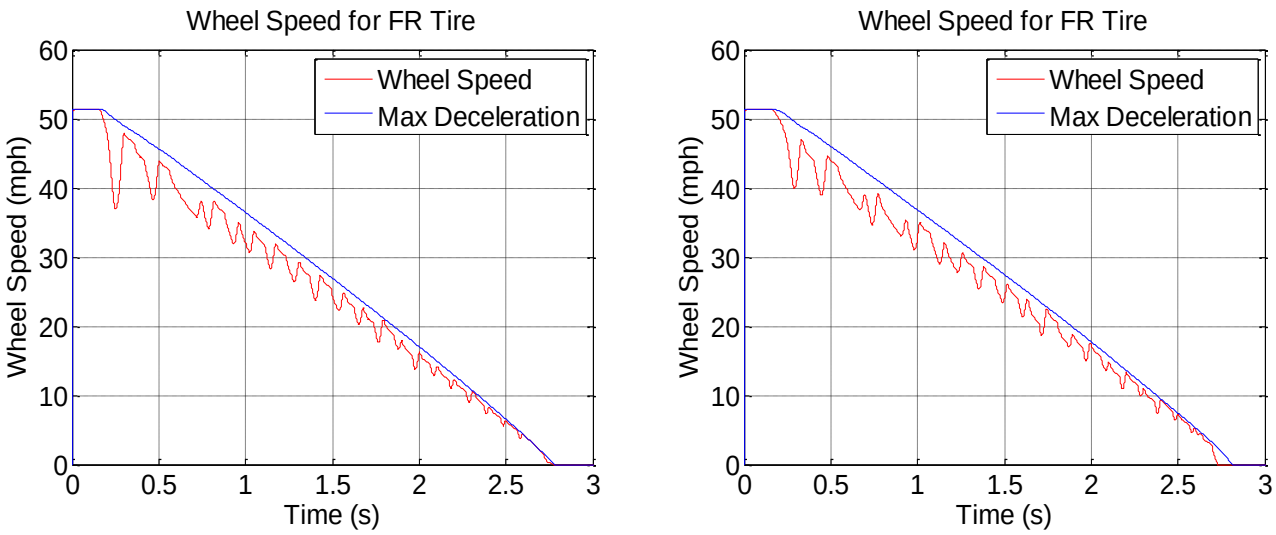

(a) (b)

Figure 38. Wheel speed response for (a) the best improvement in braking response by adjustment of parameter threshold values and (b) the baseline wheel speed response.

The total reduction in stopping distance with the newly tuned parameter values is 2.2 *ft* (0.675 *m*). The entire braking maneuver is accomplished in 118 ft (36 m). This reduction in braking distance accounts for an overall decrease in braking distance of approximately 1.9%. In order to achieve this maximum reduction in braking distance, some trade-offs were necessary, including pushing the tire close and slightly into the frictional range, which results in a decrease in vehicle lateral control. This parameter sensitivity analysis method can be expanded for use on varying surface conditions, including low-mu surfaces. Similar trends for parameter variations are expected, only occurring over longer braking maneuvers due to the reduction in available braking force.

5.4 Conclusion

The parameter sensitivity analysis clearly demonstrated which parameter gain values and threshold ranges had the greatest affect on the system. The individual parameter sensitivity analysis was able to separate and group the parameters that were insensitive to changes in system values or provided negative performance from those that would benefit the ABS. These values were then extensively tested to find the threshold range combinations that resulted in the best overall braking performance. Again, braking performance is quantified by achieving the greatest reduction in braking distance while maintaining a slip ratio within the linear region of the tire, defined as less than 0.3, to

allow for the driver to maintain steering control of the vehicle. The newly tuned system that met the braking system criteria was able to reduce overall braking distance by approximately 1.9%. The upper bound of improvement on the current ABS control algorithm is limited to minimal increases due to the available information to the control algorithm and the necessary trade-offs in ABS performance to achieve a reduction in braking distance while maintaining lateral vehicle control. Similar results are expected by applying this parameter sensitivity analysis on low-mu surfaces.

The next phase in this project is to develop a new ABS algorithm capable of controlling brake torque at the desired calculated longitudinal slip ratio relating to the point of maximum braking force using the information gained from an IT. Chapter 6 introduces a sliding mode control method for use in ABS control that is designed to control and maintain a desired slip ratio value at a specific point.

6 Sliding Mode Control

6.1 Introduction

The objective of an anti-lock braking control algorithm is the accurate control of the wheel longitudinal slip by applying the proper amount of braking torque to the wheel. In order to achieve this objective, a robust controller capable of tracking the longitudinal slip and commanding the brake torque value despite changes in the system parameters must be developed. The required parameters of the system for the development of this controller include the vehicle longitudinal velocity, longitudinal acceleration, wheel angular acceleration and longitudinal force and available friction at the tire contact patch. The type of control method used for this application is based on the theory of Variable Structure Control (VSC) as a high-frequency switching feedback control, resulting in Sliding Mode Control (SMC). This Chapter details the SMC control method development and application using force and friction information gained from an IT. SMC is discussed along with the reasons for using this type of control for an improved ABS algorithm. A simplified wheel model is developed along with the dynamic equations of motion and control equations. The vehicle model and control strategy is designed in Simulink and the results of the system are presented, followed by the concluding remarks.

6.2 Function of Sliding Mode Control

SMC is a nonlinear control method that alters the dynamics of a system by application of a high speed switching control. The purpose of the switching control law is to drive the plant's state trajectory onto a user specified surface within the state space and once the trajectory reaches this surface, to maintain the plant's state trajectory on this surface for all subsequent time [38]. This surface is referred to as the switching surface. Two gains are specified for SMC. One gain is responsible for controlling the trajectory if the plant state is "above" the switching surface. The second gain is responsible for the control of the trajectory of the plant state when it is "below" the switching surface. The switching surface defines the rule for determining the proper gain to apply. This surface

is also referred to as the sliding surface, since once the plant trajectory intercepts this surface, the switching control will maintain the plant's trajectory on this surface for all subsequent time, thus, the trajectory will "slide" along this surface. The plant dynamics, when restricted to this sliding surface, represent the controlled system's behavior. There are two main phases for developing a VSC. The first phase is to properly define a switching surface so that the plant dynamics, when restricted to this surface, display desired dynamics. The second phase is to develop a discontinuous control law that will drive the plant's state to the specified surface and maintain the plant's trajectory along this surface for all subsequent time.

A simplified example of the dynamics of the plant trajectory is shown in Figure 39. For this example, the *x*-axis at a value of zero represents the desired sliding surface. For this example, the first order system that represents the plant with a discontinuous, piecewise control are represented by Equation 14 and Equation 15, respectively,

$$\dot{x}(t) = u(x,t) \qquad \text{Equation 14}$$

and

$$u(x,t) = sgn(x) = \begin{cases} -1 & if\ x > 0 \\ 0 & if\ x = 0 \\ +1 & if\ x < 0 \end{cases} \qquad \text{Equation 15}$$

This control law guarantees that if the initial system state is greater than zero, the plant trajectory will be driven downward to the switching surface. When the initial system state is less than zero, the control law followed will change, and drive the plant trajectory upward to the switching surface. Once the trajectory reaches the switching surface, the control law will ensure that the trajectory continues along the sliding surface.

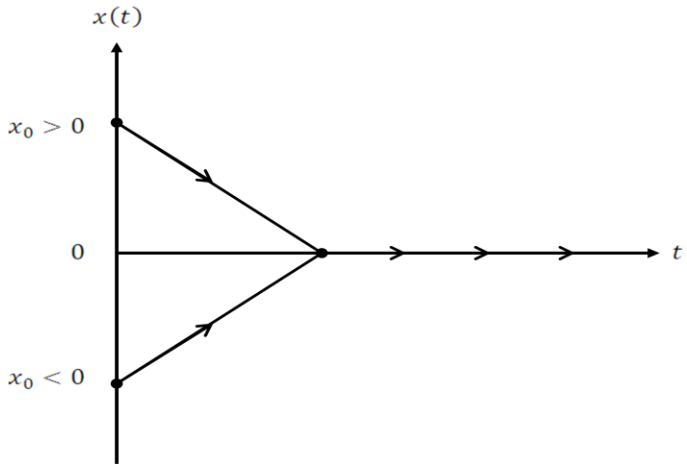

Figure 39. State trajectory dynamics of the first order system example.

The control $u(x,t)$ for the above example changes its value between ± 1 around the desired sliding surface. For any initial condition x_0, there exists a "reaching" phase, in which the trajectory of the system is forced from its initial condition to the desired sliding surface in a finite time. The control gains can be chosen in order to tune the timing of the reaching phase. A drawback to using a discontinuous piecewise control law is that the system dynamics are forced to change abruptly. This drawback, paired with the physical limitations and delay of the mechanical controller, create an area of discontinuity at the switching surface. Due to the imperfections in switching devices and delays, SMC suffers from chattering [39]. The sketch in Figure 40 shows how delays in the control switching result in chattering. The trajectory of the system approaches the switching surface from the initial condition - the reaching phase. Once the system reaches the switching surface, the delay in the controller to switch the control law allows overshoot of the surface into the region $x < 0$. When the control switches, the trajectory reverses direction and heads back to the switching surface. Once again, the trajectory overshoots the surface. The repetition of this process creates the oscillation about the switching surface, as seen in the Figure.

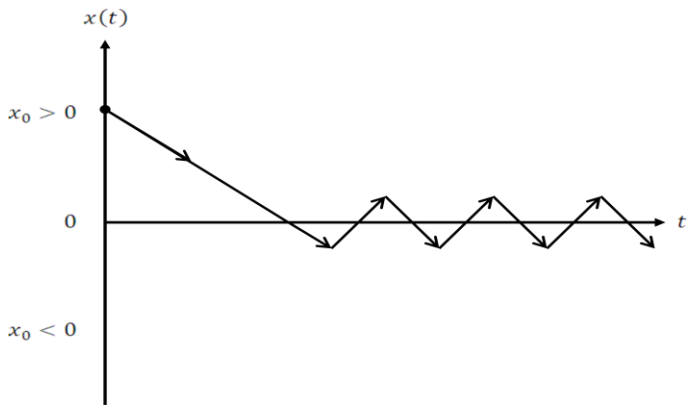

Figure 40. Chattering due to the delay in control switching.

There are two methods to help reduce or eliminate chattering from the system. The first method is to divide the control law into continuous and switching components to aid in reducing the amplitude of the switching one. The second method to eliminate chattering is to replace the signum control function with a high slope saturation function. The control law can be rewritten

$$u(x,t) = sat(x) = \begin{cases} t/\varepsilon & if\ |t| \leq 1 \\ sgn(t) & if\ |t| > 1 \end{cases} \qquad \text{Equation 16}$$

Using the control law in Equation 16, a continuous component is added to the switching function. The signum nonlinear control law results in a function approximation as shown in Figure 41 (a) and its continuous saturation approximation function is shown in Figure 41 (b). The saturation function approximation can be tuned to determine the slope of the linear portion by adjusting the value ε. Good approximation of the system requires the use of small values of ε. More complex functions can be used to define a linear approximation, but the saturation function yields a simple, tunable linear approximation. In addition, when the selection points for the linear function and gains are properly tuned, the system can accurately represent the physical controller and can effectively reduce or eliminate chattering of the control system [39].

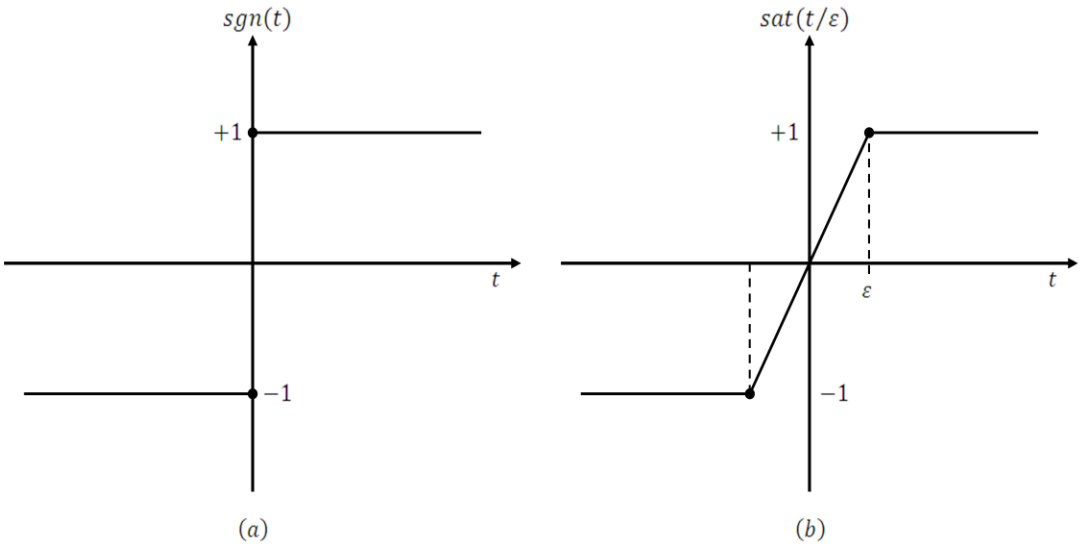

Figure 41. Comparison showing the (a) signum nonlinearity and (b) its continuous saturation function approximation.

6.2.1 Application of SMC to Vehicle ABS

The reason for high interest in SMC for ABS application is due to the insensitive system response to variations in plant parameters and to external parameters when the plant trajectory is on the sliding surface. The speed, acceleration and force parameters experienced by the vehicle and tire during hard braking are subject to large variation depending on the vehicle and road conditions. SMC is able to accept a wide range of plant parameters and still drive the system's trajectory to the specified surface.

The sliding surface is defined as the point of longitudinal slip that corresponds to the maximum available longitudinal braking force. The control laws for SMC are designed to maintain the wheel longitudinal slip at this desired value. Nonlinear control methods, including SMC, have been used in the past to show the potential for such nonlinear tracking controllers [40]. Current methods using this style of control use a predetermined slip ratio value as the sliding surface for all surface conditions. Having known friction and force information from an IT, the exact value of desired longitudinal slip can be calculated during each braking maneuver to determine the desired slip ratio value for any surface condition.

6.3 Sliding Mode Control Development

In order to present the feasibility of using a SMC algorithm for ABS, a simplified wheel model is introduced to define the wheel motion during braking. The dynamic equations of motion for the wheel are defined and used to determine the control equations for SMC. The sliding surface equation is defined in terms of the wheel motion and used to design the SMC ABS controller. The same model parameters used in the full vehicle simulation in Chapter 4 are implemented into the SMC model to compare the results for the baseline longitudinal slip based ABS control and the sliding model control ABS model. The following model is representative of a single tire, but the same control procedure can be extended to use at each wheel of the vehicle.

6.3.1 Wheel Model

The wheel model used to describe the vehicle and wheel motion is presented in Figure 42. The vehicle is represented as a mass block with no suspension compliance. The vehicle provides a vertical load on the tire due to the static weight of the vehicle as well as the load transfer experienced by the front wheels during heavy braking. The vehicle is also subject to aerodynamic resistance. The wheel is subjected to torque from the engine, T_e, acting at the center of the wheel, the braking torque necessary to decelerate the tire without causing wheel lock up, T_b, the longitudinal braking force available at the contact patch, F_x and the rolling resistance experienced by the tire, RR_x. The speed parameters for both the vehicle and wheel are measured by V_x and Ω, respectively, along with the effective rolling radius of the tire, r. The model presented in Figure 42 is representative of a front wheel of the vehicle.

The following equations are derived from the vehicle model in order to derive a dynamic equation for the longitudinal slip ratio. This dynamic slip equation is responsible for tracking the plant dynamics and defining the switching surface in order to apply the proper control law to achieve the desired dynamics of the system. This step satisfies phase one of designing a sliding mode controller.

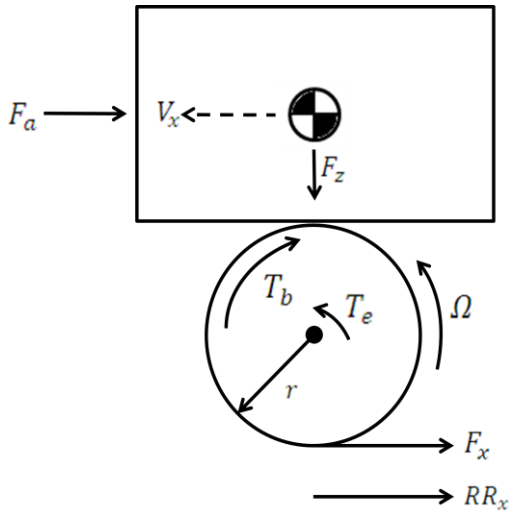

Figure 42. Simplified wheel and vehicle model for use with SMC.

Using Newton's second law to write out the force balance equation, the vehicle motion can be represented using

$$m\dot{V} = F_x - F_a \qquad \text{Equation 17}$$

Rewriting the vehicle force balance equation in terms of vehicle acceleration, Equation 18 is obtained.

$$\dot{V} = \frac{F_x - F_a}{m} \qquad \text{Equation 18}$$

The equation of motion for the wheel is written as

$$J\dot{\Omega} = (T_e - T_b) - F_x r - RR_x r \qquad \text{Equation 19}$$

Where $(T_e - T_b)$ represents the net torque, T_{net} on the wheel, with T_e as the engine torque acting on the wheel and T_b as the desired braking torque. Equation 19 can be rewritten in terms of the wheel angular acceleration,

$$\dot{\Omega} = \frac{T_{net} - F_x r - RR_x r}{J} \qquad \text{Equation 20}$$

These equations summarize the vehicle and wheel dynamics of the system in terms of known or measured parameters. The longitudinal braking, aerodynamic and rolling resistance forces acting on the wheel and vehicle are defined in the following equations.

$$F_x = \mu F_z \qquad \text{Equation 21}$$

Equation 21 defines the maximum longitudinal braking force available to the tire where F_z is the vertical load on the tire, which accounts for the static load on the tire, as well as the load transfer to the front tire during braking, which is dependent on vehicle acceleration. Equation 21 can be rewritten as

$$F_x = \mu\left(mg - \frac{Mh\dot{V}}{l}\right) \qquad \text{Equation 22}$$

In this equation, M represents the mass at one wheel, accounting for the mass seen on the quarter-car model used for SMC. h is the height of the vehicle center of gravity. This longitudinal force equation accounts for the static load on the tire as well as a simple longitudinal load transfer to the wheel during braking.

$$F_a = \frac{1}{2}\rho C_d A_f V_x^2 \qquad \text{Equation 23}$$

Equation 23 defines the aerodynamic force experienced by the vehicle, where ρ is the density of air, C_d is the measured drag coefficient of the vehicle being tested, A_f is the total frontal area of the vehicle and V_x is the vehicle speed. Equation 24 presents the rolling resistance forces for a standard passenger tire and is dependent on vehicle speed [8].

$$RR_x = 0.005 + 3.24 \cdot 0.01 V_x^2 \qquad \text{Equation 24}$$

Next, the equations for longitudinal slip estimation and the friction versus slip curves must be developed in order to define the area of operation for the system during braking. The longitudinal slip ratio defined in Equation 1, will be reiterated here for reference,

$$\kappa = \frac{V_x - r\Omega}{V_x} \qquad \text{Equation 25}$$

A commonly used friction coefficient versus longitudinal slip ratio equation is defined in Equation 26 [41]. This Equation defines the maximum friction coefficient location with respect to longitudinal slip for varying surface conditions.

$$\mu(\kappa) = 2\mu_p \kappa_p \left(\frac{\kappa}{\kappa_p^2 + \kappa^2} \right) \qquad \text{Equation 26}$$

The peak friction coefficient and peak longitudinal slip ratio are defined by μ_p and κ_p, respectively. Figure 43 shows a representation of the friction coefficient versus longitudinal slip ratio used for the SMC simulation. For these curves, a high friction coefficient of 0.8, the point of maximum available braking force, corresponds to a slip ratio of 0.1415. For a low friction surface, the maximum braking force occurs at a friction coefficient of 0.2, corresponding to a slip ratio of 0.2. This set of curves will allow the system to exhibit the maximized braking potential under varying surface conditions and peak longitudinal slip ratios.

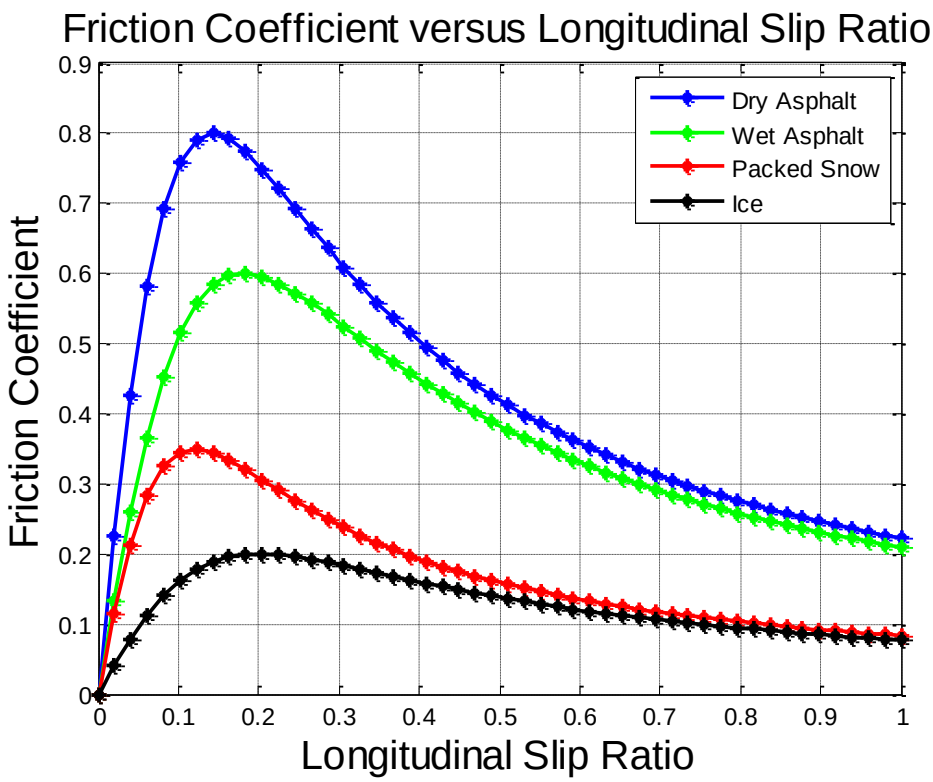

Figure 43. Simulated friction coefficient versus longitudinal slip ratio curve for varying surface conditions.

In order to develop the control law, it is easiest to define the slip ratio in state space form, following the first-order state space equation $\dot{x} = Ax + Bu$, where x represents the states of the system, u is the control input and A and B are the state and input matrices. Putting the first-order system in terms of the longitudinal slip state and braking torque control input gives the equation

$$\dot{\kappa} = A\kappa + BT_b \qquad \text{Equation 27}$$

The final goal of developing the control equation is to output the required braking torque to the wheel to maintain a desired value of slip and prevent wheel lock up. To simplify the derivation of the control law in Equation 27, the vehicle parameters will be defined in terms of the system states as,

$$x_1 = V_x \qquad \text{Equation 28}$$

$$x_2 = \Omega \cdot r \qquad \text{Equation 29}$$

$$\dot{x}_1 = \dot{V}_x \qquad \text{Equation 30}$$

$$\dot{x}_2 = \dot{\Omega} \cdot r \qquad \text{Equation 31}$$

The longitudinal slip ratio given by Equation 25, can be rewritten in terms of the state space variables

$$\kappa = \frac{x_1 - x_2}{x_1} \qquad \text{Equation 32}$$

Taking the derivative with respect to time of Equation 32 yields the dynamic equation for longitudinal slip in terms of state space variables.

$$\dot{\kappa} = \frac{x_1(\dot{x}_1 - \dot{x}_2) - (x_1 - x_2)\dot{x}_1}{x_1^2} \qquad \text{Equation 33}$$

To simplify the control law in Equation 33, Equation 32 can be rewritten in terms of x_2.

$$x_2 = x_1(1 - \kappa) \qquad \text{Equation 34}$$

Equation 34 can be substituted into Equation 33, putting the dynamic slip equation in terms of longitudinal slip and the state variables. Simplifying these terms, the final form of the dynamic equation for slip is developed.

$$\dot{\kappa} = \frac{(1 - \kappa)\dot{x}_1 - \dot{x}_2}{x_1} \qquad \text{Equation 35}$$

Now that the dynamic equation for slip has been derived in terms of the state space variables, the vehicle system variables can be input into Equation 35 to relate the dynamic slip equation to known vehicle parameters. First, $\dot{x}_1$ and $\dot{x}_2$, which were defined in Equation 30 and Equation 31, have the values of $\dot{V}$ and $\dot{\Omega}$ from the vehicle dynamic equations defined in Equation 18 and Equation 20 to yield:

$$\dot{x}_1 = \frac{F_x - F_a}{m} \qquad \text{Equation 36}$$

$$\dot{x}_2 = \frac{T_{net} - F_x \cdot r - RR_x \cdot r}{J} \qquad \text{Equation 37}$$

These two equations can be substituted in for the state variables in Equation 35 and simplified to put the dynamic longitudinal slip equation in terms of known vehicle parameters. Note that the net torque is separated from the other known vehicle parameters, since the braking torque value within this term is the value we wish to control. During braking, the engine torque provided to the wheel is zero, which puts the net torque equation solely in the terms of the braking torque, T_b.

$$\dot{\kappa} = \frac{1}{V_x}\left[\frac{1-\kappa}{mr}(F_x - F_a) + \frac{F_x \cdot r}{J} + \frac{RR_x \cdot r}{J}\right] - \frac{1}{JV_x}T_b \qquad \text{Equation 38}$$

Equation 38 represents the final form of the dynamic longitudinal slip control law in terms of known and measured vehicle parameters. This equation provides the tracking of the dynamic slip to control the braking torque input to the system, so that the longitudinal slip reaches the desired value and maintains this value for the duration of the braking maneuver.

The second phase of designing the sliding mode controller is to develop a discontinuous control law that will drive the longitudinal slip from its initial value to the specified surface and maintain the slip along this surface for all subsequent time. The first step is to define the sliding surface – the surface that will make the system operate with the desired dynamics. In order for ABS to operate at the maximum braking potential, the longitudinal slip ratio must be maintained at the point where the maximum braking force is achieved. The longitudinal slip can define the sliding surface, s, as

$$s = \kappa - \kappa_d \qquad \text{Equation 39}$$

where κ is the actual slip ratio of the tire and κ_d is the desired slip ratio that corresponds to the value where maximum braking force is available. The goal of the sliding surface equation is to minimize the value between the actual slip ratio and the desired slip ratio,

ideally resulting in a sliding surface value of zero. A zero value would mean that the actual slip ratio is being controlled to the exact value of the desired slip ratio and the system is behaving as desired. Taking the derivate of the sliding surface equation with respect to time will put the sliding surface in terms of the dynamic slip ratio equation developed in Equation 38. Taking the derivative of Equation 39,

$$\dot{s} = \dot{\kappa} \qquad \text{Equation 40}$$

where the desired value of slip drops out of the equation since it is a constant. Setting Equation 40 to zero will result in the sliding surface having a value of zero. This will correspond to an equation that will result in the desired dynamics, since this surface represents the value along the sliding surface.

$$\dot{s} = \dot{\kappa} = 0 \qquad \text{Equation 41}$$

The condition of $\dot{\kappa} = 0$ can be substituted into the dynamic longitudinal slip control law in Equation 38. Setting the right hand side of the equation equal to zero and solving for the braking torque control input yields,

$$T_b = \frac{J(1-\kappa)}{mr}(F_x - F_a) + F_x \cdot r + RR_x \cdot r \qquad \text{Equation 42}$$

Equation 42 represents the best approximation of a continuous control law for the braking torque that achieves $\dot{s} = 0$. This is the governing equation employed for determining the linear portion of the control law, when the trajectory is not on the sliding surface. The overall switching control equation is a combination of the linear control portion, Equation 42, and the switching, or nonlinear control portion about the sliding surface at $s = 0$, which can be defined as

$$U_{sw} = k \cdot sgn(s) \qquad \text{Equation 43}$$

Equation 43 can be rewritten with the signum function approximated as

$$U_{sw} = k \cdot \frac{s}{|s| + \varphi} \qquad \text{Equation 44}$$

where k and φ are proportional gain values chosen by the user to tune the response of the system, and s is the sliding surface. The linear control is responsible for the system dynamics when the trajectory is not traveling on the sliding surface and the switching control is responsible for the braking dynamics on s. The switching control in Equation 44 is responsible for smoothing the resulting dynamics of the system as the trajectory travels along the sliding surface, helping to reduce the chatter inherent in SMC.

The Simulink model that represents the simplified wheel model and SMC is shown in Figure 44. The dashed red outline highlights the vehicle and wheel dynamics of the system from the model presented in Figure 42. The dashed blue outline highlights the SMC and brake dynamics of the system. Within the SMC block is the brake subsystem, where the brake dynamic response is approximated using a transfer function. This transfer function for the braking dynamics represents the delay in braking actuation and line pressure build up [41] to help compare the SMC results with the simulation results presented in Chapter 4.

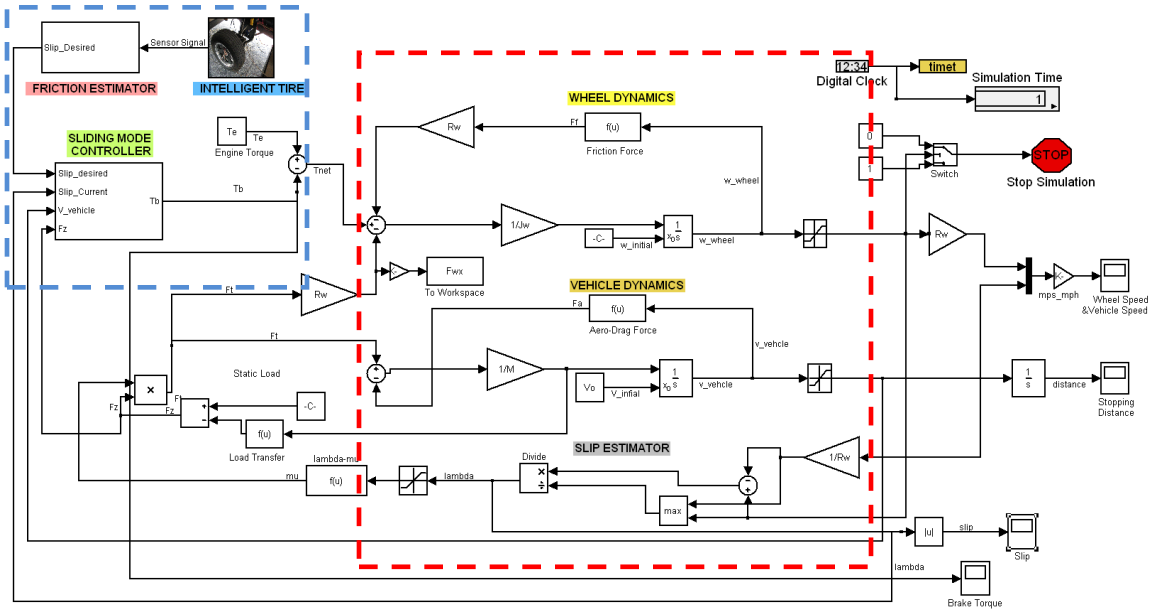

Figure 44. Simulink model of the SMC, vehicle dynamics and wheel dynamics.

6.4 Results

Executing the described SMC ABS control algorithm in Simulink shows a good braking dynamic response. For this simulation, a major assumption is that the exact

value of longitudinal slip ratio that corresponds to the maximum braking force is known, due to the use of an IT. The vehicle is traveling at a speed of 52.5 *mph* and applies full brakes at 0.15 seconds. Figure 45 shows the longitudinal slip ratio response with respect to time for the ABS braking maneuver on a high-mu surface. The longitudinal slip quickly reaches the calculated desired slip ratio of 0.1415 after brake application and oscillates about this point for the remainder of the braking maneuver, until the ABS cut-off speed is reached. The slip ratio is maintained within a close proximity to the desired slip. Due to the simplified model used, the results experience a smooth and linear response.

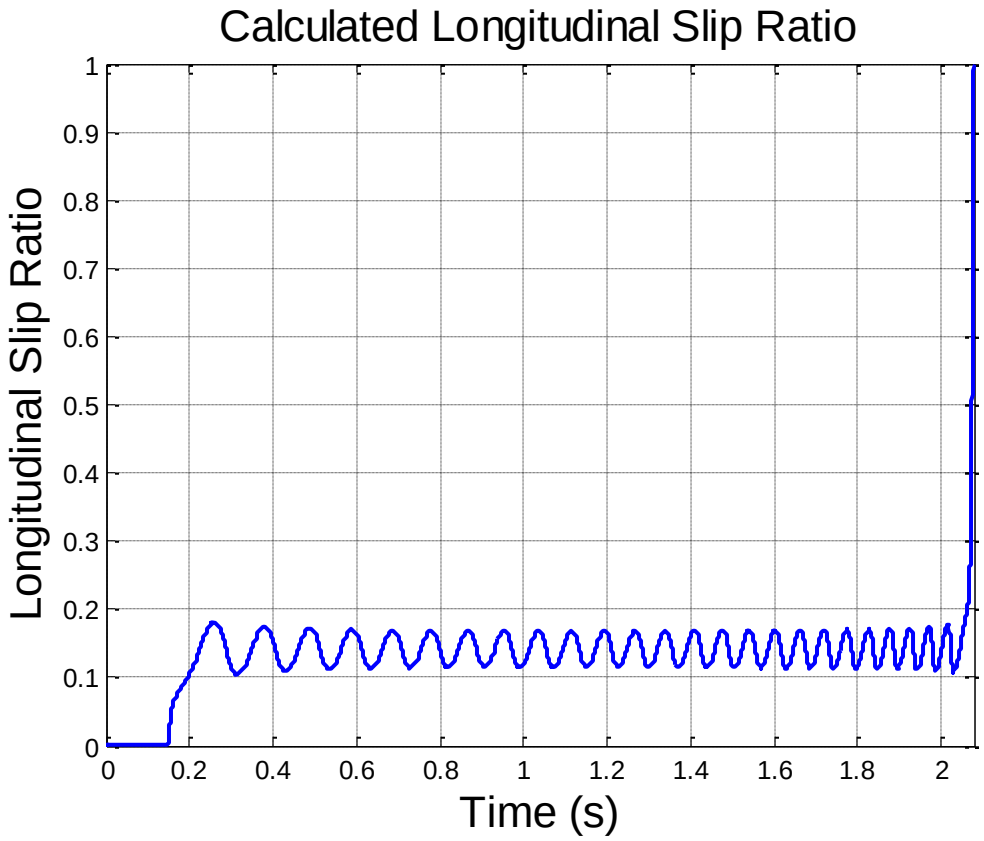

Figure 45. Longitudinal slip versus time response for ABS braking on a high-mu surface using SMC.

Figure 46 shows the longitudinal braking force versus slip ratio during the braking maneuver. For this simulation, the longitudinal force versus slip ratio curve was estimated according to Equation 26. For the high-mu surface tested here, there is a

relatively large peak just around the maximum value. The longitudinal slip is well maintained around the desired slip ratio, staying within a range from 0.12 to 0.17.

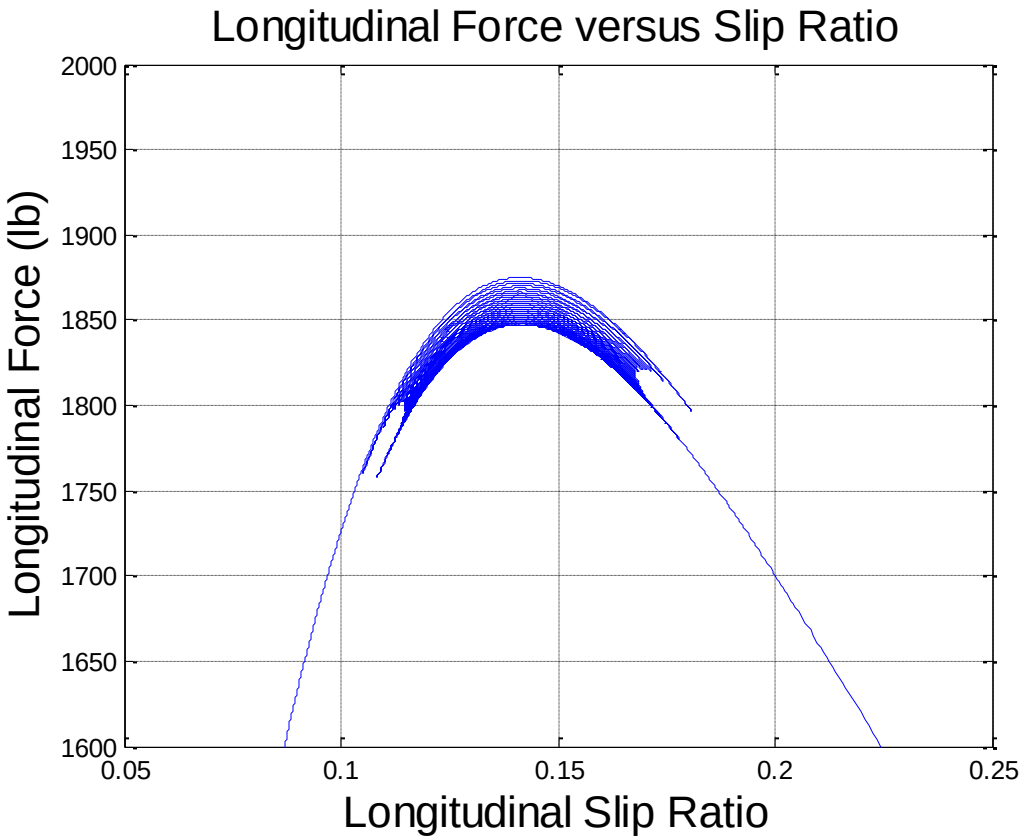

Figure 46. Longitudinal force versus longitudinal slip ratio for SMC during ABS braking maneuver for high-mu surface.

The wheel speed during the braking maneuver is shown in Figure 47. Wheel speed plotted alongside maximum wheel deceleration against time throughout ABS braking maneuver for high-mu surface.. The wheel speed experiences expected results, decreasing and increasing velocity as the brakes are applied and released for ABS operation. The proportional gains for the switching control law were chosen so that the ABS operated at approximately 14 Hz and experienced a constant oscillation value around the desired longitudinal slip value.

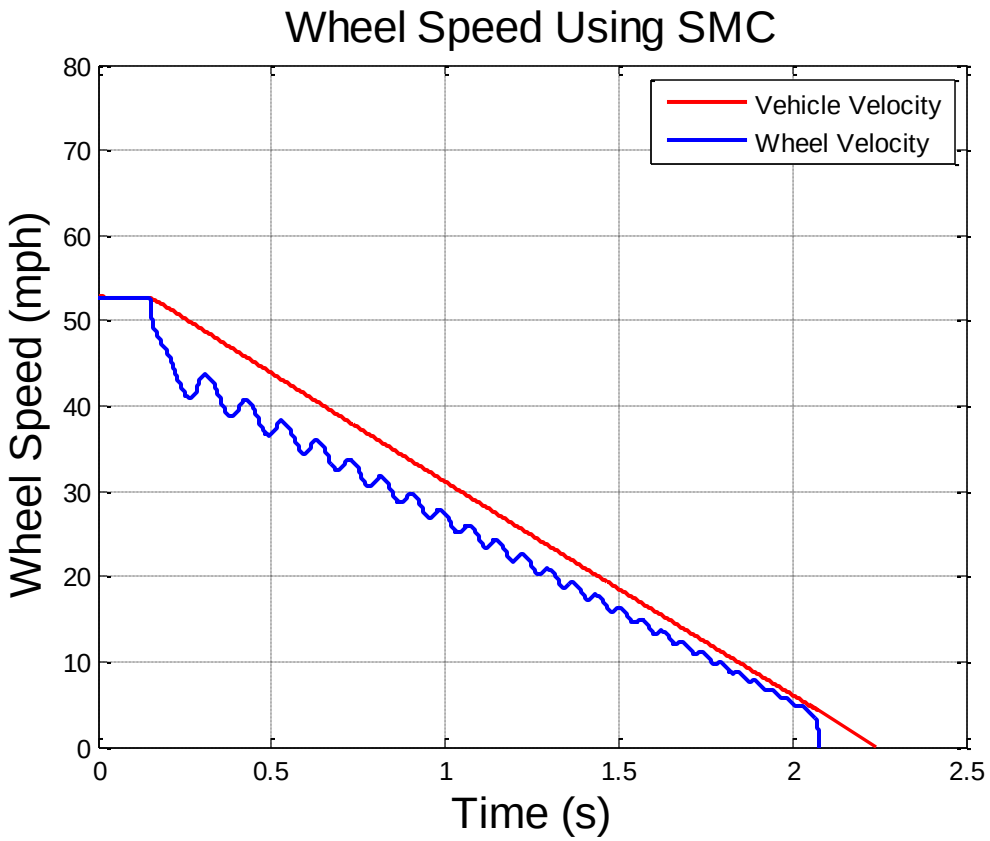

Figure 47. Wheel speed plotted alongside maximum wheel deceleration against time throughout ABS braking maneuver for high-mu surface.

The results presented from the simplified SMC control show good response and control of the braking torque to maintain the longitudinal slip ratio around the desired value. More complex switching control laws can be implemented in order to further improve the performance of SMC, but for the scope of this example, a simple sloping function is more than adequate to describe the function of SMC. This simple function also provides a good estimation of actual braking system capabilities, accounting for the delays of the mechanical components and pressure change in the system.

6.5 Discussion

The SMC simulation presented in the preceding sections is a simplified wheel model approximation used for ABS control. The purpose for using such a simple wheel model to describe SMC function for ABS is twofold. Firstly, it allows for the incorporation of an IT easily into the ABS control simulation to explain the benefit of having known tire force and friction information available to the ABS control system.

Secondly, it shows how the ABS control algorithm can be simplified with this additional information down to several control equations.

A direct comparison of the simplified SMC simulation to the current ABS system performance is difficult due to the differences in the two models, but some comparisons can be presented to show the potential benefit of implementing a SMC algorithm for ABS development. While the direct stopping distances cannot be accurately correlated between the SMC simulation and the current vehicle ABS simulation due to some of the simplifications used in for the SMC, the resulting braking dynamics can be examined. Figure 48 shows the comparison in the longitudinal slip ratio over time between (a) the SMC simulation and (b) the current upper bound ABS simulation developed in Chapter 5. The longitudinal slip with time for the SMC control oscillates around the desired slip ratio of 0.1415 after the brakes are applied up to the point where the vehicle cut-off speed is reached. The slip ratio is well controlled throughout the entirety of the braking maneuver. The slip ratio of the current ABS upper bound simulation in (b) varies quite a bit more than the SMC. There is an initial spike in the slip ratio due to the increase in braking pressure and a larger variation in the slip ratio range over the course of the braking maneuver.

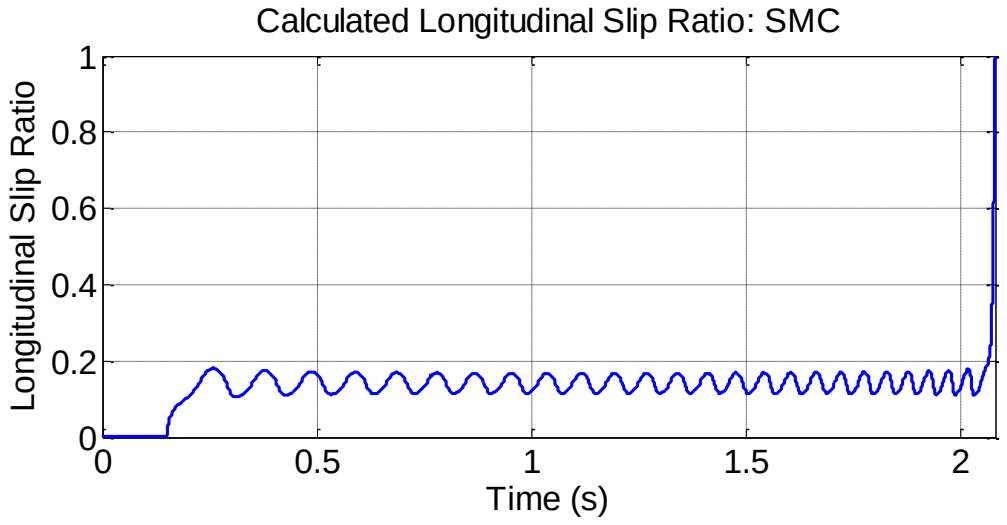

(a)

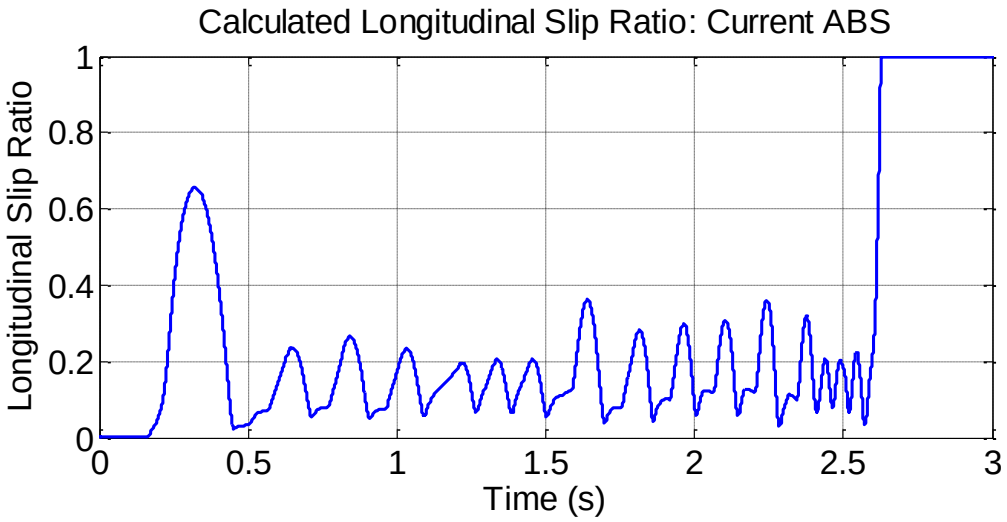

(b)

Figure 48. Comparison of longitudinal slip ratio over time between (a) SMC and (b) current ABS simulations.

The comparison of the plots shown in Figure 48 (a) and (b) show that the SMC method does a much better job of controlling the longitudinal slip ratio during emergency braking. There are no spikes in slip ratio using the SMC and less variation in the upper and lower range during ABS control. Recalling from previous desired ABS dynamics, the more closely the slip ratio range can be maintained around the desired slip ratio, the better the performance of the ABS.

Similar results are experienced in the longitudinal force versus longitudinal slip ratio plots shown in Figure 49. (a) shows the response for the SMC simulation and (b) shows the response of the upper bound ABS controller designed in Chapter 5. Again, the SMC controller shows excellent control of the longitudinal slip ratio, resulting in a slip range that operates between 0.12 and 0.17. The result of staying within these close boundaries is an increase in the average longitudinal braking force available to the tire. For the current ABS simulation shown in (b), there is a wider variation in the slip ratio range, resulting in lower and upper boundaries of 0.05 and 0.2; a range about 3 times larger than for SMC. This equates to a lower average longitudinal braking force and therefore longer braking distances.

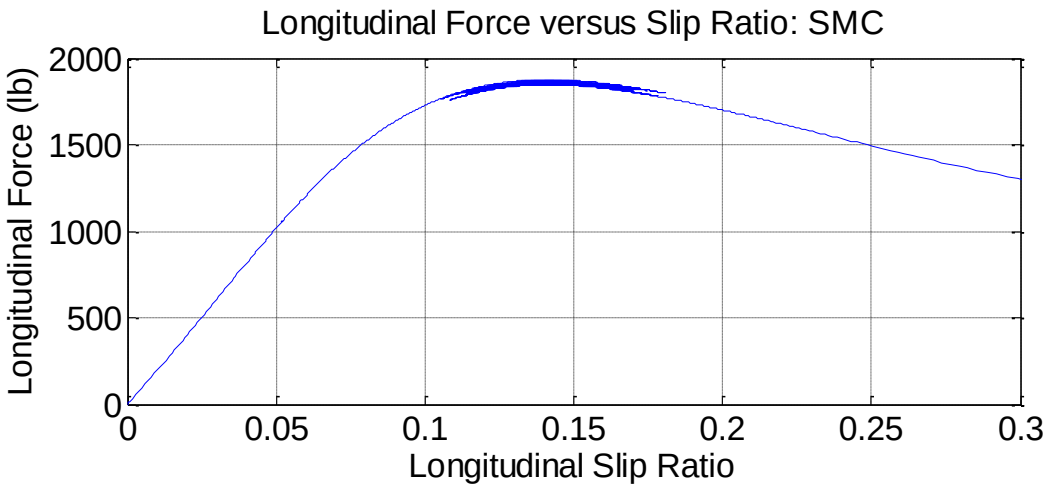

(a)

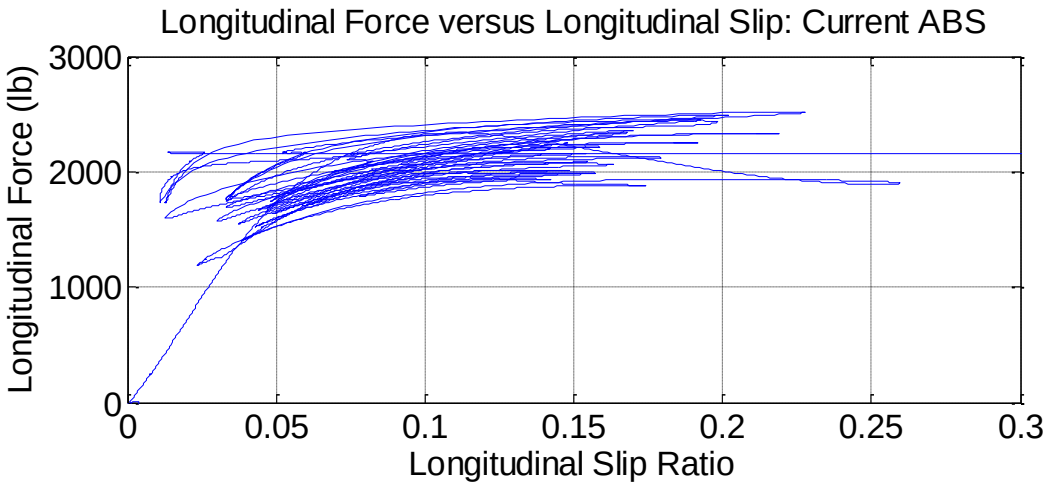

(b)

Figure 49. Longitudinal slip ratio versus longitudinal slip ratio for (a) SMC simulation and (b) upper bound ABS simulation.

The last comparison plots show the wheel speed response of the ABS systems for (a) the SMC simulation and (b) the tuned upper bound ABS response in Figure 50. The results for the wheel speed are fairly similar. The major differences that can be seen here is the variation in wheel speed due to the control of longitudinal slip and the operating frequency. The SMC wheel speed experiences a constant oscillation decrease in wheel speed, while the current ABS simulation shows variation in both oscillation amplitude and frequency, mainly in the beginning of the braking maneuver. The SMC ABS is operating at approximately 14 Hz while the current ABS system operates at 10 Hz. The control of the wheel speed is directly related to the control of the braking torque

responsible for maintaining a constant slip ratio. Since the SMC algorithm is more effective at evenly controlling the longitudinal slip, it also displays better control of the wheel speed.

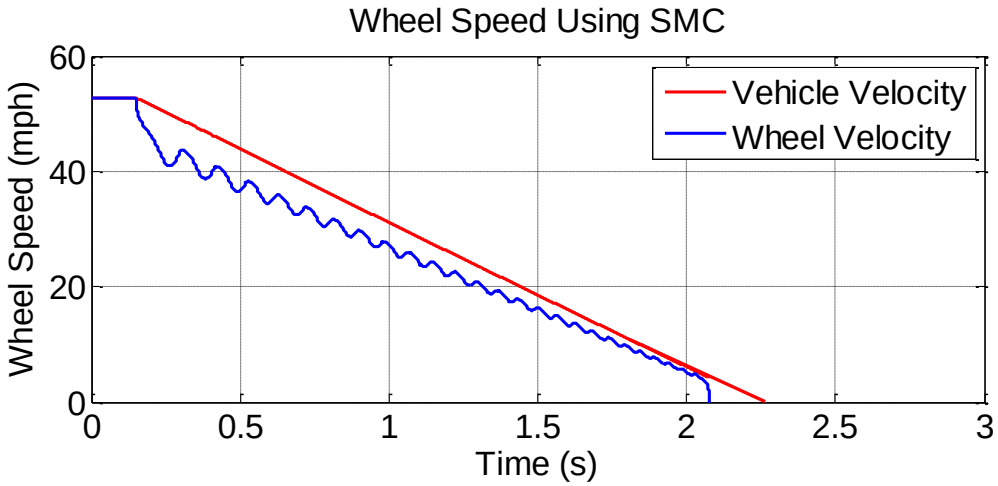

(a)

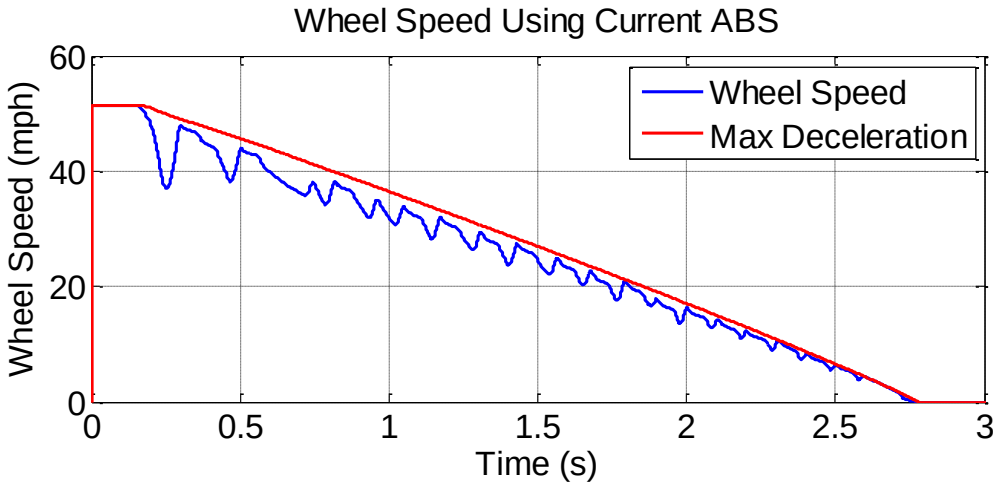

(b)

Figure 50. Wheel speed response of the ABS for (a) SMC simulation and (b) current tuned ABS simulation.

For the SMC, the estimated braking distance of the vehicle is 98.8 *ft* (30.1 *m*). For the original ABS simulation, the calculated braking distance was 118 *ft* (36 *m*). This accounts for a reduction in braking distance of 19.2 *ft* (5.85 *m*). This equates to a 16% reduction in overall braking distance, with no compromise on vehicle lateral control. It is noted that the SMC model used is a very simplified model in comparison to the model used for current ABS control, so this number is most likely an overestimate of the actual

system performance. While this difference in complexity accounts for a majority of the variations between the two control algorithms, the greater potential for increased braking dynamics is presented. The implementation of SMC using this simple model shows the feasibility and benefit of implementing a new, robust control method for use in ABS.

6.6 Conclusions

The SMC development method and operation is described and the system benefits and drawbacks are presented. SMC is an ideal candidate for use in ABS control since it is extremely robust and largely insensitive to external system parameters. The vehicle speed, wheel acceleration, longitudinal force and friction parameters experienced by the vehicle and tire during hard braking are subject to large variations depending on the vehicle and road conditions. This new SMC method is able to incorporate all of the new information gained from the IT and use this data to develop simple control laws for an ABS algorithm.

The implementation of SMC shows much greater potential for improvements in ABS braking dynamics and overall algorithm development in comparison to current ABS control methods. The use of SMC allows the designer to specify a specific desired operating point of the system and to drive the system to this control point, regardless of the system's current condition. This control point, the sliding surface, is adaptive and is calculated for each braking maneuver based on the surface condition, which is measured from the instantaneous force and friction information gained from the IT. Initial results show that using a SMC method reduces overall braking distance from the original ABS simulation by 16%. While the number is likely larger than the true value that is attainable, the SMC method shows high potential for improvement of the braking dynamics performance.

Another noteworthy point is that incorporating a SMC method will replace the current decision based algorithm with simple control laws. Current ABS algorithms have fairly complex decision processes that must determine the brake state based on currently available information. Having the additional knowledge of the instantaneous force and friction available at the tire contact patch from an IT allows for several of these decision processes to be eliminated. Current ABS algorithms must estimate the friction potential

and braking force available based on vehicle speed, wheel acceleration and other estimated tire parameters. Direct knowledge of the tire parameters will simplify the decision processes to simple switching control laws for SMC. These new control laws will result in less complex ABS algorithms and will allow for faster controller actuation times, further increasing braking performance.

7 Conclusions

The techniques and simulations explored in this work address the current commercial anti-lock braking limitations and the potential of improving ABS by developing new control algorithms. The work provides a comprehensive review of current longitudinal and lateral active vehicle control systems and introduces the IT along with an approach to exhibit the feasibility of implementing an intelligent tire into vehicle safety systems. A full-vehicle simulation is presented to detail the performance of current ABS methods. The major contributions of this research are as follows:

1) A threshold parameter sensitivity analysis is conducted for the full-vehicle anti-lock braking system simulation to identify the upper bound improvement to the current anti-lock braking system controller, and
2) Using information gained from an intelligent tire, an improvement to current anti-lock braking control systems is proposed by employing the use of a sliding-mode control method.

This work discusses the future trend of the role active safety systems will play in vehicle development. A comprehensive review of current longitudinal and lateral active vehicle control systems is presented to show the wide scope of active safety control and the potential for each system to improve vehicle safety. An intelligent tire is defined as an integral and necessary instrument in order to improve active vehicle safety systems. The use of an IT that can provide information about the dynamic behaviour of the tire at the contact patch holds potential to improve nearly every dynamic safety system. The ABS is focused on in this work due to the availability of these systems on all modern vehicles and this system stands to directly benefit from the implementation of an IT. Once successfully integrated with ABS, it can be easily adopted for other active control systems including traction control, yaw stability and rollover avoidance, to name a few.

To reiterate, the scope of this work as defined by the research sponsor included performing a study on current ABS to determine the upper bound improvement to the

current algorithms. The research then explored how employing an intelligent tire into ABS can improve braking performance. The overall goal of this study was to determine if employing an IT into new ABS algorithms improved braking performance enough to warrant further development of an IT.

A full vehicle simulation including a current longitudinal slip based ABS controller is presented and established as the current baseline standard. The performance of this commercially available ABS is presented in order to evaluate the improvement of newly proposed control methods to the system. The first method of improvement explored included performing a parameter sensitivity analysis on the current ABS control method. This establishes the upper bound of performance of current slip based control techniques, using only the vehicle and wheel parameters available to the system. The sensitivity analysis revealed that only minimal system improvement is possible utilizing current control algorithms.

A sliding mode control method was developed assuming perfect knowledge from an intelligent tire. The control algorithm now incorporates tire force and friction information from the contact patch into the control equations. The SMC simulation developed shows much greater potential for improvements in ABS braking dynamics and overall algorithm development in comparison to current ABS control methods. Due to the increased knowledge of the tire dynamics, new control algorithms are necessary in order to maximize the potential gain of the system. It is anticipated that an IT will improve the safety of many active safety systems and become an integral part to the vehicle safety system. Development of the IT should be continued for implementation into active vehicle safety systems.

References

1. NHTSA. *Fatality analysis reporting system (FARS) encyclopedia*. 2008 [cited 2010 10 February]; Available from: http://www-fars.nhtsa.dot.gov/Main/index.aspx.
2. *Intelligent tyre systems - state of the art and potential technologies deliverable D7*. APOLLO Project 23 May 2003 [cited 2010 24 February]; Available from: http://virtual.vtt.fi/virtual/proj3/apollo/deliverables/apollo_state_of_art.pdf.
3. *Vehicle Dynamics Terminology SAE J670*, in *Vehicle Dynamics Standards Committee*. 2008, SAE.
4. Hac, A. and M. Bodie, *Improvements in vehicle handling through integrated control of chassis sytems.* International Journal of Vehicle Design, 2002. 29(1/2): p. 23-50.
5. Gantz, T.a.H., G., *Seatbelts: Current Issues*, in *Prevention Institute*. 2002, University of Berkeley Traffic Safety Center: Berkeley, CA. p. 1-6.
6. Ergen, S., A. Sangiovanni-Vincentelli, and X. Sun, *The tire as an intelligent sensor.* IEEE Transactions on Computer-Aided Design of Integrated Circuits and Systems, 2009. 28(7): p. 941-955.
7. Huang, H. and C. Wang, *Intelligent control of wheeled vehicle with anti-braking systems.* International Journal of Vehicle Design, 2001. 26(2/3): p. 218-238.
8. Rajamani, R., *Vehicle dynamics and control*. 2006, New York: Springer Science.
9. Pacejka, H., *Tire and Vehicle Dynamics, 2nd Ed.* 2005: SAE International.
10. Yamakado, M. and M. Abe, *An experimentally confirmed driver longitudinal acceleration control model combined with vehicle lateral motion.* Vehicle System Dynamics: International Journal of Vehicle Mechanics and Mobility, 2008. 46(1 supp 1): p. 129 - 149.
11. Wilkin, M., W. Manning, and D. Crolla, *Estimation of non-linear friction force between tyre and road applied to a perfmrance vehicle*, in *Proceedings of AVEC'04*. 2006. p. 387-392.
12. Garrett, T., K. Newton, and W. Steeds, *The Motor Vehicle*. 2001, Warrendale, PA: SAE International.
13. Cho, W., et al., *An investigation into unified chassis control scheme for optimised vehicle stability and manoeuvrability.* Vehicle System Dynamics: International Journal of Vehicle Mechanics and Mobility, 2008. 46(1 supp 1): p. 87 - 105.
14. Dugoff, H., P. Fancher, and L. Segal, *Tyre performance characteristics affecting vehicle response to steering and braking control inputs*. 1969, Office of Vehicle Systems Research, US National Bureau of Standards.
15. Ghoneim, Y., W. Lin, and D. Sidlosky, *Integrated chassis control system to enhance vehicle stability.* International Journal of Vehicle Design, 2000. 23(1/2): p. 124-144.
16. *Intelligent tyre systems - final report including technical implementation plan deliverable 22/23*. APOLLO Project 25 July 2005 [cited 2010 24 February]; Available from: http://virtual.vtt.fi/virtual/proj3/apollo/deliverables/apollo_final%20report.pdf.
17. Trachtler, A., *Integrated vehicle dyanmics control using active brake, steering and suspension systems.* International Journal of Vehicle Design, 2004. 36(1): p. 1-12.

18. Schuller, J., P. Brangs, and R. Rothful, *Development methodology for dynamic stability control systems.* International Journal of Vehicle Design, 2002. 28(1/2/3): p. 37-56.
19. Li, J., F. Yu, and J. Zhang, *The rapid development of a vehicle electronic control system and its application to an antilock braking system based on hardware-in-the-loop simulation.* Proceedings of the Institute of Mechanical Engineering Part D: Journal of Automobile Engineering, 2002. 216: p. 95-105.
20. Baslamisli, S.Ç., İ.E. Köse, and G. Anlaş, *Gain-scheduled integrated active steering and differential control for vehicle handling improvement.* Vehicle System Dynamics: International Journal of Vehicle Mechanics and Mobility, 2009. 47(1): p. 99 - 119.
21. You, S., H. Choi, and H. Kim, *Active steering for intelligent vehicles using advanced control synthesis.* International Journal of Vehicle Design, 2006. 42(3/4): p. 244-262.
22. Yang, X., Z. Wang, and W. Peng, *Coordinated control of AFS and DYC for vehicle handling and stability based on optimal guaranteed cost theory.* Vehicle System Dynamics: International Journal of Vehicle Mechanics and Mobility, 2009. 47(1): p. 57 - 79.
23. Lynch, D. and A. Alleyne, *Velocity scheduled driver assisted control.* International Journal of Vehicle Design, 2002. 29(1/2): p. 1-22.
24. Antonov, S., A. Fehn, and A. Kugi, *A new flatness-based control of lateral vehicle dynamics.* Vehicle System Dynamics: International Journal of Vehicle Mechanics and Mobility, 2008. 46(9): p. 789 - 801.
25. Abou-Jaoude, R., *ACC radar sensor technology, test requirements, and test solutions.* IEEE Transactions on Intelligent Transportation Systems, 2003. 4(3): p. 115-122.
26. Jagtman, H., V. Marchau, and T. Heijer. *Current knowledge on safety impacts of collision avoidance systems (CAS).* in *Proceedings of the 5th International Conference on Technology, Policy and Innovation*. 2001. Delft.
27. Zador, P., S. Krawchuk, and R. Voas, *Automotive collision avoidance system (ACAS) program.*, NHTSA, Editor. 2000, Department of Transportation: Washingtion D.C.
28. Golias, J., G. Yannis, and C. Antoniou, *Classification of driver-assistance systems according to ther impact on road safety and traffic efficienty.* Transport Reviews, 2002. 22(2): p. 179-196.
29. Papadimitriou, I. and M. Tomizuka, *Lateral control of platoons of vehicles on highways: the autonomous following based approach.* International Journal of Vehicle Design, 2004. 36(1): p. 24-37.
30. Guo, K., H. Ding, and J. Zhang, *Development of a longitudinal and lateral driver model for autonomous vehicle control.* International Journal of Vehicle Design, 2004. 36(1): p. 50-65.
31. NHTSA, *Tire Pressure Monitoring System (TPMS) Final Rule*, in *http://www.nhtsa.gov/cars/rules/rulings/tirepresfinal/index.html*. 2007, DOT.
32. Fox, D., *Design of a Portable Tire Test Rig and Vehicle Roll-Over Stability Control*, in *Mechanical Engineering*. 2009, Virginia Polytechnic Institute and State University: Blacksburg.

33. Hopkins, B., *Adaptive Rollover Control Algorithm Based on an Off-Road Tire Model*, in *Mechanical Engineering*. 2009, Virginia Polytechnic Institute and State University: Blacksburg.
34. Hopkins, B., Fox, D., Caffee, J., Sides, B., Burke, W., Craft, M., Taheri, S., *Construction and Operational Verification of a Medium Duty Truck Tire Force and Moment Testing Trailer Suitable for On or Off Road Use*, in *Tire Society Conference*. 2009: Akron, OH.
35. Dhasarathy, D., *Estimation of Vertical Load on a Tire from Contact Patch Length and its use in Vehicle Stability Control*, in *Mechanical Engineering, Intelligent Transportation Lab*. 2010, Virginia Polytechnic Institute and State University: Blacksburg.
36. Salvucci, D., *Modeling Driver Behavior in a Cognitive Architecture.* Human Factors: The Journal of the Human Factors and Ergonomics Society, 2006. 48: p. 362-380.
37. Tan, D., Wang, Yanyang, *Research on the Parameter Identification of LuGre Tire Model Based on Genetic Algorithms*, in *School of Automobile and Traffic Engineering*. 2006, Shandong University of Technology: Zibo, China.
38. Levine, W., ed. *The Control Handbook*. ed. J. Claypool. 1996, CRC Press: Boca Raton, Florida. 1566.
39. Khalil, H., *Nonlinear Systems*. Third Edition ed. 2002, Upper Saddle River, NJ: Prentice Hall.
40. Taheri, S., *Slip Control Braking System Integrated with Four Wheel Steering*, in *Mechanical Engineering*. 1990, Clemson University: Clemson, SC.
41. Jin, K.H., Kyeung, H.O. and Chul, K.S. *Sliding Mode Control with Disturbance Observer for Antilock Braking System*. in *International Conference on Advanced Intelligent Mechatronics*. 2005. Monterey, CA: IEEE.

Appendix A Nomenclature

a	Multiplication factor for the tire
A	State matrix
$\mathrm{A_f}$	Frontal area of vehicle
B	Input matrix
$\mathrm{C_d}$	Coefficient of drag
CG	Vehicle center of gravity
d	Effective rolling diameter of the tire
F	Magnitude of combined longitudinal and lateral forces
F_{aero}	Aerodynamic drag force
F_a	Aerodynamic drag force
F_x	Longitudinal force acting on the tire at the contact patch
F_y	Lateral force acting on the tire at the contact patch
F_z	Vertical force acting on the tire at the contact patch
g	Acceleration due to gravity
h	Center of gravity height
J	Wheel moment of inertia
K	Vertical stiffness of tire
k	Proportional gain value
L	Length of tire contact patch
l	Wheelbase of vehicle
l_f	Length from vehicle center of gravity to front axle
l_r	Length from vehicle center of gravity to rear axle

m	Mass of vehicle
M	Mass of quarter-car model
M_x	Overturning moment of tire
M_y	Rolling resistance moment of tire
M_z	Self-aligning moment of tire
r	Effective rolling radius of the tire
RR_x	Longitudinal rolling resistance
s	Sliding surface
$\dot{s}$	Rate of change of sliding surface
T_b	Required brake torque for ABS
T_e	Engine torque
T_{net}	Net torque acting on the wheel
u	State space control input
V_x	Longitudinal velocity of the vehicle
V_y	Lateral velocity of the vehicle
x	Current longitudinal vehicle heading
x_0	Initial longitudinal vehicle heading
x_1	State space variable
$\dot{x}_1$	State space variable
x_2	State space variable
$\dot{x}_2$	State space variable
x-axis	Longitudinal direction of travel, positive forward
y-axis	Lateral direction of travel, positive to the right of the vehicle
z-axis	Vertical direction of travel, positive downward

α	Lateral slip angle
γ	Inclination / Camber angle
ε	Saturation gain value
δ	Steering angle
κ	Longitudinal slip ratio
$\dot{\kappa}$	Rate of change of longitudinal slip ratio
κ_d	Desired longitudinal slip ratio
κ_p	Peak longitudinal slip ratio
μ	Friction coefficient
μ_p	Peak friction coefficient
ρ	Density of air
σ	Total combined longitudinal and lateral slip component
σ_x	Longitudinal slip component
σ_y	Lateral slip component
τ	Ratio of normal load to vertical stiffness at particular inflation pressure
φ	Proportional gain value
Ω	Wheel angular velocity
$\dot{\Omega}$	Wheel angular acceleration

Appendix B Simulation Nomenclature

brk_pdl	Brake command (on / off)
$delt$	Change in slip angle
$delt\_f$	Driver corrected change in slip angle
Fwx	Calculated maximum longitudinal braking force
p	Damper velocity of vehicle
Q_u	Combined longitudinal velocity at each wheel
Q_v	Combined lateral velocity at each wheel
Q_r	Combined yaw velocity at each wheel
Q_p	Combined damper velocity at each wheel
r	Yaw velocity of vehicle
$slip$	Combined longitudinal and lateral slip
T_b	Calculated required brake torque for ABS
T_d	Driver desired braking torque
u	Longitudinal vehicle velocity
U	Longitudinal vehicle velocity corrected with yaw velocity
v	Lateral velocity of vehicle
w	Wheel rotational velocity
X	Longitudinal position of vehicle in test plane
Y	Lateral position of vehicle in test plane

Appendix C Simulation Parameters

```
% "Control Tire, Lateral Force"
% LATERAL_COEFFICIENTS
PCY1 =    1.4108e+000; % Shape factor Cfy for lateral forces
PDY1 =   -1.0492e+000; % Lateral friction Muy
PDY2 =    1.2588e-001; % Variation of friction Muy with load
PDY3 =   -8.3638e+000; % Variation of friction Muy with squared camber
PEY1 =    2.5099e-001; % Lateral curvature Efy at Fznom
PEY2 =   -3.3880e-001; % Variation of curvature Efy with load
PEY3 =   -3.3237e-001; % Zero order camber dependency of curvature Efy
PEY4 =    5.4411e-001; % Variation of curvature Efy with camber
PKY1 =   -3.4020e+001; % Maximum value of stiffness Kfy/Fznom
PKY2 =    4.0162e+000; % Load at which Kfy reaches maximum value
PKY3 =    1.5864e+000; % Variation of Kfy/Fznom with camber
PHY1 =    2.0123e-003; % Horizontal shift Shy at Fznom
PHY2 =    7.8600e-004; % Variation of shift Shy with load
PHY3 =   -3.3716e-002; % Variation of shift Shy with camber
PVY1 =   -3.6945e-003; % Vertical shift in Svy/Fz at Fznom
PVY2 =    9.2123e-003; % Variation of shift Svy/Fz with load
PVY3 =    2.6803e-001; % Variation of shift Svy/Fz with camber
PVY4 =    3.3248e-001; % Variation of shift Svy/Fz with camber and load
RBY1 =    1.3281e+001; % Slope factor for combined Fy reduction
RBY2 =    1.2241e+001; % Variation of slope Fy reduction with alpha
RBY3 =    5.1095e-004; % Shift term for alpha in slope Fy reduction
RCY1 =    1.0286e+000; % Shape factor for combined Fy reduction
RHY1 =   -2.3794e-002; % $Shift factor for combined Fy reduction
RVY1 =   -1.9826e-001; % Kappa induced side force Svyk/Muy*Fz at Fznom
RVY2 =   -6.4294e-001; % Variation of Svyk/Muy*Fz with load
RVY3 =   -4.6050e-002; % Variation of Svyk/Muy*Fz with camber
RVY4 =    1.0000e+003; % Variation of Svyk/Muy*Fz with alpha
RVY5 =    2.2937e+000; % Variation of Svyk/Muy*Fz with kappa
RVY6 =    1.6352e+001; % Variation of Svyk/Muy*Fz with atan(kappa)
PTY1 =    0.0000e+000; % Peak value of relaxation length SigAlp0/R0
PTY2 =    0.0000e+000; % Value of Fz/Fznom where SigAlp0 is extreme
%-------------------------------------------------rolling resistance
%[ROLLING_COEFFICIENTS]
QSY1 =    0.0000e+000; % Rolling resistance torque coefficient
QSY2 =    0.0000e+000; % Rolling resistance torque depending on Fx
%-------------------------------------------------aligning
%[ALIGNING_COEFFICIENTS]
QBZ1 =   -6.6937e+000; % Trail slope factor for trail Bpt at Fznom
QBZ2 =   -9.9403e-001; % Variation of slope Bpt with load
QBZ3 =    6.2090e-001; % Variation of slope Bpt with load squared
QBZ4 =   -4.0098e-001; % Variation of slope Bpt with camber
QBZ5 =   -1.3916e+000; % Variation of slope Bpt with absolute camber
QBZ9 =    2.9983e+001; % Slope factor Br of residual torque Mzr
QCZ1 =    2.1405e+000; % Shape factor Cpt for pneumatic trail
QDZ1 =    5.8367e-002; % Peak trail Dpt" = Dpt*(Fz/Fznom*R0)
QDZ2 =    1.2300e-002; % Variation of peak Dpt" with load
QDZ3 =   -2.3011e-001; % Variation of peak Dpt" with camber
QDZ4 =    1.4196e+000; % Variation of peak Dpt" with camber squared
QDZ6 =    6.5662e-004; % Peak residual torque Dmr" = Dmr/(Fz*R0)
```

```
QDZ7 =   -2.1288e-004; % Variation of peak factor Dmr" with load
QDZ8 =   -9.1201e-002; % Variation of peak factor Dmr" with camber
QDZ9 =    2.4666e-001; % Var. of peak factor Dmr" with camber and load
QEZ1 =    7.7762e-001; % Trail curvature Ept at Fznom
QEZ2 =    6.9822e-001; % Variation of curvature Ept with load
QEZ3 =   -3.1869e-001; % Variation of curvature Ept with load squared
QEZ4 =    5.5030e-002; % Variation of curvature Ept with sign of Alpha-
t
QEZ5 =   -1.5623e+000; % Variation of Ept with camber and sign Alpha-t
QHZ1 =    9.1788e-003; % Trail horizontal shift Sht at Fznom
QHZ2 =   -8.8192e-003; % Variation of shift Sht with load
QHZ3 =    1.1678e-001; % Variation of shift Sht with camber
QHZ4 =   -5.6332e-001; % Variation of shift Sht with camber and load
SSZ1 =   -5.7866e-002; % Nominal value of s/R0: effect of Fx on Mz
SSZ2 =    2.4197e-002; % Variation of distance s/R0 with Fy/Fznom
SSZ3 =   -1.0000e+000; % Variation of distance s/R0 with camber
SSZ4 =   -1.0000e+000; % Variation of distance s/R0 with load and
camber
QTZ1 =    0.0000e+000; % Gyration torque constant
MBELT =   0.0000e+000; % Belt mass of the wheel

lr = 0.6; % tire lateral relaxation length, m

a = 1.255; % Cg to front axle
b = 1.657; % Cg to rear axle
tr = 1.613; % wheel track at front
m = 1950; % Vehicle mass, kg
ms = 1810.5; % Sprung mass, kg
hs = 0.59; % CG Height
kroll = 71592.8; % calculated from linear stiffness of front and rear
sunspensions
croll = 4360; % calculated from front and rear damper rates of 2 N/mm/s
Ix = 474.5; % Roll moment of inertia
Iz = 3522; % Yaw moment of inertia

% LuGre tire model
% normal tire
sigma_0 = 32.5; % normal tire, 1/m
sigma_1 = 0.76; % 1/m
sigma_2 = 0.0063; % s/m
mu_c = 0.965; % the normalized Coulomb friction
mu_s = 2.5; % the normalized static friction
v_s = 1; % the Stribeck relative velocity, m/s
alpha = 0.515; % exponent for dynamic friction function g(vr)
kappa_0 = 1; % a parameter relating distribution of normal force

% ABS thresholds
a1_ini_f = - 15.68; % m/s^2
a1_ini_r = - 21.6; % m/s^2
a2_f = 2.5; % m/s^2
a2_r = 1.5; % m/s^2
Ak_f = 10.5; % m/s^2
Ak_r = 9; % m/s^2
a_hold = -11; % m/s^2
```

```
% high friction, normal stiffness
smpl_prd = 0.00025; % sampling period, s
m1_f = 0.01 / smpl_prd; % increase-constant for step-increase of front
wheels, 10 ms
m1f_f = 0.021 / smpl_prd; % increase-constant for fast step-increaseof
front wheels, 15 ms
m1_r = 0.014 / smpl_prd; % increase-constant for step-increase of rear
wheels, 10 ms
m1f_r = 0.021 / smpl_prd; % increase-constant for fast step-increaseof
rear wheels, 20 ms
n_1 = 0.049 / smpl_prd; % hold-constant for step-increase, 0.075 s

time_3 = 0.21 / smpl_prd; % maximum time for brake state 3
time_rls = 0.48 / smpl_prd; % time for brake release
P_pushout = 0.535; % pressure of pushout, MPa

pi = 3.1416;
g = 9.8066;
T = 0.8; % preview time of driver, s
tao = 0.2; % reaction time of driver, s
L = a + b;
esp = .001;

u_d = 23.0; % desired vehicle speed, m/s

% extra parameters for "DirectLyapunov1.mdl"
R = 0.3215; % loaded radius of tire, m
Iwf = 1.8; % rotary moment of inertia of a front wheel
Iwr = 1.2; % rotary moment of inertia of a rear wheel
%Cp_f = 500; % braking torque gain of front wheels, Nm/MPa
Cp_f = 560; % braking torque gain of front wheels, Nm/MPa
Cp_r = 260; % braking torque gain of rear wheels, Nm/MPa
mu_max_left = 0.8; % maximum tire-road friction coefficient on left
side
mu_max_right = 0.8; % maximum tire-road friction coefficient on right
side
CD = 0.3; % Coefficient of Air Drag
A = 2.25; % Front wind area
f = 0.015; % rolling friction coefficient
KP = 60; % P coefficient of PI controller for vehicle speed
KI = 40; % I coefficient of PI controller for vehicle speed
```